December 2019

Simulation-Based Evaluation and Optimization of the Seismic Performance of Buildings with Passive Energy Dissipation System

Yuting Cheng
Clemson University, yutingc8912@gmail.com

SIMULATION-BASED EVALUATION AND OPTIMIZATION OF THE SEISMIC PERFORMANCE OF BUILDINGS WITH PASSIVE ENERGY DISSIPATION SYSTEM

A Dissertation
Presented to
the Graduate School of
Clemson University

In Partial Fulfillment
of the Requirements for the Degree
Doctor of Philosophy
Civil Engineering

---

by
Yuting Cheng
December 2019

Accepted by:
Dr. Qiushi Chen, Committee Chair
Dr. Weichiang Pang, Co-Chair
Dr. Brandon Ross
Dr. Laura Redmond

ABSTRACT

Earthquakes are one of the major natural hazards that could directly cause damages to or collapse of buildings, leading to significant economic losses. In this dissertation research, analytical tools and simulation-based optimization framework are developed to improve our understanding of and the ability to design more seismic-resilient structures with passive energy dissipation systems. The main objectives of this dissertation are to (1) investigate the seismic performance of structures with energy dissipation systems and evaluate the effectiveness of damping coefficient dissipation methods using three-dimensional numerical models; (2) develop a simulation-based multi-objective optimization framework to evaluate and optimize the seismic performance of buildings with energy dissipation systems; (3) incorporate and evaluate the influence of soil-structure interaction in the performance-based seismic design of structures.

Aiming at these objectives, this dissertation consists of three related studies. In the first study, the seismic performance of structures with energy dissipation systems, specifically fluid viscous dampers (FVD), was investigated using three-dimensional (3D) numerical models. Four different damping coefficient distribution methods for FVD were extended to 3D numerical models. Then, their effectiveness in terms of improving structural seismic performance was evaluated through a series of nonlinear dynamic analysis. The seismic performance of the structure has been significantly improved by applying the FVD, and this significance of the improvement depends on the distribution of damper's damping coefficient within the 3d numerical model. Among the four different damping coefficient distribution methods, the story shear strain energy distribution

(SSSED) method was found to be an optimal distribution method that can improve the inter-story drift of the structure while it can also provide the most uniformly distributed inter-story drift.

In the second study, a performance-based optimization framework for the structural design was developed that considers multiple conflicting objectives: initial material cost, structural repair cost, and record-to-record variability of ground motions. The developed optimization framework was effective in improving the seismic performance of structures. All obtained optimum designs can dramatically decrease the inter-story drift and peak floor acceleration of the structure. This study also provided a practical approach to select the optimal design variables of the energy dissipation systems. The selected design can achieve the desired performance level of the structure with moderate initial material cost, structural repair cost, and robustness measure.

In the third study, the effect of soil-structure interaction was incorporated into the optimization framework developed in the second study. Two scenarios were considered in the analysis: one with a fixed foundation, and the other one with a flexible foundation. In this study, the selection of soil properties was based on site class D. The frame with a flexible foundation was found to have a larger inter-story drift in each floor when compared to the frame with a fixed foundation. The guideline for selecting the best-performance design was developed based on the inter-story drift ratio. The improvement of the inter-story drift (compared to a bare frame without energy dissipation systems) and the

uniformity of the inter-story drift, were proposed as two performance indices to evaluate the effectiveness of the selected designs.

Finally, based on findings of this dissertation work, recommendations for seismic design of buildings with energy dissipation systems and directions for future research are given.

DEDICATION

I dedicate this dissertation to my parents for their love and support all these years.

ACKNOWLEDGMENTS

I would foremost like to express my deepest gratitude to my advisors, Dr. Qiushi Chen and Dr. Weiqiang Pang, for giving me the opportunity to work with them. I am genuinely grateful for their encouragement, support, and advice throughout my research. I would also like to thank my committee members, Dr. Brandon Ross, and Dr. Laura Redmond, for their help and constructive feedback on this dissertation study.

I appreciate Kristin Baker, Monica A. Hughes, and all the teachers and staff of the Glenn Department of Civil Engineering. Thanks for their consistent help and advice through my master's and doctoral studies at Clemson University.

I would also like to thank my friends and colleagues, Wenxin Liu, Feiyang Chen, Weiwei Zhan, Zakia Tasnim, Fanfu Fan, and Ke Tang, who are always willing to help in life and study over the years.

Last but not least, I am greatly thankful to my family for their understanding and unconditional support. Thanks to them for always stand by my side through the tough and stressful time and made this achievement possible.

TABLE OF CONTENTS

Page

TABLE OF CONTENTS (CONTINUED)

Page

LIST OF TABLES

Table Page

LIST OF TABLES (CONTINUED)

Table Page

LIST OF TABLES (CONTINUED)

Table Page

LIST OF FIGURES

Figure Page

LIST OF FIGURES (CONTINUED)

Figure Page

LIST OF FIGURES (CONTINUED)

Figure Page

LIST OF FIGURES (CONTINUED)

Figure Page

LIST OF FIGURES (CONTINUED)

Figure Page

CHAPTER I
INTRODUCTION

1.1. Problem Statement

Earthquakes are one of the major natural hazards that could directly damage to or cause the collapse of a structure (Otani 1999; Achour et al. 2011; Lu et al. 2013; Raghunandan and Liel 2013; Tong et al. 2013; Xie et al. 2015). Earthquake could also induce landslide (Bommer et al. 1999; Gorum et al. 2011; Meunier et al. 2008) and soil liquefaction (Ishihara 1993; Obermeier 1996), posing threats to buildings and infrastructures. For instance, in the 1994 Northridge earthquake, thousands of buildings and 228 bridges were damaged (Basoz et al. 1999). Over 8,000 buildings collapsed in the 2016 Kumamoto earthquake (Liu and Yamazaki 2018).

In conventional seismic designs and the retrofitting of structures, the following methods have been frequently used to improve the seismic capacity of structures and mitigate the earthquake-induced structure damages: (1) constructing shear walls (Kaplan et al. 2011); (2) adding diagonal braces, e.g., buckling-restrained brace (Aristizabal-Ochoa 1986; Güneyisi 2012); (3) installing base isolation, e.g., high-damping rubber bearing (Matsagar and Jangid 2008). In recent years, the passive energy dissipation system has been used instead of the conventional brace and been applied to retrofit structures and for seismic protection of new structures. Fluid viscous damper (FVD) is a passive energy dissipation system widely implemented in engineering projects (Soong and Spencer 2002). Pictures of FVD and its major components are shown in Figure 1-1.

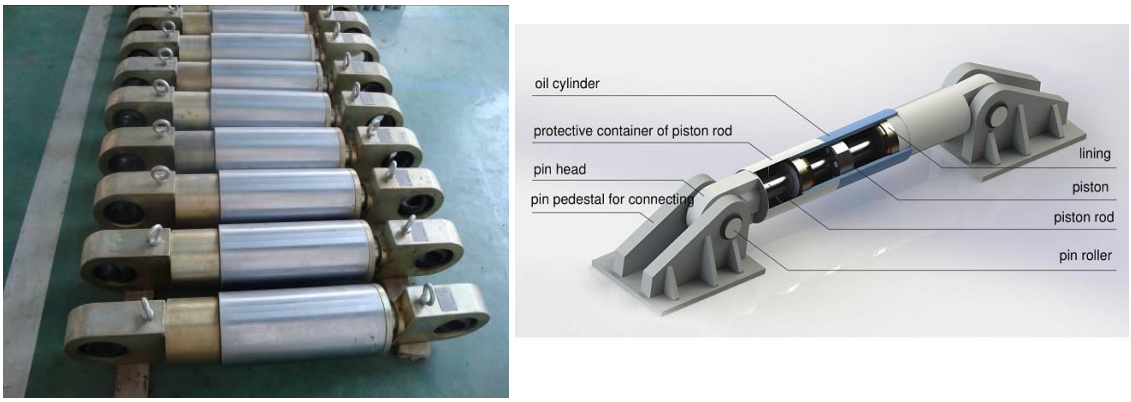

Figure 1-1 Fluid viscous damper (left); major components of a fluid viscous damper (right)
(https://www.techstar-inc.com/products/seismic/viscous-dampers/damper1; http://www.roadjz.com/en/show.asp?id=12)

FVD can affect the seismic responses of structure by improving the damping ratio of structure. The damping force of the FVD mainly depends on the properties of the viscous fluid and the piston head orifices, which can be characterized by its damping coefficient. Previous research on the damping coefficient of FVD can be divided into two categories: (1) calculating the required damping coefficient of FVD and its distribution in the structure (FEMA-273 1997; FEMA-356 2000; Hwang et al. 2013); (2) optimizing and selecting the optimum design parameters of the FVD (Sorace and Terenzi 2008).

Seismic design document (e.g., FEMA 356) has specified the uniform distribution method to determine the damping coefficient of FVD in each story. Various damping coefficient distribution methods were proposed based on the seismic capacity of different stories of the structure, e.g., the inter-story drift proportional distribution method (Landi et al. 2015), and the story shear strain energy distribution method (Hwang et al. 2013). These damping coefficient distribution methods have been applied to the numerical models of structures. The two-dimensional numerical models were used to evaluate the effectiveness

of these distribution methods on the seismic performance of the structure. However, there is a lack of knowledge about assigning damping coefficients in three-dimensional numerical models in the current seismic standards of the structural design.

For optimizing and selecting the optimum design parameters of the FVD, Lavan et al. (2008) have conducted a genetic algorithm-based multi-objective optimization study. The inter-story drift and floor acceleration were treated as the conflicting performance measures of the structure to formulate the optimization study. These conflicting performance measures were frequently used to construct single or multi-objective optimization of the structural design. The design that can simultaneously reduce these two performance measures is considered as the optimal design. In Lavan's study, the distribution of nonlinear FVD was determined by simultaneously minimizing the inter-story drift and absolute floor acceleration of a five-story shear frame. Moreover, Hejazi et al. (2013) have defined the damping coefficient of dampers as the design parameters. The optimum values of the design parameters were selected by reducing the three-directional displacements of a five-story reinforced concrete building.

In general, reducing the amounts of performance measures usually results in the increasing costs of dampers. However, most studies have only considered the costs of dampers as the critical optimization objectives to select the cost-effective design parameters of the dampers. For instance, most studies only considered the effects of manufacturing, repair, or even the life-cycle costs of dampers as the optimization objectives when determining design parameters of the dampers (Gidaris and Taflanidis

2015; Del Gobbo et al. 2018; Lavan and Amir 2014; Pollini et al. 2016). Hence, it has great significance in developing a performance-based optimization framework for structural design that considers both performance measures of the structure and the costs of dampers.

The traditional shaking table test can evaluate the seismic responses of the structure with FVD. Nowadays, the shaking table test has been evolved from testing scaled-down structural models to full-scale structures (Kasai et al. 2010). However, the shaking table test has restrictions on the weight of the structure being tested and the site where the tests being performed. Moreover, the experiment is non-reproducible, especially the collapse experiment. Numerical modeling-based seismic performance analysis, as an alternative method, can effectively alleviate those limitations. Numerical methods have relatively low cost and are applicable to a variety of architecture types. Open System for earthquake engineering simulation (OpenSees) is one of the finite element-based modeling tools, which is developed at UC Berkeley and supported by Pacific Earthquake Engineering Research Center (PEER) and Network for Earthquake Engineering Simulation (NEES) (Jiang and Usmani 2013). OpenSees can be used to perform nonlinear static and dynamic seismic analysis of the structures (Ferracuti et al. 2009), and has been applied to simulate the seismic performance of steel structures, concrete structures, and masonry walls (Bao and Kunnath 2010; Furtado et al. 2015; Lignos et al. 2011; Tang and Zhang 2011). Most existing studies using OpenSees have focused on two-dimensional structural models with FVD (Karavasilis 2016; Seo et al. 2014; Silwal et al. 2015, 2016).

The seismic responses of the structure with FVD can be affected by the properties of FVD and the rationality of the structural design, e.g., sizes of beams and columns. Moreover, it has been found that the soil-structure interaction also influences the overall performance of a structure. Namely, the interaction between the structure, the foundation, and the soil properties of the underlying and surrounding of the foundation during the ground shaking (Ghosh and Madabhushi 2004). The soil-structure interaction typically affects the performance of a structure in three ways: (1) alter the period of the structure by foundation movement; (2) reduce structural force demand by the nonlinear behavior and hysteretic energy dissipation; (3) alter the input ground motion by the foundation flexibility (Raychowdhury 2011). The foundation movements can induce significant flexibility to the braced system, so that result in an inaccurate estimation of seismic performance of structure (Stewart et al. 1999). Thus, the flexibility of the foundation is urgently needed to be incorporated in a conservative performance-based structural design. However, it has not been specified how to consider the flexibility of foundation in the structural design. In this research, the impact of soil-structure interaction will be evaluated and incorporated in the performance-based optimization framework for structural design.

In this dissertation, a comprehensive study is conducted on investigating the seismic performance of structures with energy dissipation systems using three-dimensional numerical models. Numerical analysis with the finite element method is applied to simulate the nonlinear dynamic responses of the structure under different intensities of biaxial ground motions. The seismic performance of the structure is improved by the application of the energy dissipation system. The existing damping coefficient distribution methods of

the energy dissipation system are extended and applied to the three-dimensional numerical models. Their effectiveness is evaluated by the nonlinear dynamic analysis of the three-dimensional numerical models. The cost-effective optimum design and performance-based structural design are integrated to develop a performance-based optimization framework for structural design. Furthermore, the effect of soil-structure interaction is evaluated and incorporated in the proposed performance-based optimization framework. The selection guidelines of optimum performance and cost-effective design is proposed based on the improvement and uniformity of inter-story drift.

1.2. Objectives and Scope

The research efforts of how to improve and simulate the seismic performance of the structure, and how to choose an optimum-performance and cost-efficient structural design have always been the critical topics in seismic engineering researches.

By addressing these questions, the main objectives of this research are to (1) investigate the seismic performance of structures with energy dissipation systems and evaluate the effectiveness of damping coefficient dissipation methods using three-dimensional numerical models; (2) develop a simulation-based multi-objective optimization framework to evaluate and optimize the seismic performance of buildings with energy dissipation systems; (3) incorporate and evaluate the influence of soil-structure interaction in performance-based seismic design of structure.

Revolving around these objectives, the scope of this research covers the application of energy dissipation systems on structural steel frames and the investigation of their seismic performance using the three-dimensional numerical models. It includes the evaluation of the effectiveness of different damping coefficient distribution methods of the energy dissipation system. It also covers the development of the performance-based optimization framework for structural design and the selection guideline of design parameters of FVD. It also includes the assessment of soil-structure interaction and its impact on the performance-based structural design.

1.3. Dissertation Organization

This dissertation is organized into six chapters. Chapter I presents the problem statement, the objectives and scope, and the organization of this dissertation. Chapter II introduces the background and methodologies that are required for conducting the dissertation research. This chapter covers the illustrations of the theoretical knowledge of the fluid viscous damper and the Non-Dominated Sorting Genetic Algorithm II based multi-objective optimization method.

In Chapter III, the seismic performance of structures with energy dissipation systems is investigated by using three-dimensional numerical models. Four damping coefficient distribution methods are presented and applied to the three-dimensional numerical models of steel moment-resisting frame. The effectiveness of different damping coefficient distribution methods is evaluated by considering different intensities of biaxial ground motions.

Chapter IV presents a performance-based optimization framework for structural design that considers multiple conflicting objectives. The manufacturing costs of the energy dissipation system, repair costs of the structure, and the robustness measure of record-to-record variability of ground motion are minimized simultaneously. The applicability and capability of the proposed framework are demonstrated by applying it to the simulation-based seismic design of the steel frame with the energy dissipation system. The Non-Dominated Sorting Genetic Algorithm II based multi-objective optimization method is conducted to optimize the conflicting objectives. The optimal design parameters of the energy dissipation system are selected with moderate initial material cost, structural repair cost, and robustness measure. The effectiveness of the selected design is evaluated by the extent of improvement of the seismic performance of structures.

In Chapter V, the effect of soil-structure interaction is incorporated in the evaluation of the seismic performance of the steel frame with the energy dissipation system. The seismic responses of the structures are evaluated using three-dimensional numerical models. The performance-based optimization framework, as introduced in Chapter IV is applied to the numerical models of the steel frame with fixed and flexible foundations. The optimum properties of the design parameters of the fluid viscous dampers are selected based on the comparison of improvement and uniformity of inter-story drift.

In Chapter VI, as a conclusion of this dissertation, the main findings of this dissertation and the recommendations for future research are presented.

CHAPTER II
BACKGROUND AND METHODOLOGY

2.1. Background and Principle of Fluid Viscous Damper

2.1.1. Background of Fluid Viscous Damper

Over the past two decades, various types of passive energy dissipation systems have been developed and applied in structural designs. The supplemental damping devices can absorb a portion of seismic energy to improve structural performance. The following time-dependent energy conservation equation can clearly illustrate the effect of the supplemental damping devices to a structure in resisting the seismic force (Uang and Bertero 1990):

$$E_e(t) = E_k(t) + E_s(t) + E_h(t) + E_d(t) \tag{2.1}$$

where E_e is the absolute earthquake input energy, t is the time, E_k is the absolute kinetic energy of the masses, E_s is the recoverable elastic strain energy, E_h is the irrecoverable hysteretic energy dissipated by the structure, and E_d is the energy dissipated by the supplemental damping system. The right-hand side of the equation represents the energy capacity of the structure, and the left-hand side represents the energy demand of the structure under the ground motion. For a stable structural design, the energy capacity of the structure should be larger than the energy demand.

In conventional seismic design, the term E_d is equal to zero. The seismic input energy is mainly dissipated by the irrecoverable hysteretic energy of the structure. The structural components are inelastically deformed to dissipate the seismic induced energy. The principle of the damping devices is to dissipate the input energy before the primary

structural components. Thus, the structures with damping devices can effectively dissipate the seismic induced energy and reduce the inelastically deformation of the structural components.

In the late 1980s and early 1990s, fluid viscous dampers (FVDs) were used in structural engineering. FVD typically consists of a stainless-steel piston with an orifice head. The piston is contained in a cylinder filled with highly viscous fluid, such as silicone or a similar type of oil, as shown in Figure 2-1. The liquid in the cylinder is in a vacuum environment. Due to the movement of the piston rod region, the FVD can generate the resistance force, which always resists the structure motion during a seismic event (Lee and Taylor 2001; Oesterle 2003; Ras and Boumechra 2016).

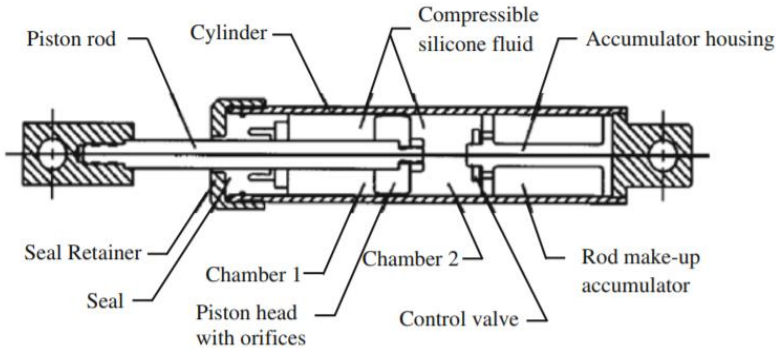

Figure 2-1 Diagrammatic sketch of the viscous damper (Symans and Constantinou 1998)

The resistance force is proportional to the relative velocity between the ends of the damper, and can be expressed as follows:

$$F_d = C_d \operatorname{sgn}(v)|v|^{\alpha} \tag{2.2}$$

where C_d is the supplemental damping coefficient, sgn is the signum function, v is the relative velocity between the ends of the damper, α is the velocity exponent of the damper with a typical range 0.3 to 1.95 (Liu 2010). The damping coefficient and velocity exponent have primarily controlled by the configuration of the piston head orifices. When α=1, the FVD is called a linear viscous damper. The FVD behaves as a nonlinear viscous damper with α smaller than unity. FVD with α larger than unity is rarely used in practical applications. The force-velocity relationship of FVD with different values of velocity exponent is given by Figure 2-2. The resistance force generated by the nonlinear viscous damper increases rapidly and then begin to flatten. The linear viscous damper can provide a larger damper force than the nonlinear viscous damper when the relative velocity is larger than unity.

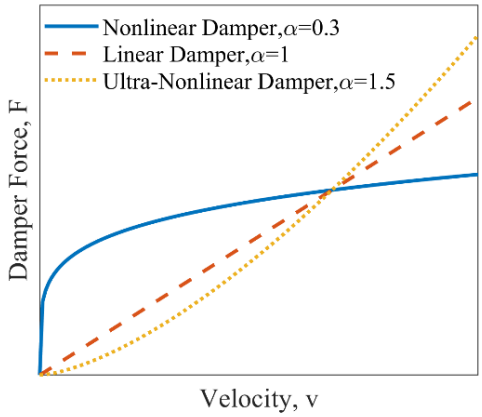

Figure 2-2 Force-velocity relationship of the viscous damper

2.1.2. Damping Coefficient of Linear Viscous Damper

For a structure with FVD, the total effective damping ratio ξ_e of the structure consists of the structural inherent damping ratio ξ_i and damper's damping ratio ξ_d, as shown in equation (2.3). The inherent damping ratio is usually assumed to be 5%. As specified in

FEMA 356 and ASCE 41-17 (FEMA-356 2000; ASCE 41-17 2017), in each principal horizontal direction, the damper's damping ratio should be less than 30% of critical damping in the fundamental mode of the rehabilitated building. The damper's damping ratio is related to the damping coefficient of the damper and the critical damping coefficient of the structure, as shown in equation (2.4).

$$\xi_e = \xi_i + \xi_d \tag{2.3}$$

$$\xi_d = \frac{C_d}{C_{cr}} \tag{2.4}$$

$$C_{cr} = 2\sqrt{Km} \tag{2.5}$$

where K, m, and C_{cr} represent the stiffness, mass, and the critical damping coefficient of the structure, respectively.

The critical damping coefficient of the structure is based on the inherent properties of the structure, as shown in equation (2.5). Hence, the damping coefficient of the damper needs to be determined to achieve a certain amount of damper's damping ratio. The derivation of C_d for the linear viscous damper is presented as follows:

Considering a single degree of freedom (SDOF) system equipped with a linear viscous damper. The SDOF system is assumed to subject to a sinusoidal displacement time history:

$$u(t) = u_0 \sin \omega t, \quad 0 < t < \frac{2\pi}{\omega} \tag{2.6}$$

where u, u_o and ω represent the displacement of the damper, the amplitude of the displacement and the loading frequency. Recall equation (2.2), the energy dissipated by a damper in one cycle of vibration can be calculated as follows:

$$\begin{aligned} E_d &= \oint F_d d_u = \oint C_d \dot{u} d_u = \int_0^{2\pi/\omega} C_d \dot{u}^2 d_t \\ &= C_d u_0^2 \omega^2 \int_0^{2\pi} \cos^2(\omega t) d(\omega t) = \pi C_d u_0^2 \omega \end{aligned} \tag{2.7}$$

where ω_o represents the natural frequency of the system, which essentially equals ω under the seismic ground motion (Ras and Boumechra 2016). Then, equation (2.7) can be rewritten based on equations (2.3), (2.4) and (2.5), as:

$$\begin{aligned} E_d &= \pi C_d u_0^2 \omega \\ &= \pi \xi_d C_{cr} u_0^2 \omega \\ &= 2\pi \xi_d \sqrt{Km} u_0^2 \omega \\ &= 2\pi \xi_d K u_0^2 \omega / \omega_0 \\ &= 4\pi \xi_d E_s \omega / \omega_0 \end{aligned} \tag{2.8}$$

The elastic strain energy of the system, E_s can be calculated as:

$$E_s = K u_0^2 / 2 \tag{2.9}$$

Hence, the damper's damping ratio can be calculated as:

$$\xi_d = \frac{E_d}{4\pi E_s} \frac{\omega_0}{\omega} = \frac{E_d}{4\pi E_s} \tag{2.10}$$

The equation of damper's damping ratio can be extended to a multi-degree of freedom (MDOF) system. For the MDOF system, assume that the linear viscous dampers are installed on each floor. The damper's damping ratio can be calculated as:

$$\xi_{d,n} = \frac{\sum_{i=1}^{N_F} E_{d,in}}{4\pi \sum_{i=1}^{N_F} E_{sn}} \tag{2.11}$$

where $E_{d,in}$ represents the dissipated energy by the i-th dampers in one cycle of vibration within the system, and N_F is the number of stories of the system. This equation was derived based on the shear building assumption and adopted in FEMA 356 and ASCE 41-17 (ASCE 41-17 2017; FEMA-356 2000). The formula of damper's damping ratio is derived based on the assumption of the n-th vibration mode of the system. The damping coefficient of each damper is identical. The formula of energy dissipation by dampers can be expressed as follows:

$$\begin{aligned} \sum_{i=1}^{N_F} E_{d,in} &= \sum_{i=1}^{N_F} \pi C_d {u_{in}}^2 \omega_n \\ &= \frac{2\pi^2}{T_n} \sum_{i=1}^{N_F} C_d {u_{in}}^2 \\ &= \frac{2\pi^2}{T_n} \sum_{i=1}^{N_F} C_d (f_i \phi_{d,in})^2 \end{aligned} \tag{2.12}$$

where C_d represents the damping coefficient of dampers at the i-th story, u_{in} and $\phi_{d,in}$ are the relative axial displacement and relative horizontal displacement of dampers at the i-th story, T_n is the period of n-th vibration mode, f_i is the scale factor that depends on the

installation plan of the dampers (Hwang et al. 2008). The formula of elastic strain energy can be rewritten as:

$$\begin{aligned}\sum_{i=1}^{N_F} E_{sn} &= \frac{1}{2}\Phi^T K \Phi = \frac{1}{2}\Phi^T \omega_n{}^2 m \Phi \\ &= \frac{1}{2}\sum_{i=1}^{N_F} \omega_n{}^2 m_i \phi_{in}{}^2 = \frac{2\pi^2}{T_n{}^2}\sum_{i=1}^{N_F} m_i \phi_{in}{}^2\end{aligned} \tag{2.13}$$

where m_i represents the mass of the i-th floor, Φ and ϕ_{in} represent the n-th mode shape of the system and the horizontal displacement of the i-th floor. The linear damper's damping ratio $\xi_{d,n}$ is given as follows:

$$\xi_{d,n} = \frac{\frac{2\pi^2}{T_n}\sum_{i=1}^{N_F} C_d (f_i \phi_{d,in})^2}{4\pi \frac{2\pi^2}{T_n{}^2}\sum_{i=1}^{N_F} m_i \phi_{in}{}^2} = \frac{T_n \sum_{i=1}^{N_F} C_d (f_i \phi_{d,in})^2}{4\pi \sum_{i=1}^{N_F} m_i \phi_{in}{}^2} \tag{2.14}$$

The damping coefficient C_d of the linear viscous damper at each floor can be derived from equation (2.14) as:

$$C_d = \frac{4\pi \xi_{d,n} \sum_{i=1}^{N_F} m_i \phi_{in}{}^2}{T_n \sum_{i=1}^{N_F} (f_i \phi_{d,in})^2} \tag{2.15}$$

2.1.3. Damping Coefficient of Non-Linear Viscous Damper

The derivation of C_d for the nonlinear viscous damper is presented in this section. For a given SDOF system, the system is assumed to subject to a sinusoidal displacement time history, expressed as:

$$u(t) = u_0 \sin \omega t, \quad 0 < t < \frac{2\pi}{\omega}$$
$$u_0 = f_i \phi_{d,i} \tag{2.16}$$

where u, u_o and ω represent the displacement of the damper, the amplitude of the displacement and the loading frequency, f_i is the scale factor, $\phi_{d,i}$ is the relative horizontal displacement of dampers at the i-th story.

For a single cycle of harmonic motion, the energy dissipated by the nonlinear viscous damper can be expressed as:

$$\begin{aligned} E_d &= \oint F_d d_u = \oint C_d \operatorname{sgn}(\dot{u}) |\dot{u}|^{\alpha} d_u \\ &= \int_0^{2\pi/\omega} C_d \operatorname{sgn}(\dot{u}) |\dot{u}|^{\alpha} \dot{u} d_t \\ &= \frac{4 C_d (2\omega)^{\alpha} (u_0)^{\alpha+1} \Gamma^2 (1 + \frac{\alpha}{2})}{\Gamma(2+\alpha)} \end{aligned} \tag{2.17}$$

All the nonlinear viscous dampers are assumed to have the same value of α to simplify the derivation. According to equations (2.11) and (2.13) , the formula of ξ_d can be written as equation (2.18), where Γ is the gamma function.

$$\xi_d = \frac{T^{2-\alpha} \sum_{i=1}^{N_F} C_d (f_i \phi_{d,i})^{\alpha+1}}{(2\pi)^{3-\alpha} \sum_{i=1}^{N_F} m_i \phi_i^2} \cdot \sum_{i=1}^{N_F} \frac{\Gamma^2 (1 + \frac{\alpha}{2})}{\Gamma(2+\alpha)} \tag{2.18}$$

C_d of the nonlinear damper device at each floor can be derived from equation (2.18) as:

$$C_d = \frac{(2\pi)^{3-\alpha}\xi_d \sum_{i=1}^{N_F} m_i \phi_i^2}{T^{2-\alpha}\sum_{i=1}^{N_F}(f_i \phi_{d,i})^{1+\alpha}} \cdot \sum_{i=1}^{N_F} \frac{\Gamma(2+\alpha)}{\Gamma^2(1+\frac{\alpha}{2})} \tag{2.19}$$

As known, the seismic capacity of each story of the structure is quite different. It is not an optimum and cost-effective approach that assumes all dampers have identical design properties. In order to find the optimal design properties and the placement of dampers, Constantinou and Tadjbakhsh (1983) claimed to place the dampers in the first story of a building by the parametric studies. The genetic algorithm has been proposed to find the optimal properties and location of dampers by Singh and Moreschi (2002).

Moreover, the cost of damper devices is proportional to its peak damper force. It is critical to find a cost-effective design that also maintains the seismic performance of the structure. This trade-off problem brings into the optimization problem to find a cost-effective design. In this dissertation, a performance-based optimization framework of structural design will be presented to seek the optimal design properties of the dampers.

2.2. Multi-Objective Optimization Method

2.2.1 Multi-Objective Optimization Methodology

In the context of performance-based structural design, multi-objective optimization problems arise when more than one objective needs to be optimized, each in a conflicting manner. As described above, the seismic performance of a structure and the cost of the damper are always acting as the conflicting objectives. In multi-objective optimization design, the conflicting objectives can be optimized simultaneously under given constraints.

Generally, the multi-objective optimization problem can be expressed as follows (Kuczera 1997; Madsen 2003; Madsen et al. 2002):

$$\begin{aligned} &\text{Minimize}: Y(x) = [f_1(x), f_2(x) \ldots f_n(x)],\ x \in \theta \\ &\text{Subject}: h(x) \le 0 \end{aligned} \tag{2.20}$$

where f represents an individual objective function, n is the number of objective functions, x is the set of design variable within a feasible input parameter space θ, and h represents the constraining function.

Multi-objective optimization problem results in a set of compromising solutions, which represents the trade-off between at least two conflicting objectives (Aittokoski and Miettinen 2008; Liu and Sun 2010; Veerappa and Letier 2011). The Pareto front is formed by the optimal solutions for which improving one objective is not possible without degrading the other(s) (Confesor and Whittaker 2007; Zitzler 1999). Therefore, obtaining a single optimal solution becomes possible when objectives do not conflict, thus obviating the need for multi-objective optimization (Deb 2001).

2.2.2 The Non-Dominated Sorting Genetic Algorithm II (NSGA-II)

NSGA-II is one of the evolutionary algorithms to solve the multi-objective optimization problem. The basic operators of NSGA-II are selection, recombination, and mutation to populate a new generation until the solution reaches an optimum state or satisfies the stopping criteria (Deb et al. 2000). Users should predefine the number of generations, which is used to limit the number of iterations as the stopping criteria.

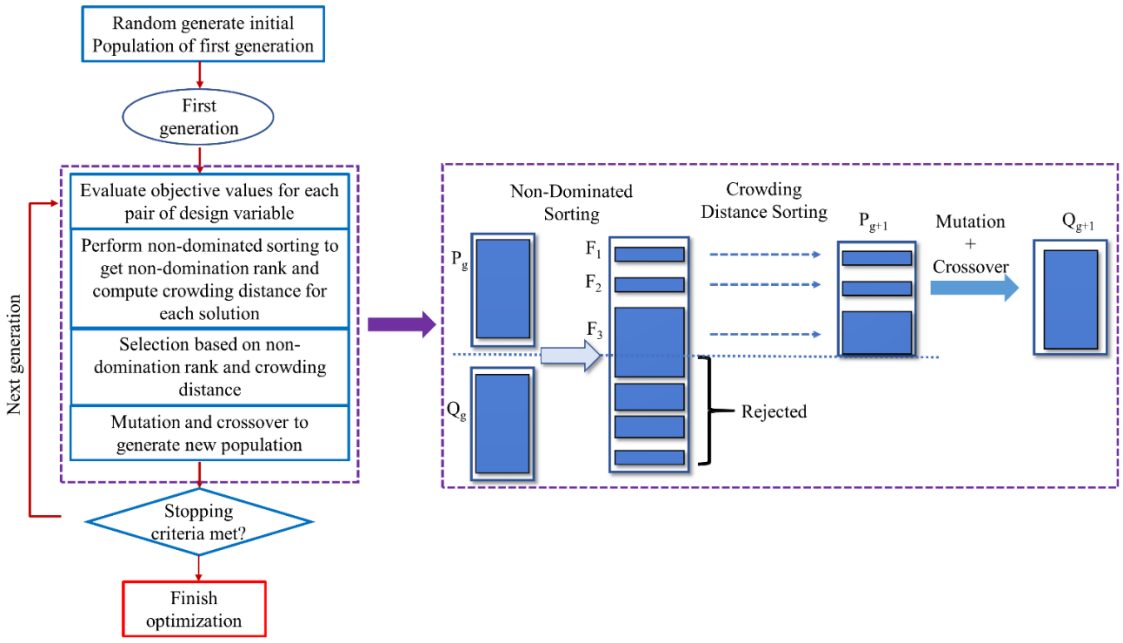

Figure 2-3 Main processes of NSGA-II approach

The main procedure of NSGA-II is shown in Figure 2-3. Initially, a parent population of input design variables, P_g is randomly created as the size of N. The 'population' represents a group of paired input design variables. Then, a child population, Q_g of size N is created from the parent population by using the general genetic operators such as mutation operators. A combined population $R_g = P_g \cup Q_g$ is then formed as the size of $2N$. The following steps are repeatedly used in every generation, after creating the initial combined population. The entire combined population R_g needs to be evaluated by the objective functions. The obtained values of the objective functions are sorted into different ranks based on the non-dominated sorting procedure in ascending order of dominance.

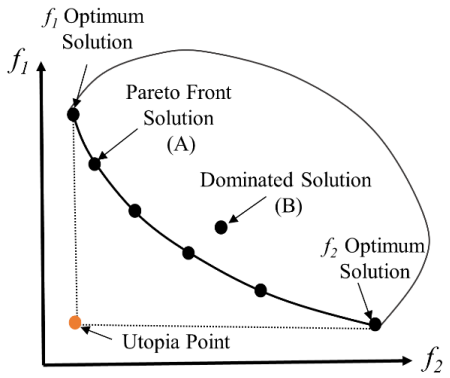

Figure 2-4 Domination relation between Pareto Front and dominated solution

The non-dominated sorting procedure relies on the domination relation. For the two objectives case, f_1 versus f_2 is presented to describe the domination relation, as shown in Figure 2-4. The solution (A) dominates the solution (B) as long as solution A is better than solution B in at least one objective (Mishra and Harit 2010). If no solution dominates the other one, they collectively form the Pareto front and transfer to become the new parent population, P_{g+1}, so that the elitism is ensured.

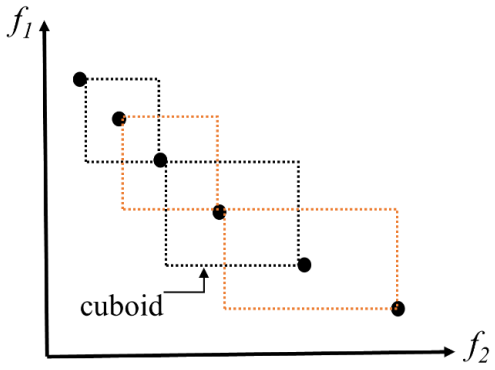

Figure 2-5 Illustration of the crowding distance computation

The new parent population, P_{g+1} is formed by adding the solutions from the first rank till reaching the size of N. The solution in the last rank will be selected by comparing the values of crowding distances, as shown in Figure 2-5. For each solution, the crowding

distance value is calculated by adding the average length of its two neighboring solutions in each objective function. The solution locates in the less crowded region is selected as the new parent population. The boundary solutions are assumed to have infinite crowing distance values so that they are always selected. The population P_{g+1} will produce a new child population, $Q_{g+1,}$ through mutation and crossover operators. This iterative procedure will continue until the predefined stopping criteria are met.

In the context of NSGA-II, the Pareto front consists of a set of optimal non-dominated solutions. For the Pareto front shown in Figure 2-4, one extreme point represents the parameter set generating the f_1 optimal solution while the other extreme point represents the parameter set producing the f_2 optimal solution. The shape of the Pareto front visually displays the level of compromise needed from one objective to improve the other. The tendency of this compromise decreases as the solutions approach the extreme points of the Pareto front. In this dissertation, the NSGA-II based multi-objective optimization method is applied in the proposed performance-based optimization framework for structural design.

CHAPTER III
DAMPING COEFFICIENT DISTRIBUTION OF ENERGY DISSIPATION SYSTEM APPLIED TO THE 3D NUMERICAL MODEL OF BUILDING

3.1. Introduction

Mitigating the impact of seismic loadings on a structure is one of the critical considerations in structural design. During the past decades, researchers and structural engineers have been persistently exploring the techniques of improving the performance of structures against earthquake hazards. One outcome of the previous research is the incorporation of structural control systems into the modern structural seismic design. The passive control system is one of the structural control systems that is used to decrease structural response against dynamic loads, such as earthquakes and intense winds (Ou and Li 2009). It acts passively without requiring any external power supply (Torunbalci 2004). The passive control systems typically include the tuned mass damping system, the seismic isolation system, and the energy dissipation system (Buckle 2000). Among them, the energy dissipation system which is incorporated into structural frames has significantly reduced wind-induced and seismic-induced structural responses. The energy dissipation system has been applied to various types of structures such as office, retail, hotel, and hospital buildings (Gonzalez et al. 2013; Guo et al. 2014; Kumar et al. 2016; Miyamoto et al. 2007; Sorace and Terenzi 2009).

Fluid viscous damper (FVD) is a kind of velocity-dependent passive energy dissipation system (Constantinou et al. 1998). The FVD has been incorporated in the structural design because of its applicability to both new and retrofit constructions (Soong

and Dargush 1997). Other appealing features of FVD include quick installation, negligible mass, and easy maintenance over its lifespan. Existing studies of FVD have mainly focused on the experimental testing and analytical/numerical modeling of its seismic performance. For example, Kasai et al. (2010) conducted the shaking table experiment to test the seismic performance of FVD, and Wong (2011) studied the nonlinear time history structural responses of using the linear FVD. In Kasai et al. (2010), one full-scale 5-story steel building with dampers was tested using a large-scale shake table, E-Defense. This building was repeatedly tested with four types of damper, i.e., steel, oil, viscous, and viscoelastic dampers. The researchers concluded that the building with viscous and viscoelastic dampers have better seismic performance than the building with other types of dampers.

Experimental testing is typically time-consuming and costly. As a supplement to experimental studies, a validated numerical model can be used to evaluate the seismic performance of various types of dampers and to assist the selection of optimal damper properties and placements (Sirois and Francesco 2015). In this study, the seismic performance of a three-dimensional (3D) numerical structure model will be simulated by the Open System for earthquake engineering simulation (OpenSees) software.

The damping force of a FVD is defined as its capability to dissipate seismic energy and can be characterized by its damping coefficient. The damping force of a FVD depends on the properties of the viscous fluid and the piston head orifice. Many studies have concerned about the damper placement and its distribution corresponding to different building heights. Wu et al. (1997) used the transfer function matrix method and concluded

that the optimal location of viscoelastic damper is the place with the maximum relative displacement in the structure. The same conclusion was drawn by Takewaki (1997) and Shukla and Datta (1999).

Moreover, the latest damping coefficient distribution methods can be generally divided into iterative and non-iterative methods. The sequential search algorithm (SSA) is one of the pioneering damping coefficient distribution methods, first proposed by Zhang and Soong (1992). It acts as an iterative process by adding the supplemental damper device to the location with the maximum structural response in sequence. This step is repeated until reaching the predefined value of the damping coefficient.

Examples of the non-iterative method include the uniform distribution method (UD), the inter-story drift proportional distribution method (IDPD), the story shear strain energy distribution method (SSSED), and the effective story shear strain energy distribution method (ESSSED). The ESSSED only distributes the damping coefficient to the "efficient stories", which have the shear strain energy more significant than the average story shear strain energy (Del Gobbo et al. 2018; Hwang et al. 2013). The formulas of these non-iteration methods were derived based on the shear building assumption and only considered the first mode of vibration. The effectiveness of these damping coefficient distribution methods was estimated by the two-dimensional numerical study (Landi et al. 2015). However, the following problems are not specified when the existing damping coefficient distribution methods need to be applied to the 3D numerical models: (1) how to distribute the damping coefficients in two principle horizontal directions of the structure;

(2) how to consider the impact of different vibration modes; (3) how to select the mode shapes and periods.

This chapter will extend and apply the conventional non-iterative damping coefficient distribution methods (UD, IDPD, SSSED, and ESSSED) to the three-dimensional (3D) numerical models that can solve the problems as mentioned above. A series of 3D numerical simulations are conducted to evaluate the effectiveness of these damping coefficient distribution methods. Because the distribution of damping coefficient is constrained by the achieved damping ratio, two levels of the added damping ratio: 20% and 30% are selected to compare the effectiveness of those damping coefficient distribution methods.

This remainder of this chapter is organized as following: Section 3.2 provides the background of the fluid viscous damper; Section 3.3 describes the application of damping coefficient distribution methods for 3D models; Section 3.4 describes the prototype building design and its numerical model; Section 3.5 evaluates the seismic behavior of the four-story steel frame by applying different damping distribution methods; Section 3.6 provides a summary of this study.

3.2. Model of the Fluid Viscous Damper

In this section, we briefly describe the model of the fluid viscous damper (FVD), and the design formulations for the supplemental linear viscous damper to the structure. FVD is a velocity-dependent energy-dissipation device that consists of a cylinder filled with silicone fluid, a stainless-steel piston, and a seal retainer, as shown in Figure 3-1 (a)

(Miyamoto et al. 2010). During an earthquake, the movement of the piston head causes the pressure difference across the piston head to generate the resistive force in the opposite direction of the input motion (Narkhede and Sinha 2012).

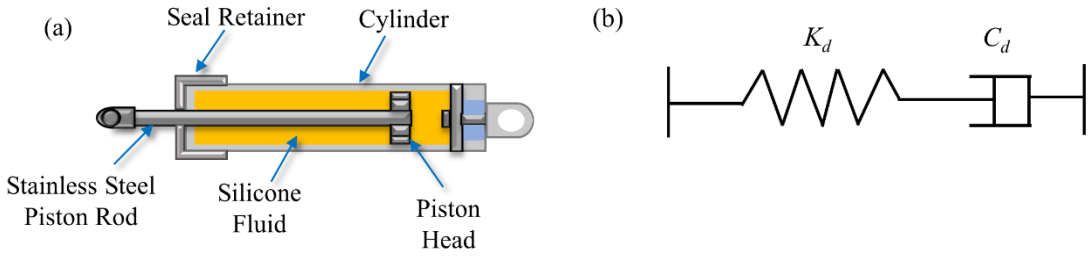

Figure 3-1 (a) Schematic drawing and major components of the fluid viscous damper; (b) Maxwell model.

The mechanical behavior of FVD can be described by the Maxwell model, which is composed of a linear spring and a nonlinear dashpot connected in series, as shown in Figure 3-1 (b). The stiffness of the linear spring, K_d, expresses the combined effect of supporting brace and the inner damper portion. The force-velocity relationship of the nonlinear dashpot can be expressed using a fractional power law as:

$$F_d = C_d \operatorname{sgn}(v)|v|^{\alpha} \tag{3.1}$$

where C_d is the supplemental damping coefficient, sgn is the signum function, v is the relative velocity between the ends of the damper, and α is the velocity exponent of the damper with a typical range 0.3 to 1.95 (Liu 2010).

The structure with a FVD is considered as a dual system. The total effective damping ratio, ξ_e, of the system can be expressed as:

$$\xi_e = \xi_i + \xi_d \tag{3.2}$$

where ξ_i is the inherent damping ratio of the structure, which is usually assumed to be 5%. ξ_d is the damper's damping ratio. Corresponding to the n-th vibration mode, the damper's damping ratio, $\xi_{d,n}$, is given as equation (3.3). This equation was derived based on the shear building assumption and has been adopted in FEMA 356 and ASCE 41-17.

$$\xi_{d,n} = \frac{T_n \sum_{i=1}^{N_F} C_{d,i} (f_i \phi_{d,in})^2}{4\pi \sum_{i=1}^{N_F} m_i \phi_{in}^{\ 2}} \tag{3.3}$$

where $C_{d,i}$ represents the damping coefficient of the damper at the i-th story, N_F is the total number of stories, m_i represents the mass of the i-th floor, ϕ_{in} and $\phi_{d,in}$ are the n-th mode horizontal and the relative horizontal displacement of the i-th story, T_n is the n-th mode period of the structure, f_i is the scale factor that depends on the installation plan of the damper. For a diagonal-brace damper, f_i equals cos(θ).

As specified in FEMA 356 and ASCE 41-17 (FEMA-356 2000; ASCE 41-17 2017), for each principal horizontal direction, the ξ_d should be less than 30% of the critical damping in the fundamental mode of the rehabilitated building. As described in equation (3.3) that there exist unlimited combinations of the $C_{d,i}$ to achieve the same amount of $\xi_{d,n}$ of the structure with known m_i, f_i, ϕ_{in}, $\phi_{d,in}$, and T_n.

In order to alleviate the problem of the infinite number of selection of $C_{d,i}$ under the constraint of a prescribed ξ_d, the damping coefficient distribution methods were

proposed to determine the $C_{d,i}$ for each story. In the conventional structural design, the simplified UD method intends to distribute the identical damping coefficient to each story (Hwang et al. 2013). The IDPD method suggests distributing the damping coefficient proportional to the inter-story drift of the structure (Landi et al. 2015). For a more thorough consideration, Hwang et al. (Hwang et al. 2013) proposed the SSSED method, which distributes the damping coefficient proportional to the story shear strain energy along with the building height. They also proposed the ESSSED method, which more efficiently distributes the damping coefficient to the stories with higher story shear strain energy than the average story shear strain energy. All these existing damping coefficient distribution methods were proposed based on the first vibration mode of the structure and applied to the two-dimensional numerical model. However, these existing methods have not specified how to apply their methods to the 3D numerical models and how to select the ϕ_{in}, $\phi_{d,in}$, and T_n for higher vibration modes. In this case, an extension of the existing damping coefficient distribution methods to the 3D models is presented in the following section.

3.3. Damping Coefficient Distribution Methods

On the basis of the existing methods, this section will discuss in detail how to apply these methods in the 3D models. The existing damping coefficient distribution methods will be extended and applied to the two principal horizontal directions of the numerical model. The modal analysis of the 3D numerical model is executed first. The ϕ_{in} and $\phi_{d,in}$ are selected based on the primary mode of each principal horizontal direction. Then, the corresponding mode periods, T_n are determined to obtain the damping coefficient of each horizontal direction.

3.3.1. Uniform Distribution (UD)

The simplified UD method assumes the damping coefficient of each story is identical. Recalling equation (3.3), the damping coefficient of each story can be calculated as:

$$C_d = \frac{4\pi\xi_{d,n}\sum_{i=1}^{N_F} m_i\phi_{in}{}^2}{T_n\sum_{i=1}^{N_F}(f_i\phi_{d,in})^2} \tag{3.4}$$

In order to illustrate the distribution of the damping coefficient in a 3D model, the model is assumed to be composed of two horizontal directions: *X* and *Z*, and one vertical direction: *Y*. The damping coefficients are assumed to be independently distributed in two horizontal directions. The equation (3.4) is extended into two directions: X and Z, as:

$$C_{d,X} = \frac{4\pi\xi_d\sum_{i=1}^{N_F} m_i\phi_{i,X}{}^2}{T_X\sum_{i=1}^{N_F}(f_i\phi_{d,i,X})^2} \tag{3.5}$$

$$C_{d,Z} = \frac{4\pi\xi_d\sum_{i=1}^{N_F} m_i\phi_{i,Z}{}^2}{T_Z\sum_{i=1}^{N_F}(f_i\phi_{d,i,Z})^2} \tag{3.6}$$

where $C_{d,X}$ represents the distributed damping coefficient in the *X*-direction, $\phi_{i,X}$ represents the horizontal displacement of the *i*-th floor in the *X*-direction. The horizontal displacement is determined by the primary mode shape in the *X*-direction, $\phi_{d,i,X}$ represents the relative horizontal displacement of the *i*-th floor in the *X*-direction, T_X is the corresponding period

of the primary vibration mode in the *X*-direction. The same symbol rule is applied to the *Z*-direction through changing subscript 'X' to 'Z'. It is noted that the primary vibration mode of each horizontal direction is determined based on the 3D numerical modal analysis. The fundamental mode will be considered if the model has a coupled effect of both horizontal directions.

3.3.2. Inter-Story Drift Proportional Distribution (IDPD)

As a more cost-efficient and pertinence method, IDPD is implemented to distribute the damping coefficient according to the distribution of inter-story drifts within the structure. The damping coefficient of the *I*-th story corresponding to the *n*-th mode can be expressed as:

$$C_{d,I} = q\phi_{d,In} \tag{3.7}$$

where q is a proportionality constant; $\phi_{d,In}$ is the inter-story drift of the I-th floor. The total damping coefficient of the system is equal to the summation of the damping coefficient of each story:

$$\sum_{i=1}^{N_F} C_{d,i} = q\sum_{i=1}^{N_F} \phi_{d,in} \tag{3.8}$$

Substituting equation (3.7) into equation (3.8):

$$C_{d,I} = \frac{\phi_{d,In}}{\sum_{i=1}^{N_F} \phi_{d,in}} \cdot \sum_{i=1}^{N_F} C_{d,i} \tag{3.9}$$

Substituting equation (3.9) into equation (3.3).

$$\xi_{d,n} = \frac{T_n \sum_{i=1}^{N_F} [\phi_{d,In} \sum_{i=1}^{N_F} C_{d,i} (f_i \phi_{d,in})^2]}{4\pi (\sum_{i=1}^{N_F} \phi_{d,in})(\sum_{i=1}^{N_F} m_i {\phi_{in}}^2)} \tag{3.10}$$

The total damping coefficient of the system can be calculated as:

$$\sum_{i=1}^{N_F} C_{d,i} = \frac{4\pi \xi_{d,n} (\sum_{i=1}^{N_F} \phi_{d,in})(\sum_{i=1}^{N_F} m_i {\phi_{in}}^2)}{T_n \sum_{i=1}^{N_F} [\phi_{d,in} (f_i \phi_{d,in})^2]} \tag{3.11}$$

Substituting equation (3.11) into equation (3.9). The damping coefficient of each story can be expressed as:

$$C_{d,I} = \frac{4\pi \xi_{d,n} \phi_{d,In} (\sum_{i=1}^{N_F} m_i {\phi_{in}}^2)}{T_n \sum_{i=1}^{N_F} [\phi_{d,in} (f_i \phi_{d,in})^2]} \tag{3.12}$$

Extending the equation (3.12) to consider the multiple directions in the 3D model:

$$C_{d,I,X} = \frac{4\pi \xi_d \phi_{d,I,X} (\sum_{i=1}^{N_F} m_i {\phi_{i,X}}^2)}{T_X \sum_{i=1}^{N_F} [\phi_{d,i,X} (f_i \phi_{d,i,X})^2]} \tag{3.13}$$

$$C_{d,I,Z} = \frac{4\pi \xi_d \phi_{d,I,Z} (\sum_{i=1}^{N_F} m_i {\phi_{i,Z}}^2)}{T_Z \sum_{i=1}^{N_F} [\phi_{d,i,Z} (f_i \phi_{d,i,Z})^2]} \tag{3.14}$$

where $C_{d,I,X}$ and $C_{d,I,z}$ represent the distributed damping coefficient of the I-th floor in the X-direction and Z-direction, respectively.

3.3.3. Story Shear Strain Energy Distribution (SSSED)

The SSSED (Hwang et al. 2013) distributes the damping coefficient along with the building height by considering their story shear strain energy. The story shear force is proportional to the parameter S_I, which is defined as follows:

$$S_I = \sum_{i=I}^{N_F} m_i \phi_i \tag{3.15}$$

The story shear strain energy is defined as the product of the shear force and the inter-story drift, which proportional to the $S_I \phi_{d,I}$. Following the similar derivation process from equation (3.7) to equation (3.12), the damping coefficient of the I-th story corresponding to the n-th vibration mode can be expressed as:

$$C_{d,I} = \frac{4\pi \xi_{d,n} S_{In} \phi_{d,In} (\sum_{i=1}^{N_F} m_i \phi_{in}^{\ 2})}{T_n \sum_{i=1}^{N_F} [S_{in} \phi_{d,in} (f_i \phi_{d,in})^2]} \tag{3.16}$$

Extending the equation (3.16) to consider the multiple directions in the 3D model:

$$C_{d,I,X} = \frac{4\pi \xi_d S_{I,X} \phi_{d,I,X} (\sum_{i=1}^{N_F} m_i \phi_{i,X}^{\ 2})}{T_X \sum_{i=1}^{N_F} [S_{i,X} \phi_{d,i,X} (f_i \phi_{d,i,X})^2]} \tag{3.17}$$

$$C_{d,I,Z} = \frac{4\pi\xi_d S_{I,Z}\phi_{d,I,Z}(\sum_{i=1}^{N_F} m_i {\phi_{i,Z}}^2)}{T_Z \sum_{i=1}^{N_F}[S_{i,Z}\phi_{d,i,Z}(f_i\phi_{d,i,Z})^2]} \tag{3.18}$$

3.3.4. Efficient Story Shear Strain Energy Distribution (ESSSED)

The ESSSED method is a modification of the SSSED method. Two steps are considered in the application of ESSSED method: (a) determine the 'efficient stories' which have larger shear strain energy than the average story shear strain energy:

$$S_{In}\phi_{d,In} > \frac{\sum_{i=1}^{N_F} S_{in}\phi_{d,in}}{N_F} \tag{3.19}$$

(b) distribute the damping coefficients to the 'efficient stories':

$$C_{d,I} = \frac{4\pi\xi_{d,n} S_{In}\phi_{d,In}(\sum_{i=1}^{N_F} m_i {\phi_{in}}^2)}{T_n \sum_{i=1}^{k}[S_{in}\phi_{d,in}(f_i\phi_{d,in})^2]} \tag{3.20}$$

where k represents the number of stories that have larger shear strain energy than the average.

The application of the ESSSED method to the 3D model also includes two steps: the determination and distribution steps. These two steps are applied to each horizontal direction separately. For the *X*-direction, the distributed damping coefficient is calculated as the following steps:

$$S_{I,X}\phi_{d,I,X} > \frac{\sum_{i=1}^{N_F} S_{i,X}\phi_{d,i,X}}{N_F} \tag{3.21}$$

$$C_{d,I,X} = \frac{4\pi\xi_d S_{I,X}\phi_{d,I,X}(\sum_{i=1}^{N_F} m_i {\phi_{i,X}}^2)}{T_X \sum_{i=1}^{k}[S_{i,X}\phi_{d,i,X}(f_i\phi_{d,i,X})^2]} \tag{3.22}$$

For the *Z*-direction, the distributed damping coefficient is calculated as:

$$S_{I,Z}\phi_{d,I,Z} > \frac{\sum_{i=1}^{N_F} S_{i,Z}\phi_{d,i,Z}}{N_F} \tag{3.23}$$

$$C_{d,I,Z} = \frac{4\pi\xi_d S_{I,Z}\phi_{d,I,Z}(\sum_{i=1}^{N_F} m_i {\phi_{i,Z}}^2)}{T_Z \sum_{i=1}^{k}[S_{i,Z}\phi_{d,i,Z}(f_i\phi_{d,i,Z})^2]} \tag{3.24}$$

3.4. Office Building Design and OpenSees Numerical Model

3.4.1. Office Building- Steel Moment-Resisting Frame Design

The seismic performance of a four-story steel moment-resisting frame is considered as the comparison metric to evaluate the effectiveness of the four different damping distribution methods. The design of the four-story steel moment frame is adopted from the Lignos (2008) study. This steel frame was designed in accordance with IBC-2003, AISC-2002, and AISC-2005 design codes. The steel frame is assumed to be an office building with a moveable penthouse. It is assumed to built on type D soil site located in Los Angeles and is classified as risk category II.

A detailed plan view of the office building is shown in Figure 3-2. For a typical floor, all effective seismically dead weights are summarized in Table 3-1. The designed seismic weights of each story are summarized in Table 3-2. The first three modal periods are 1.26 sec, 1.04 sec, and 0.65 sec based on modal analysis of the 3D numerical model. The maximum considered earthquake (MCE) spectral response acceleration at short periods (S_{MS}) and 1-sec period (S_{M1}) and design spectral response acceleration at short periods (S_{DS}) and 1-sec period (S_{D1}) are listed in Table 3-3.

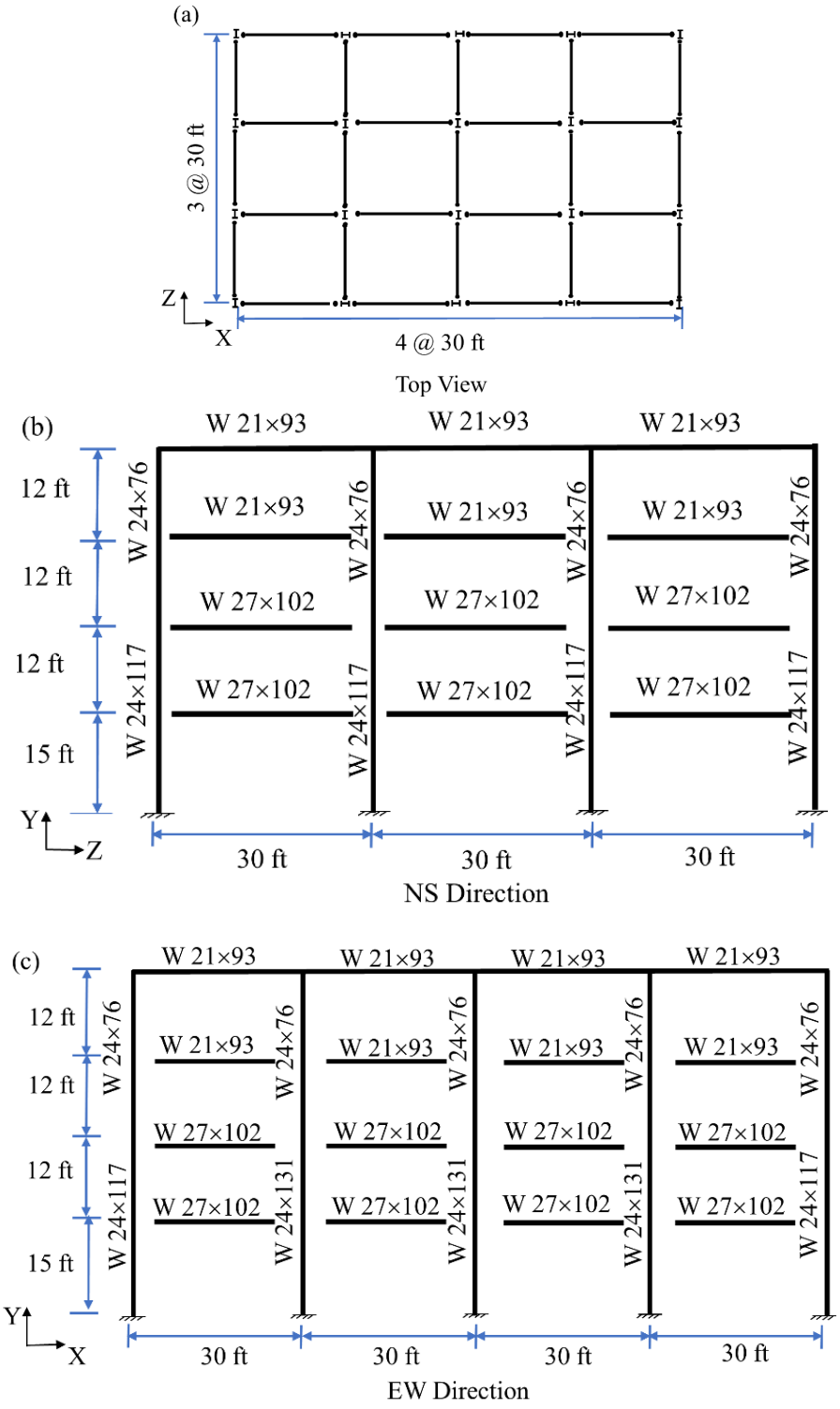

Figure 3-2 Plan view of the office building

Table 3-1 Details of seismically effective dead weight for a typical floor

Load Description	Weight (kips)
4.25-inch concrete slab	518
18 ga. Steel deck	54
Interior partitions	108
Roofing systems	162
Exterior cladding	101
Floor beams	63
Girders (average)	30
Columns(average)	48
others	130

Table 3-2 Design seismic weight for each floor

Floor	Design Seismic Weight (kips)
Second floor	1070
Third floor	1050
Fourth floor	1050
Roof	1200

Table 3-3 Spectral response acceleration values adjusted for site class

Hazard Level	Short-Period (0.2sec) Sa	1-Sec Period Sa
10%/50yr (DBE)	S_{DS}=1.0 g	S_{D1}=0.6 g
2%/50yr (MCE)	S_{MS}=1.5 g	S_{M1}=0.9 g

3.4.2. OpenSees Numerical Model

In this study, the office building is modeled as a 3D numerical model in the OpenSees software, as shown in Figure 3-3. The 3D numerical model can consider the influence of seismic waves in multiple directions, which provides a more comprehensive and accurate seismic analysis result.

The inherent damping ratio of the frame is assumed to be 2%. All structure components are made of the A992 Grade 50 steel. The “non-linear beam-column” elements are used to model columns with Gauss-Lobatto integration and five integration points along with the element. All columns of the numerical model are assumed to be fixed at the bases.

The beams and girders are modeled using the 'elastic beam-column' element with Young's Modulus as 200 GPa.

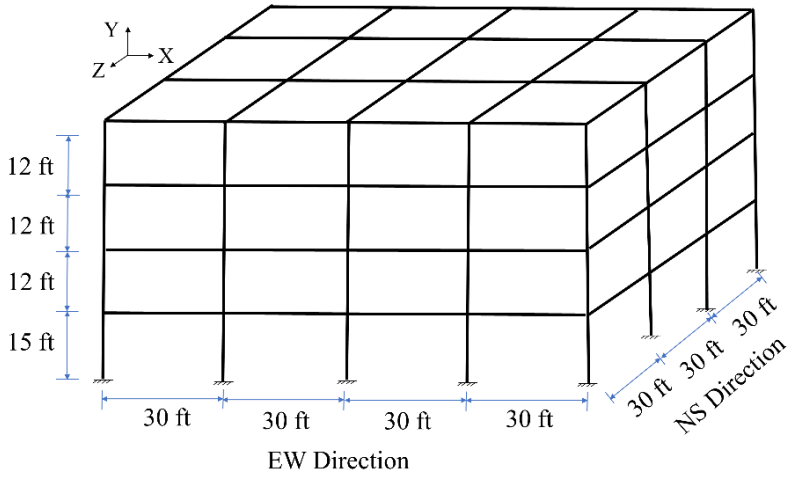

Figure 3-3 Three-dimensional OpenSees model of the steel frame

3.4.3. Validation of OpenSees Model

In order to verify the ability of the 3D numerical model to predict its seismic performance, the experimental verification is required for the beam and column properties and the scaled floor weight of the model. Hence, an OpenSees model of the 4-story steel frame is developed to validate against the experimental results in this section. Herein, only two-bay of the steel moment-resisting frame in the EW direction is represented. The reason for representing only the part of the building is the availability of the experimental result.

The experimental test was conducted by the shake table test of one 1:8 scale-down model. The 1:8 scale model of the 4-story steel frame was designed and tested by Lignos (2008) at the State University of New York at Buffalo. The shaking table experiments were conducted to predict the collapse capacity, to quantify the engineering demand parameters of story drifts, floor accelerations, and story forces and to evaluate the effects of the

connections of the beam and column on the collapse capacity of the steel frame. Due to the cost and the weight limitation of the shaking table, only the middle two-spans of the frame in the EW direction was designed for testing, as shown in Figure 3-4. The actual and target weights of each floor are listed in Table 3-4.

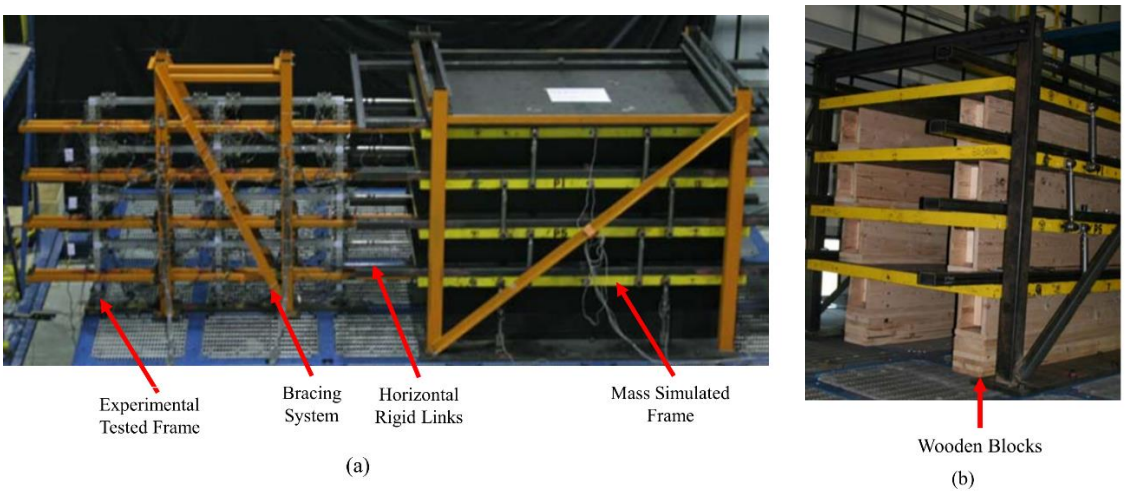

Figure 3-4 (a) experimentally tested frame; (b) installation of mass plates on the shaking table (modified from (Lignos 2008))

The test frame consists of elastic beams and columns. Plastic hinge elements connect all the beams and columns of the test frame. A mass simulator frame is used to simulate the P-Delta effect. The mass simulator frame is connected to the steel frame with rigid links at each floor level, as shown in Figure 3-4 (a). Two wooden blocks are placing on each floor on the plates of the mass simulator to protect the shaking table facility, as shown in Figure 3-4 (b). These blocks limit the maximum rotation of each floor of the test frame by 0.25 radians. A separate bracing system serves as the lateral support and safety mechanism for the shaking table facility. The maximum allowable drift of the roof floor relative to the ground is 26% as limited by the brace system.

Table 3-4 Actual and target floor weights of the test frame

Floor	Second Floor	Third Floor	Fourth Floor	Roof
Actual Weight (kips)	8.6	8.6	8.6	8.8
Target Weight (kips)	8.4	8.2	8.2	9.4

The seismic performance of the tested frame is evaluated under the Northridge 1994 Canoga Park ground motion. This ground motion is scaled to five different levels of seismic intensities to test the response of the structure from the elastic range to collapse. The unscaled time history of the 1994 Northridge record represents the design level earthquake, as shown in Figure 3-5. The frame is sequentially tested under the service level earthquake (SLE), design level earthquake (DLE), maximum considered earthquake (MCE), collapse level earthquake (CLE), and the final collapse level earthquake (CLEF). The scale factors of each seismic intensity level are listed in Table 3-5.

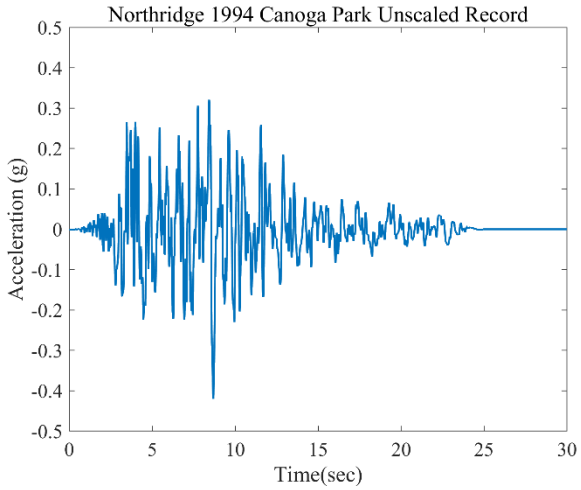

Figure 3-5 Acceleration time history of Northridge 1994 Canoga Park

Table 3-5 Scale factors of each seismic intensity level

Seismic Intensity	SLE	DLE	MCE	CLE	CLEF
Scale Factor	0.4	1.0	1.5	1.9	2.2

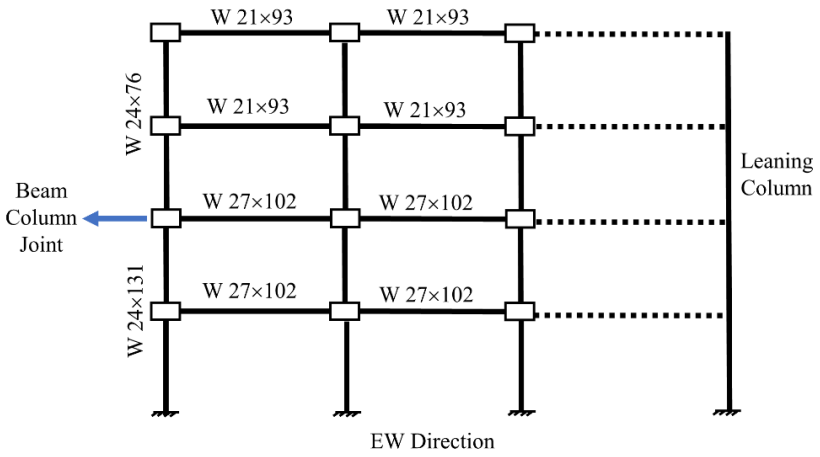

Figure 3-6 OpenSees model of the tested frame

In order to simulate the experimental frame more accurately, all beams and columns are modeled as elastic elements in the numerical model. A leaning column with gravity loads is linked to the frame to simulate the P-Delta effect, as shown in Figure 3-6. The IK connection model proposed by Lignos and Krawinkler (2010) is used to simulate the deteriorating strength and stiffness properties of all plastic hinge regions. The moment-rotation relationship of the IK model is illustrated in Figure 3-7. The effective yielding moment (M_y), capping moment (M_c), and residual moment (M_r) are characterized as the strength parameters. The post-yield strength ratio is defined as M_c/M_y. Moreover, the yield rotation (θ_y), pre-capping plastic rotation (θ_p), post-capping plastic rotation (θ_{pc}), and the ultimate plastic rotation capacity (θ_u) are characterized as the deformation parameters. The parameters of the modified IK model of each beam and column sections are listed in Table 3-6.

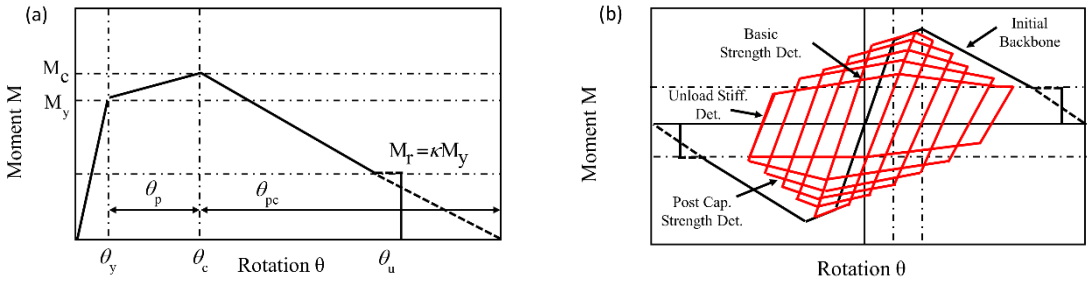

Figure 3-7 Modified IK model

Table 3-6 Parameters of IK models of the four-story numerical model

Section	M_c / M_y	κ	θ_p	θ_{pc}	$\Lambda = E_t / M_y$
W21x93	1.05	0.40	0.025	0.19	1.90
W24x76	1.05	0.40	0.025	0.35	1.50
W27x102	1.05	0.40	0.020	0.16	1.50
W24x131	1.05	0.40	0.025	0.30	1.50

The experimental results are used to validate the numerical model in two steps. In the first step, the deformation of the model is validated by comparing it with the simplified experimental incremental dynamic analysis (IDA) curve. The IDA curve is composed of the peak roof drift versus four levels of seismic intensities: SLE, DLE, MCE, and CLE levels, as shown in Figure 3-8. The result of the CLEF level does not include in the curve due to the early collapse of the numerical model. If the drift of the roof floor reaches the maximum allowable value (26%), the test frame is defined as collapsed.

In experiments, the recorded peak roof drift ratios of the tested frame approximately equal to 0.42%, 2.26%, 4.37%, and 10.80% for each seismic intensity level. The corresponding results of the numerical model are 0.46%, 2.35%, 4.98%, and 16.20%. The differences between the simulation and the experimental arise due to the collapse induced non-convergence of the model under the CLE level. The differences between the recorded peak roof drift ratios from numerical simulations and experimental tests are 0.04%, 0.09%,

and 0.6% under the SLE, DLE, and MCE levels. Generally, the simulation results are in good agreement with the experimental tests in the first validation step.

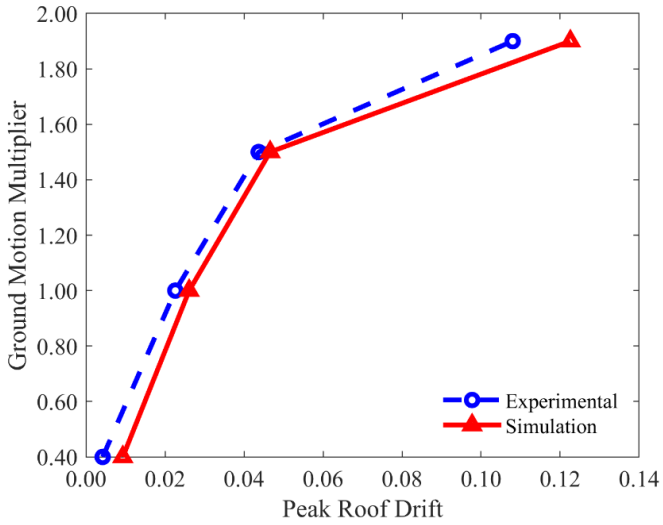

Figure 3-8 Peak roof drift under different ground motion intensities

In the second step, the displacement of each floor obtained from the numerical model is compared with the experimental results. The displacement of each story is normalized to the total height of the frame, as shown in Figure 3-9. The non-convergence of the model causes a relatively large difference under the CLE level. At the DLE level, the normalized displacement values of each floor from the experimental tests are 0.64%, 1.33%, 1.96%, and 2.35%. The recorded displacement values from the numerical simulation are 0.75%, 1.38%, 1.99%, and 2.61% which are almost coincided with the results of the experimental tests. At the SLE and MCE levels, the maximum differences of normalized story displacements between numerical simulation and experimental tests are close to 0.41% and 0.26%. Hence, it is concluded that the numerical model is capable of simulating engineering demand parameters for the experimental test of the structure.

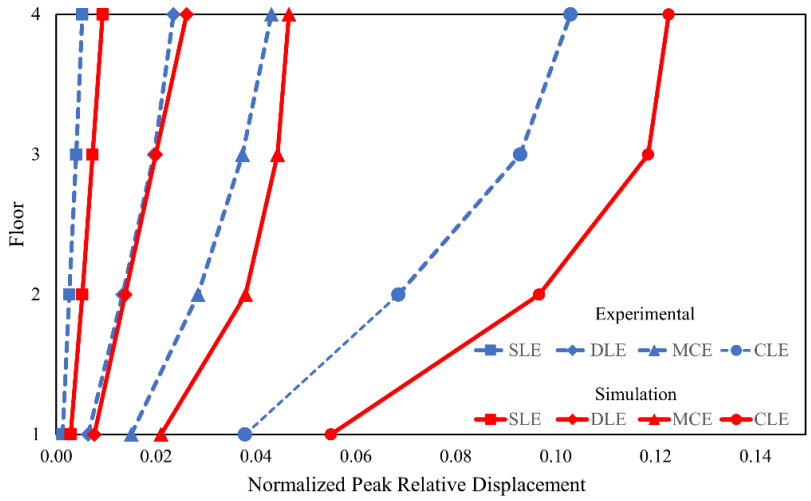

Figure 3-9 Peak displacement of each floor normalized to the total height of the frame

3.5. Numerical Analysis Results

In this section, the numerical model of the bare frame (steel frame without damping devices) is presented first as a benchmark model. Then, it shows the results of the numerical models with supplemental linear viscous dampers designed according to the four damping coefficient distribution methods: UD, IDPD, SSSED, and ESSSED.

3.5.1. Performance of Steel Frame without Damping Devices

In structural seismic design, the structural response is highly sensitive to the characteristics of the ground motion. A series of ground motions must be applied to allow statistical evaluation of record-to-record variability. Thus, the far-field record set of the FEMA-P695 PEER NGA database is used to account for the record-to-record variability in this case study. The far-field record set is a set of 22 biaxial ground motions, which recorded at sites located a distance ≥ 10 km from the fault rupture. The 22 biaxial ground motions are applied to the steel frame in two orthogonal directions. First, the first component of far-field ground motions is applied along the EW-direction of the numerical

model and the second component is applied along NS-direction. Then, the records are rotated by 90 degrees and applied to the numerical model again. Hence, a total of 44 biaxial ground motions is considered in this case study.

According to the requirements of ASCE 7-10, the 22 biaxial ground motions should be scaled to the MCE level to simulate the seismic performance of the structure under the collapse prevention level, as shown in Figure 3-10 (ASCE 07-10 2010). In the figure, the grey lines represent the scaled response spectrum for the MCE level, the blue line represents the design response spectrum (RS), the dashed red line represents the mean of the scaled Square-Root-of-Sum-of-Squares (SRSS) RS, and the solid red line represents scaled maximum SRSS RS.

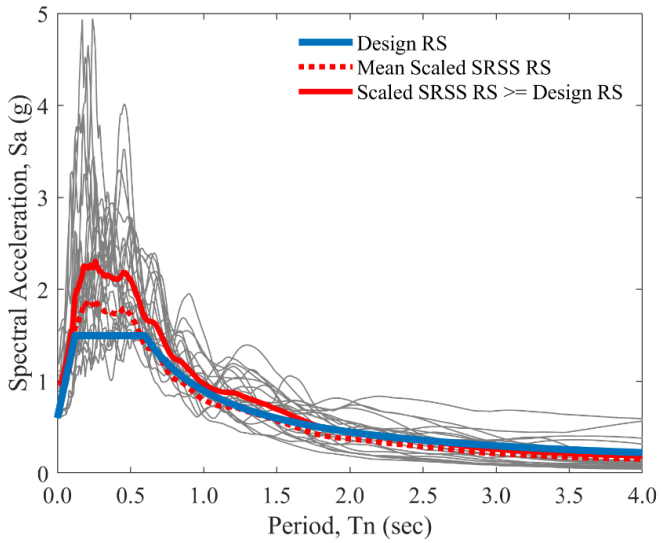

Figure 3-10 Acceleration response spectra for the far-field ground motions scaled to MCE level

The most accurate nonlinear dynamic analysis, nonlinear time history analysis is implemented to analyze the numerical model under the earthquake loading (Xiaoyun 2014). The maximum inter-story drift of each floor and the peak floor acceleration are

selected as the performance measures. The maximum inter-story drifts of each story in both EW and NS-directions are plotted in Figure 3-11 (a) and Figure 3-11 (b). Meanwhile, the peak floor accelerations in both EW and NS-directions are plotted in Figure 3-12 (a) and Figure 3-12 (b). The grey lines represent the maximum inter-story drift of each floor or the peak floor acceleration under the 44 biaxial ground motions. The blue and red lines represent the mean and median values of the inter-story drift ratio or the peak floor acceleration. Those median values will be used to compare the effectiveness of four damping coefficient distribution methods in the following section.

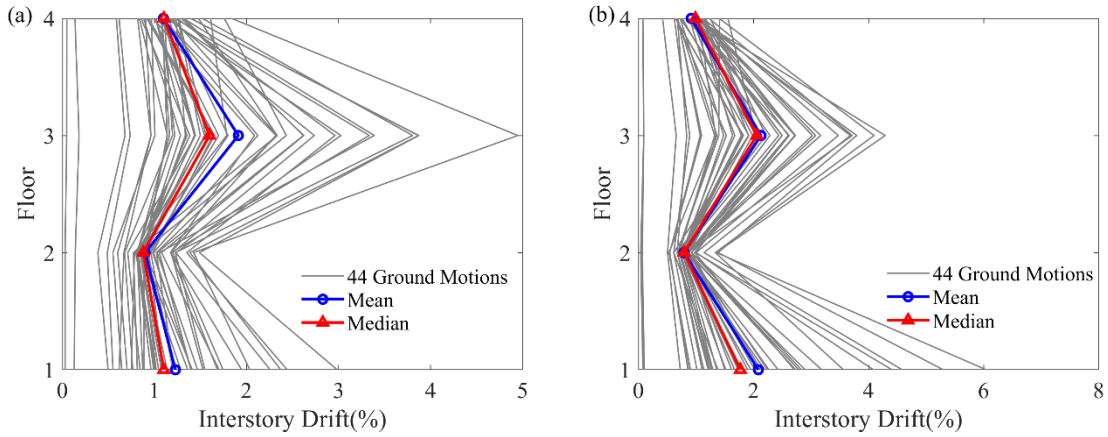

Figure 3-11 Maximum inter-story drift ratio of each floor in the (a) EW-direction; (b) NS-direction

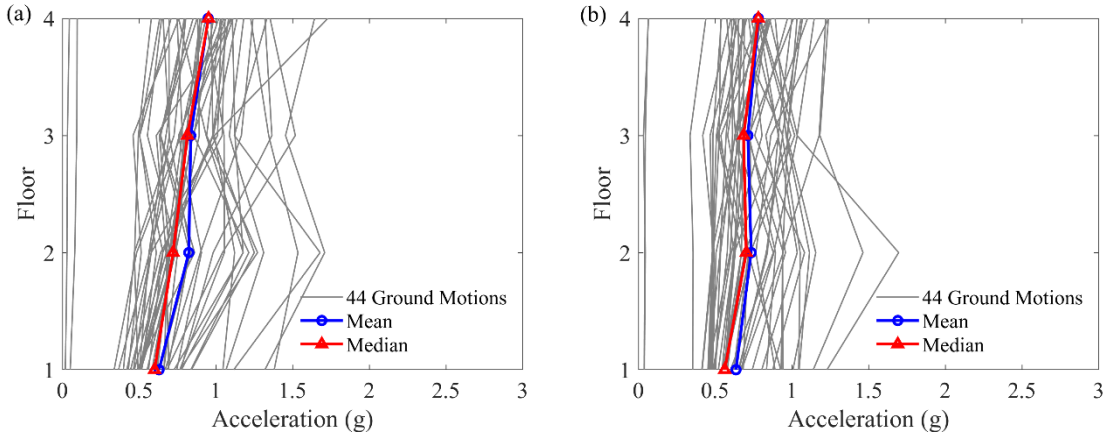

Figure 3-12 Peak floor acceleration of each floor in the (a) EW-direction; (b) NS-direction

As shown can be seen from Figure 3-11, the third floor is the relatively weak story in the EW direction, which has a maximum inter-story drift of 4.95%. While the 6.07% maximum inter-story drift occurs on the first floor in the NS direction. As specified in the FEMA 356 specification, the maximum inter-story drift of steel moment-resisting frame cannot exceed 5% under the collapse prevention level. Hence, the first floor of the NS direction needs to be increased its resistance capacity against the ground shaking in the retrofitted seismic design.

Similarly, the third story of the EW direction requires significant improvement of its resistance capacity against the ground shaking. Furthermore, as shown in Figure 3-12, the maximum peak floor acceleration is approximately 1.73g (roof floor) in the EW direction and 1.69g (second floor) in the NS direction. In order to improve the inter-story drift and the peak floor acceleration, the fluid viscous damper will be applied to the bare frame, as presented in the following section.

3.5.2. Comparison of Damping Coefficient Distribution Methods

In this section, the numerical modal analysis of the bare frame is presented first. Then, the distributed damping coefficients are calculated based on the obtained mode shapes and periods. The damping coefficients of each floor are determined by using the UD, IDPD, SSSED, and ESSSED methods in sequence. According to the obtained damping coefficients, the fluid viscous dampers are applied to the numerical models of the steel frame. The effectiveness of different damping coefficient distribution methods is evaluated by considering 44 biaxial ground motions.

To calculate the damping coefficients more accurately, the values of the mode shape and period are extracted from the 3D modal analysis in the OpenSees software. The first and second mode shapes of both EW and NS directions are listed in Table 3-7.

Table 3-7 Recorded mode shapes and modal effective mass based on 3D modal analysis

Floor	EW Direction		NS Direction	
	1st Mode	2nd Mode	1st Mode	2nd Mode
1	-3.44E-07	0.11	0.14	2.60E-04
2	3.76E-06	0.20	0.23	-5.93E-05
3	2.92E-06	0.33	0.33	1.73E-04
4	4.31E-06	0.42	0.40	1.68E-04
Modal Effective Mass (%)	0%	83.27%	89.04%	0%

The primary mode shape of the EW direction is the translation in the second mode. The primary mode shape of the NS direction is the translation in the first mode. Hence, the mode shapes and period of the second vibration mode are used to calculate the damping coefficient in the EW direction. Similarly, the calculation of damping coefficient in the NS direction is based on the first vibration mode. In order to compare the effectiveness of the damping coefficient methods with different achieved damping ratios, 20% and 30% of damper's damping ratios are considered in this case study. The 30% damping ratio in the

viscous dampers is selected as it corresponds to the upper bound specified in FEMA 356 and ASCE 41-17. The 20% damping ratio is frequently used for structures with supplemental viscous dampers (Banazadeh and Ghanbari 2017; Hwang et al. 2004) and is selected as a comparison to the 30% case.

Table 3-8 EW direction: damping coefficient of each floor (20% damping ratio)

Floor	UD (kip-sec/in)	IDPD (kip-sec/in)	SSSED (kip-sec/in)	ESSSED (kip-sec/in)
1	62.98	62.50	80.84	88.95
2	62.98	55.02	64.21	70.65
3	62.98	72.92	68.05	74.87
4	62.98	53.55	29.70	
Sum	251.91	243.99	242.80	234.47

Table 3-9 NS direction: damping coefficient of each floor (20% damping ratio)

Floor	UD (kip-sec/in)	IDPD (kip-sec/in)	SSSED (kip-sec/in)	ESSSED (kip-sec/in)
1	55.64	69.68	79.76	119.72
2	55.64	41.33	41.34	
3	55.64	49.70	38.49	
4	55.64	31.79	14.23	
Sum	222.56	192.49	173.81	119.72

Table 3-10 EW direction: damping coefficient of each floor (30% damping ratio)

Floor	UD (kip-sec/in)	IDPD (kip-sec/in)	SSSED (kip-sec/in)	ESSSED (kip-sec/in)
1	94.46	93.74	121.27	133.43
2	94.46	82.54	96.32	105.98
3	94.46	109.37	102.07	112.31
4	94.46	80.33	44.55	
Sum	377.84	365.98	364.21	351.72

Table 3-11 NS direction: damping coefficient of each floor (30% damping ratio)

Floor	UD (kip-sec/in)	IDPD (kip-sec/in)	SSSED (kip-sec/in)	ESSSED (kip-sec/in)
1	83.46	104.51	119.64	179.58
2	83.46	62.00	62.01	
3	83.46	74.55	57.73	
4	83.46	47.68	21.34	
Sum	333.84	288.74	260.72	179.58

The obtained damping coefficient of each floor in each direction are listed from Table 3-8 to Table 3-11. As illustrated in section 3.3.1, the UD assigns the identical damping coefficient to each floor. The IDPD assigns the damping coefficient proportional to the inter-story drift (see Section 3.3.2). Hence, IDPD assigns the highest damping coefficient of 72.92 kip-sec/in to the third floor in the EW direction and 69.68 kip-sec/in to the first floor in the NS direction for the model with a supplemental 20% damping ratio (see Table 3-8 and Table 3-9).

Moreover, the SSSED assigns the damping coefficient proportional to the story shear strain energy (see Section 3.3.3), e.g., the SSSED assigns the highest damping coefficient 80.84 kip-sec/in to the first floor, followed by the third floor with 68.05 kip-sec/in (see Table 3-8).

The ESSSED assigns the damping coefficient to the "efficient stories": the first, second, and third floor in the EW direction, and the first floor in the NS direction (see Section 3.3.4). For the NS direction, the first story has the highest damping coefficient, which compares to the IDPD and SSSED method (see Table 3-9 and Table 3-11). The same trends are observed for the model with a supplemental 30% damping ratio. For a more visualized comparison of the obtained damping coefficients, the damping coefficient of each floor is plotted in the bar charts, as shown in Figure 3-13 and Figure 3-14.

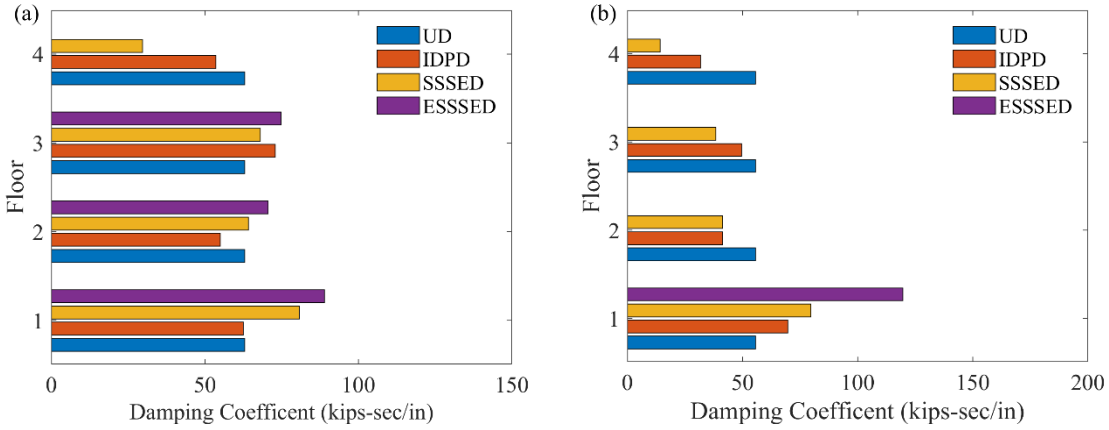

Figure 3-13 Damping coefficient of each floor with 20% damping ratio: (a) EW-direction; (b) NS-direction

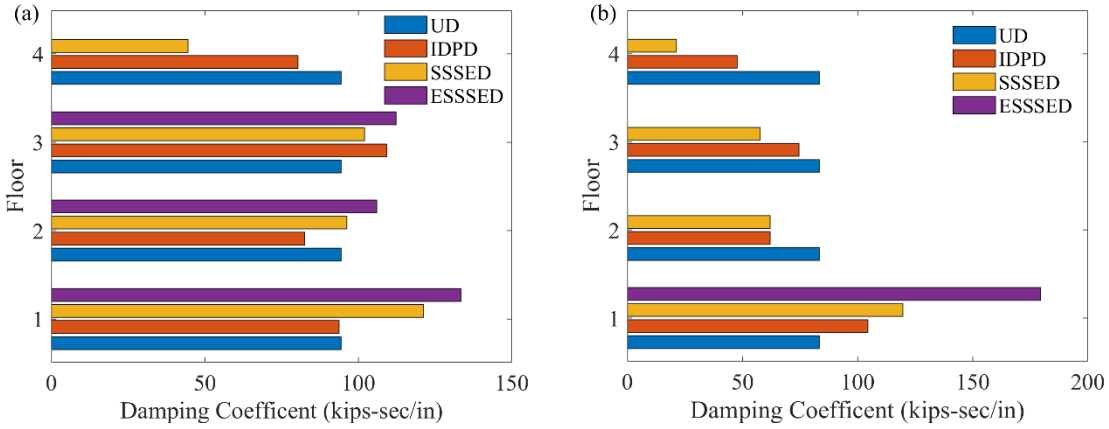

Figure 3-14 Damping coefficient of each floor with 30% damping ratio: (a) EW-direction; (b) NS-direction

The linear fluid viscous dampers are assigned in the 3D model corresponding to the obtained damping coefficients of each floor, as shown in Figure 3-15. The bold black line indicates the position of the dampers, as shown in Figure 3-15 (a). The same layout applies to the UD, IDPD, and SSSED methods, as shown in Figure 3-15 (b). The layout applies to the ESSSED method is shown in Figure 3-15 (c). If more than one damper is installed in one direction of the structure, the damping coefficient of each installed damper is equal to

the total assigned damping coefficient of this floor divided by the number of dampers. For instance, the distributed damping coefficient of the first floor in the EW direction is 94.46 kip-sec/in with a supplemental 30% damping ratio. The damping coefficient of each damper is 47.23 kip-sec/in if two dampers are installed in the first floor of the EW direction.

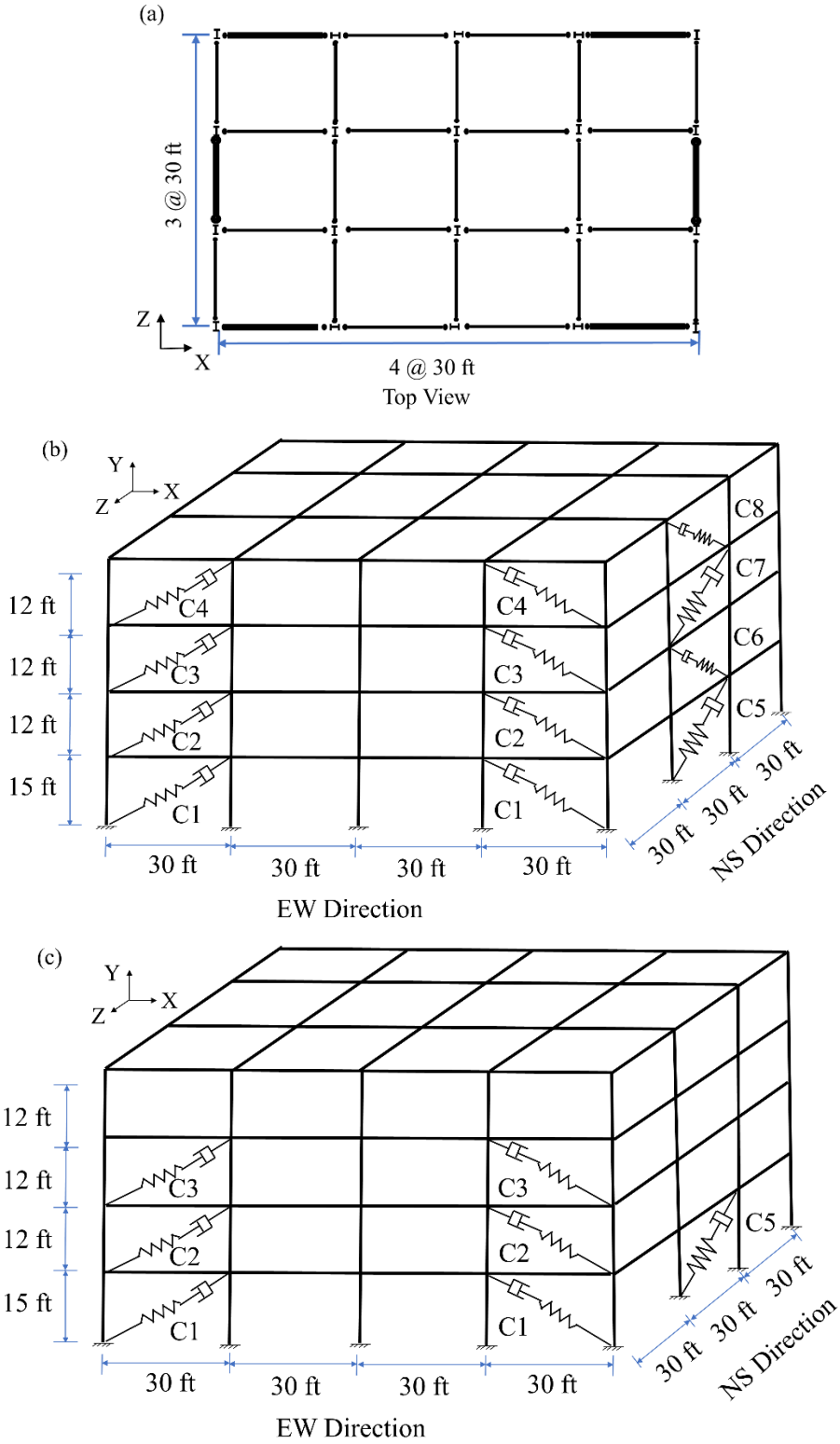

Figure 3-15 Layout of the steel frame with viscous dampers: (a) top view of the 3D model; (b) 3D model for the UD, IDPD and SSSED methods; (c) 3D model for the ESSSED method

In order to facilitate the comparison of simulation results, this section only presents the median values of peak inter-story drift and acceleration of each floor under the 44 biaxial ground motions. The simulation results for the model with a supplemental 20% damping ratio are presented first. The corresponding median values of the maximum inter-story drift of each floor are listed in Table 3-12 and Table 3-13. The median values of peak floor acceleration are listed in Table 3-14 and Table 3-15. These results are plotted in Figure 3-16. The black line represents the median values of the performance measures of the bare frame.

It is observed that the peak inter-story drift and acceleration of the frame are significantly reduced by using the UD, IDPD, and SSSED methods. In the EW direction, the peak median value of the inter-story drift has decreased from 1.60% to 0.76%, 0.75%, and 0.77%. The peak median value of the floor acceleration has reduced from 0.95g to 0.83g, 0.83g, and 0.85g. In the NS direction, the peak median value of the inter-story drift has decreased from 2.06% to 0.88%, 0.97%, and 1.08%. The peak median value of the floor acceleration has reduced from 0.78g to 0.72g, 0.72g, and 0.74g. The obtained results based on the UD and IDPD methods are very close but generally smaller than the results of the SSSED method.

The ESSSED method has significantly reduced the peak inter-story drift and acceleration of all floors in the EW direction. In the NS direction, the values have reduced on the first floor but slightly increased on other floors. This finding presents that the floor

installed the damper can enhance its seismic performance but reduce the seismic resistance of the adjacent floors at the same time.

Table 3-12 EW direction: median value of maximum inter-story drift (20% damping ratio)

Floor	Bare Frame (%)	UD (%)	IDPD (%)	SSSED (%)	ESSSED (%)
1	1.10	0.66	0.66	0.63	0.62
2	0.88	0.64	0.65	0.62	0.62
3	1.60	0.76	0.75	0.77	0.80
4	1.10	0.52	0.54	0.64	0.83

Table 3-13 NS direction: median value of maximum inter-story drift (20% damping ratio)

Floor	Bare Frame (%)	UD (%)	IDPD (%)	SSSED (%)	ESSSED (%)
1	1.77	1.17	1.06	0.99	0.77
2	0.79	0.75	0.79	0.80	0.87
3	2.06	0.88	0.97	1.08	2.05
4	0.99	0.51	0.61	0.73	1.08

Table 3-14 EW direction: median value of peak floor acceleration (20% damping ratio)

Floor	Bare Frame (g)	UD (g)	IDPD (g)	SSSED (g)	ESSSED (g)
1	0.60	0.40	0.40	0.41	0.42
2	0.72	0.57	0.57	0.59	0.65
3	0.82	0.68	0.68	0.68	0.73
4	0.95	0.83	0.83	0.85	0.90

Table 3-15 NS direction: median value of peak floor acceleration (20% damping ratio)

Floor	Bare Frame (g)	UD (g)	IDPD (g)	SSSED (g)	ESSSED (g)
1	0.56	0.45	0.46	0.43	0.52
2	0.70	0.59	0.59	0.58	0.72
3	0.69	0.67	0.68	0.66	0.74
4	0.78	0.72	0.72	0.74	0.82

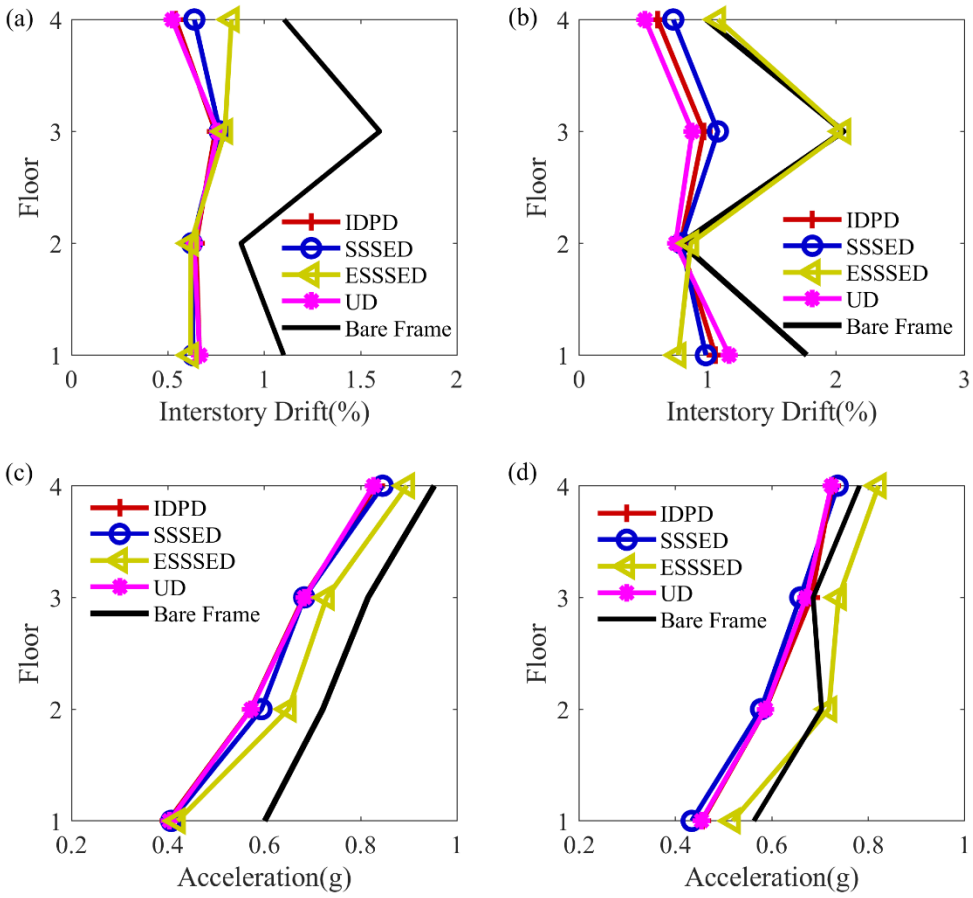

Figure 3-16 Peak inter-story drift ratio and floor acceleration with 20% damping ratio: (a) EW direction; (b) NS direction; (c) EW direction; (d) NS direction

For the model with a supplemental 30% damping ratio, the median values of the maximum inter-story drift of each floor are listed in Table 3-16 and Table 3-17. The median values of peak floor acceleration are listed in Table 3-18 and Table 3-19. The results are plotted in Figure 3-17. The median values of inter-story drift are slightly decreased compared to the model with a supplemental 20% damping ratio. However, the median values of peak floor acceleration have somewhat increased, i.e., the peak median value of the floor acceleration has reduced from 0.78g to 0.76g with applying the UD method, in

the NS direction. However, the value has reduced to 0.72g with a supplemental 20% damping ratio.

Table 3-16 EW direction: median value of maximum inter-story drift (30% damping ratio)

Floor	Bare Frame (%)	UD (%)	IDPD (%)	SSSED (%)	ESSSED (%)
1	1.10	0.61	0.61	0.57	0.56
2	0.88	0.59	0.60	0.58	0.57
3	1.60	0.65	0.63	0.65	0.70
4	1.10	0.46	0.48	0.59	0.89

Table 3-17 NS direction: median value of maximum inter-story drift (30% damping ratio)

Floor	Bare Frame (%)	UD (%)	IDPD (%)	SSSED (%)	ESSSED (%)
1	1.77	1.02	0.93	0.85	0.68
2	0.79	0.70	0.74	0.75	0.89
3	2.06	0.77	0.82	0.93	2.14
4	0.99	0.48	0.58	0.73	1.12

Table 3-18 EW direction: median value of peak floor acceleration (30% damping ratio)

Floor	Bare Frame (g)	UD (g)	IDPD (g)	SSSED (g)	ESSSED (g)
1	0.60	0.40	0.40	0.41	0.43
2	0.72	0.58	0.57	0.58	0.67
3	0.82	0.68	0.68	0.67	0.73
4	0.95	0.82	0.82	0.84	0.93

Table 3-19 NS direction: median value of peak floor acceleration (30% damping ratio)

Floor	Bare Frame (g)	UD (g)	IDPD (g)	SSSED (g)	ESSSED (g)
1	0.56	0.48	0.47	0.46	0.53
2	0.70	0.62	0.62	0.59	0.75
3	0.69	0.70	0.70	0.70	0.74
4	0.78	0.76	0.77	0.77	0.83

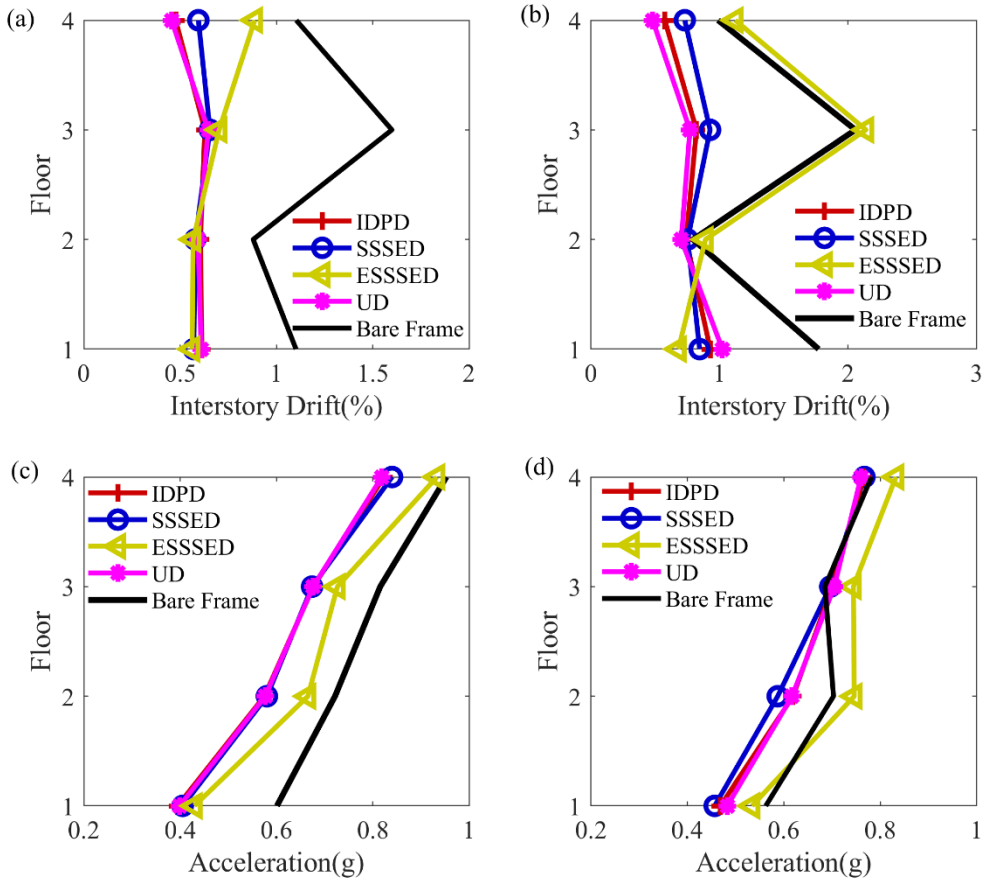

Figure 3-17 Peak inter-story drift ratio and floor acceleration with 30% damping ratio: (a) EW direction; (b) NS direction; (c) EW direction; (d) NS direction

The effectiveness of the four damping coefficient distribution methods is evaluated in two steps: (1) quantifying the uniformity of the inter-story drifts; (2) quantifying the improvement of structural performance over the bare frame. In the structural seismic design, an ideal design intends to have a uniformly distributed inter-story drift along with the building height. For such a design, the seismic capacity, strength, and stiffness of each story are more appropriately designed (Liu 2013). Herein, the inter-story drift of each floor is recorded under the 44 biaxial ground motions. The median values of those recorded

inter-story drifts of each floor are used to quantify the uniformity of the inter-story drifts, as:

$$COV = \frac{\sigma}{\mu} \tag{3.25}$$

where μ represents the mean value of the inter-story drifts, σ represents the standard deviation of the inter-story drifts, the coefficient of variance (COV) of the inter-story drift ratios is served as the index to quantify the uniformity.

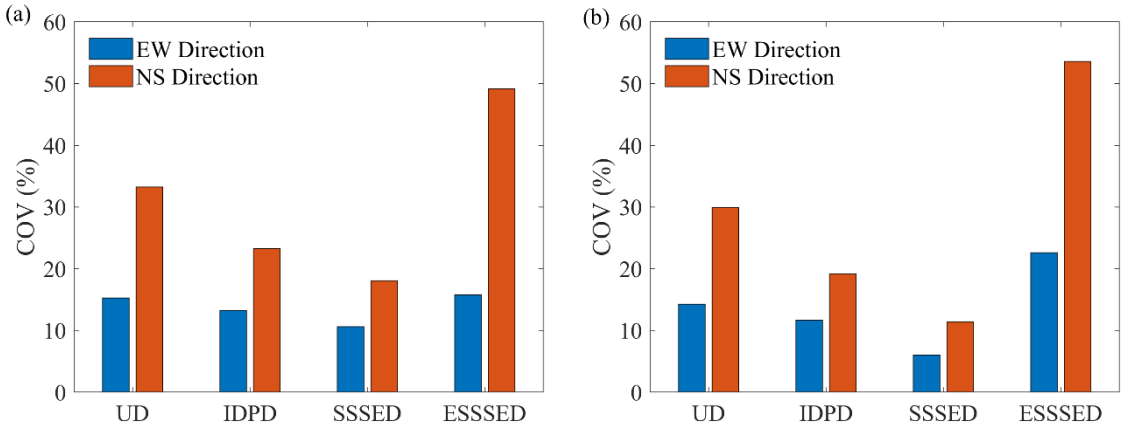

Figure 3-18 Coefficient of variance (*COV*) of the inter-story drift uniformity: (a) 20% damping ratio; (b) 30% damping ratio

The smaller the COV represents the more uniformly distributed inter-story drift, and the more similar seismic capacity of each story. The COV values corresponding to each damping coefficient distribution method are presented in Figure 3-18. It can be observed that the SSSED method can provide the most uniformly distributed inter-story drift of each story, followed by the IDPD, UD, and ESSSED methods. For the ESSSED method, the COV values of NS direction are dramatically larger than the values of the EW

direction. Hence, the ESSSED method cannot provide the uniformly distributed inter-story drift of the entire structure.

For the second step, a mean value of inter-story drifts (μ_{IDR}) is used as the index to quantify the improvement of structural performance over the bare frame. This mean value is calculated as:

$$\mu_{IDR} = \frac{\sum_{i=1}^{N_F} (IDRB_i - IDRD_i)}{N_F}, \quad \text{i=1,2}\ldots N_F \tag{3.26}$$

where the *IDRB* and *IDRD* represent the inter-story drift ratio of the bare frame and the frame with dampers, respectively. If a negative number is obtained, the general seismic performance of the structural is declined. If a positive number is obtained, the general seismic performance of the structure is enhanced. The larger the value of μ_{IDR}, the more the seismic performance of the structure is improved. The obtained mean values of the inter-story drift are shown in Figure 3-19. Overall, the damping coefficient distribution methods can effectively allocate the damping to improve the seismic performance of the structure. The UD method can significantly improve the seismic performance of the structure, followed by the IDPD, SSSED, and ESSSED methods.

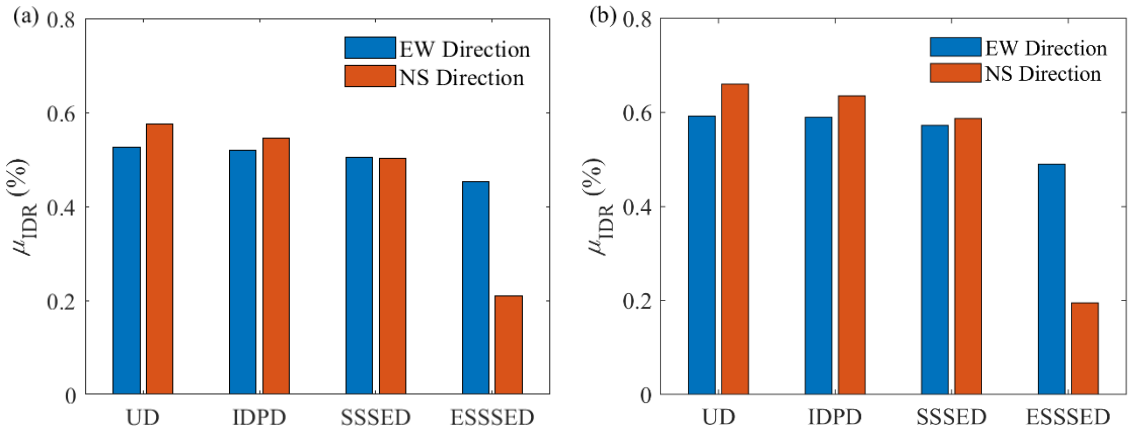

Figure 3-19 Mean value of the inter-story drift improvement over the bare frame: (a) 20% damping ratio; (b) 30% damping ratio

Comparing the improvement of structural performance as well as the uniformity of the inter-story drift is an efficient method to evaluate the effectiveness of different damping coefficient distribution methods. The SSSED method is considered as the optimum damping coefficient distribution method. The SSSED method can improve the seismic performance of the structure and provide the most uniformly distributed inter-story drift for the three-dimensional numerical model.

3.6. Summary

The fluid viscous damper has been widely used to improve the seismic performance of the structure because of its characteristics of reliable performance and easy operation. In this study, four different damping coefficient distribution methods of the fluid viscous damper were extended to the 3D numerical models. Then, their effectiveness in terms of improving structural seismic performance is evaluated through a series of nonlinear dynamic analysis. Although the formula derivation and application were based on the linear

viscous damper, the methodology described in this study can be extended to the implementation of the nonlinear viscous damper by considering the effects of velocity exponent.

In this study, the 3D numerical model of a four-story steel moment-resisting frame was developed in OpenSees. A series of 3D numerical simulations were conducted to evaluate the effectiveness of the four damping coefficient distribution methods. In this case, both the inter-story drift and acceleration were improved over the bare frame by applying the UD, IDPD, SSSED, and ESSSED methods. Among the four methods, the SSSED method was found that can improve and provide the most uniformly distributed inter-story drift of the structure. The ESSSED method could not provide the stable seismic performance of the structure when extending the method to 3D numerical models.

Moreover, the inter-story drift and acceleration are the contradictory performance measures, so that keep increasing the supplemental damping ratio cannot continuously enhance the seismic capacity of the structure. An optimization method is worth to find the optimum value of damping ratio that can seek the balance between inter-story drift and acceleration of the structure in the future research work.

CHAPTER IV
PERFORMANCE-BASED OPTIMIZATION FOR SEISMIC DESIGN OF STEEL FRAME WITH ENERGY DISSIPATION SYSTEM

4.1. Introduction

Earthquake is one of the most destructive natural disasters that could cause significant damages to infrastructure, leading to economic and human life losses. After the devastating 1994 Northridge Earthquake, the Structural Engineers Association of California started to develop a new methodology of performance-based structural seismic design (Zou et al. 2007). The primary objective is to increase the seismic capacity of a structure so that it satisfies the desired performance levels (Bertero and Bertero 2002; Ghobarah 2001).

FEMA 273 (1997) and FEMA 356 (2000) specified four performance levels, i.e., operational, immediate occupancy, life safety, and collapse prevention, to quantify the very light, light, moderate, and severe damage states of a structure (FEMA-273 1997; FEMA-356 2000). In the latest ASCE 41-17 (2017), six performance levels, i.e., immediate occupancy, damage control, life safety, limited safety, collapse prevention, and not considered, were proposed to signify the damage states of the structure. The damage states are usually evaluated by two effective performance measures: inter-story drift ratio (IDR) and peak floor acceleration (PFA). These two measures can be used to quantify the performance of the primary structural components and non-structural components under seismic loading (Lavan and Dargush 2009).

In the traditional seismic design of structures, the shear walls (Kaplan et al. 2011) and diagonal braces, e.g., buckling-restrained brace (Aristizabal-Ochoa 1986; Güneyisi 2012) have been frequently used to enhance the seismic performance of the structure. The traditional methods intend to increase the stiffness of the structure, which can alter the period of the structure. In the latest structural design, the energy dissipation systems were incorporated into the structural frames. The energy dissipation systems can significantly improve the seismic performance of the structure by only increasing the damping ratio of the structure (Del Gobbo et al. 2018).

Fluid viscous damper (FVD) is a kind of energy dissipation system that can effectively reduce both IDR and PFA of the structure. FVD dissipates the seismic energy by producing the velocity-dependent resistance force in the opposite direction of an earthquake motion (Pollini et al. 2017). The peak resistance force of FVD is typically proportional to its cost. Hence, a "trade-off" problem arises as to how to achieve the desired structural performance level while maintaining a relatively low cost of FVD.

The performance-based optimization for the seismic design of structure, which combined the performance-based structural design with optimization algorithms can solve the "trade-off" problems. This optimization method can simultaneously optimize single or multiple objective functions of the structural design. The performance-based structural optimization design has been applied to optimize the performance measures and/or the initial construction cost of the structure (Dogruel et al. 2008; Kaveh et al. 2010; Lavan et al. 2008; Lin and Chopra 2003; Zou and Chan 2004). For example, Askari et al. (2017) set

up three objective functions to seek minimum values of three performance measures: peak IDR, PFA, and base shear force of the structure. Gholizadeh and Baghchevan (2017) defined the steel sections as design variables to seek the minimum values of initial construction cost and the peak IDR. Charmpis et al. (2012) considered the performance measures and initial construction cost to minimize the peak IDR, base displacement, and the cost of the seismic isolation system. From the same line of thinking, the cost of FVD, the IDR, and PFA of the structure are treated as the optimization objectives to form the performance-based optimization framework for structural design in this dissertation.

The FEMA P-58 specification can assess the seismic performance of the structure in terms of repair costs (FEMA P-58-1 2018; FEMA P-58-2 2018). Generally, IDR and PFA are used to obtain the fragility curves of each structural and non-structural components and determine the corresponding repair costs of each component (Zeng et al. 2016). The total repair cost of the structure can be formulated as the sum of the repair costs of individual components. The FEMA P-58 method has been applied to estimate the repair costs of different building types, e.g., tall concrete building (Yang et al. 2012), tall steel building (Wang et al. 2017), and the office building with energy dissipation systems (Terzic et al. 2014). In this study, the FEMA P58 methodology is incorporated in the optimization framework to evaluate the repair cost of the structure. Both the IDR and PFA will be used to determine the repair cost of the structure.

IDR and PFA of the structure are sensitive to the record-to-record variability, also known as ground motion uncertainty (Deng et al. 2017). Typically, the ground motion

uncertainty is accounted for in the design process by applying a series of ground motions to the structure model. In order to consider the influence of the ground motion uncertainty, the far-field record dataset of FEMA P695 (2009) is applied in the formulated performance-based optimization framework for structural design. This far-field record dataset contains 22 biaxial ground motions, which applied twice to the structure model by rotating 90 degrees. Hence, a total of 44 ground motions is taken into consideration in the formulated performance-based optimization framework for structural design. In this case, the IDR of each floor is recorded under the impact of 44 ground motions. For each floor, the coefficient of vibration (COV) value of the IDRs is calculated, and the peak COV value is selected as the robustness measure. A smaller COV indicates the structure is more robust against ground motion uncertainty.

Hence, in this study, the repair cost of the structure, the cost of FVD, and the robustness measure form the optimization objective functions. These objective functions are selected based on the safety, economic, and robustness design perspective. The genetic algorithm-based multi-objective optimization approach is used to seek the minimum values of the three conflicting objectives simultaneously. This multi-objective optimization design can supply a family of compromise solutions between the conflicting objectives. This family of solutions forms the widely-known Pareto front, which visually displays the trade-off between the conflicting objectives. The design parameters of FVDs are selected as the design variables. These design variables determine the peak resistance force of FVD, which in turn influences the cost of FVD and the seismic performance of the structure. The optimum design variables of FVDs are selected based on two optimization scenarios:

maximum considered earthquake and design-based earthquake levels. These two levels can consider the probability of the occurrence of earthquakes. The maximum considered earthquake level has a 2% probability of being exceeded in 50 years. The design-based earthquake level has a 10% probability of being exceeded in 50 years.

4.2. Performance-Based Optimization Framework for Structural Design

4.2.1. Initial Material Cost: Fluid Viscous Damper Cost

The structure with supplemental damper devices is considered as a dual system. The resistance force of the dual system generates from both the lateral load resisting components and the damper devices. For a given single degree of freedom (SDOF) system with FVD, the main governing motion equation of the SDOF system can be expressed as:

$$m \cdot \ddot{u}(t) + c \cdot \dot{u}(t) + k \cdot u(t) + F_D(t) = -m \cdot \ddot{x}_g(t) \tag{4.1}$$

where m, c, and k are the mass, damping coefficient, and stiffness of the structure, respectively. $u(t)$, $\dot{u}(t)$ and $\ddot{u}(t)$ are the displacement, velocity, and acceleration of the structure. $\ddot{x}_g(t)$ is the earthquake ground acceleration, and F_D is the resistance force of FVD.

Maxwell Model

Figure 4-1 Maxwell Model

Generally, the behavior of FVD is simulated by the Maxwell model, which is composed of a linear spring, and a nonlinear dashpot in series, as shown in Figure 4-1. The stiffness of the linear spring, K_d expresses the combined effect of supporting brace and the

inner damper portion. The damping coefficient of the nonlinear dashpot is denoted as C_d. The force-velocity relationship of the nonlinear dashpot can be written as the fractional power law:

$$F_D = C_d \operatorname{sgn}(\dot{u}) |\dot{u}|^{\alpha} \tag{4.2}$$

where α is the velocity exponent, which typically varies between 0.3 to 1.95 (Liu 2010).

The resistance force of the FVD can be expressed as:

$$F_D = K_d u(t) = C_d \operatorname{sgn}(\dot{u}) |\dot{u}|^{\alpha} \tag{4.3}$$

Herein, α, K_d, and C_d are the critical factors to control the resistance force of FVD, which directly influences the cost of FVD. Some commonly used peak resistance forces of FVDs and the corresponding unit costs are listed in Table 4-1 (Liu 2010). The interpolation method is used when the peak resistance damper force is found between the provided values.

Table 4-1 Unit damper device cost for different peak force (based on data from Liu 2010)

Peak Force (kips)	Cost (Dollars, $)
55	3,200
110	3,600
220	6,400
330	8,700
440	11,000

4.2.2. FEMA P-58 Methodology

Recent researches revealed that FVD not only can effectively improve the seismic capacity of structural components but also improve the performance of non-structural

components. The FEMA P-58 method assesses the seismic performance of the structure in terms of the repair cost, which includes the repair costs related to the structural and non-structural components (FEMA P-58-1 2018; FEMA P-58-2 2018). Fragility curves and consequence functions are developed for both structural and non-structural components. The fragility curve describes the probability that a component will reach or exceed a specific damage state as a function of the engineer demand parameter (EDP), as shown in Figure 4-2. The components that are vulnerable to the same EDP can be categorized into the same performance group (PG). Typical examples of EDPs include the IDR, PFA, peak floor velocity, and the residual drift. The probability that a component experiences in one damage state for given a particular EDP value can be expressed as:

$$P[DS|EDP] = \Phi[\frac{1}{\beta_{DS}} \cdot \ln \frac{EDP}{\overline{EDP}_{DS}}] \tag{4.4}$$

where the EDP is assumed to follow the lognormal distribution, $\overline{EDP}_{DS}$ and β_{DS} are the median and standard deviation values of the lognormal distribution.

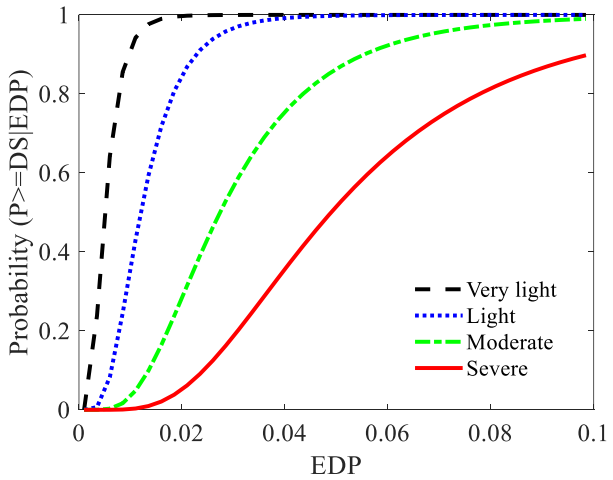

Figure 4-2 Example of fragility curves for very light, light, moderate and severe states

FEMA P-58 method generally consists of four analysis steps to assess the repair costs: (1) determine the loss prediction method; (2) assemble the structural model; (3) analyze damages by evaluating the EDPs of structure; (4) estimate the total repair cost of the structure. The intensity-based nonlinear performance assessment method is one of the loss prediction methods, which requires the user to specify the earthquake intensity. The other two methods are scenario-based and time-based methods, which require more details of building sites or information about seismic hazards. In this study, the intensity-based nonlinear performance assessment method is adopted to estimate the seismic losses, and the nonlinear time history dynamic analysis is utilized to simulate the structural behavior under the effect of ground motion (Wu 2014). The obtained EDPs are used with the fragility functions to determine the probable damage states of each PG. For example, assume a component may be experienced in four damage states. The probability of this component in each damage state can be calculated as:

$$P[D = DS_i \mid EDP] = \begin{cases} P[DS_i \mid EDP] - P[DS_{i+1} \mid EDP] & 1 \le i \le 3 \\ P[DS_i \mid EDP] & i = 4 \end{cases} \tag{4.5}$$

Then, the consequence functions are used to estimate the repair cost of each PG. The total repair cost of each PG is the summation of the repair cost of this PG in each damage state, expressed as:

$$RC[C_{repair}] = \sum_{i=1}^{4} P[D = DS_i \mid EDP] \cdot RC[C_{repair} \mid DS_i] \tag{4.6}$$

where $RC[C_{repair}|DS_i]$ represents the repair cost of each PG under each damage state. $RC[C_{repair}]$ represents the total repair cost of each PG

The total repair cost of the structure, $RC[C_{repair\_total}]$ is the summation of costs due to the damages of structural and non-structural components, expressed as:

$$RC[C_{repair\_total}] = RC[C_{repair\_SS}] + RC[C_{repair\_NS}] \tag{4.7}$$

where $RC[C_{repair\_SS}]$ and $RC[C_{repair\_NS}]$ represent the repair cost of structural and non-structural components, respectively. If the total repair cost of the structure exceeds 40% of replacement costs, the owners often choose to demolish the existing building and replace it with a new one (FEMA P-58-1 2018).

4.2.3. Record-to-Record Variability of Ground Motion

Regardless of sophistication and extent of detail of the numerical model, to be able to at best simulate the seismic performance of the structure, the uncertainties in the structural responses must be considered in the performance-based seismic design of the structure. These uncertainties may arise from the loads, particularly the seismic loads, numerical modeling assumptions, simplifications, or the input parameter uncertainties. In practice, one or more ground motion records can apply to the numerical model, so that account for the ground motion uncertainty in performance-based structural design.

The required number of ground motion records is explicitly defined in ASCE 7-10, in which a minimum of three ground motion records should be applied in the structural design (ASCE 07-10 2010). In such a situation, although different ground motions are

considered, the sensitivity of the structure to the ground motion uncertainty cannot be alleviated. In order to alleviate this difficulty, the robust structural design was proposed to make the responses of a structure insensitive to the sources of uncertainties (called "noise factors") (Kang 2005). The robust design method aims to reduce the effect of noise factors without eliminating them, thereby providing a reliable and efficient structural design.

Recently, the robust optimization design was proposed to combine the optimization algorithms with robustness measures. Generally, two objective functions formulate the robust optimization design of the structure, in which the mean and standard deviation values of the performance measures are minimized simultaneously (Doltsinis and Kang 2004). In this study, the maximum COV value of the IDRs is treated as the robustness measure and is sought for the minimum value, expressed as:

$$COV_D = \max\left(\frac{\sigma_{NF}\left(IDR_i\right)}{u_{NF}\left(IDR_i\right)}\right),\ i = 1, 2, \ldots, 44 \tag{4.8}$$

where NF is the number of stories of the structure, μ and σ represent the mean and standard deviation of IDRs of each story, i represents the number of ground motions, COV_D is the maximum COV value. A smaller COV_D means that the structure is more robust against ground motion uncertainty.

Herein, the performance-based structural optimization design can be formulated as: find optimal sets of design parameters (i.e., α, K_d, and C_d of FVD) such that the initial construction cost (i.e., the cost of FVD), the repair cost of the structure ($RC[C_{repair\_total}]$), and the robustness measure (COV_D) are minimized.

4.3. Multi-Objective Optimization Method

In the context of performance-based structural optimization design, multi-objective optimization problems arise when more than one objectives need to be optimized, each in a conflicting manner. A generic multi-objective optimization problem can be formulated as (Kuczera 1997; Madsen 2003; Madsen et al. 2002):

$$\begin{aligned} &\text{Minimize}: Y(x) = [f_1(x), f_2(x) \ldots f_n(x)],\ x \in \theta \\ &\text{Subject to: } h(x) \le 0 \end{aligned} \tag{4.9}$$

where f represents an individual objective function, n is the number of objective functions, x is the set of design variables within a feasible input parameter space θ, and h represents the constraint function.

In this study, the Non-dominated Sorting Genetic Algorithm II (NSGA-II) is implemented to solve the multi-objective optimization problem. NSGA-II uses a fast non-dominated sorting procedure, a parameterless niching operator, and an elitist persevering approach. The basic principles of NSGA-II are selection, recombination, and mutation to populate a new generation until the solution reaches an optimum state (Deb et al. 2002). NSGA-II is used to determine the Pareto front since it maintains a good distribution of solutions that converge in a non-dominated front and preserve a diversity (a similar alternative solution to any solution of the Pareto Front) of solutions (Erbas et al. 2006).

In the context of NSGA-II, the Pareto front consists of a set of optimal non-dominated solutions. A two-objective case is presented to describe the domination relation, as shown in Figure 4-3. The solution A dominates the other solution B if one of the

following two conditions are satisfied: (1) solution A is better than other solution B in both objectives (2) solution A is better than other solution B in at least one objective (Mishra and Harit 2010). If no solution dominates the other one, they collectively form the Pareto front.

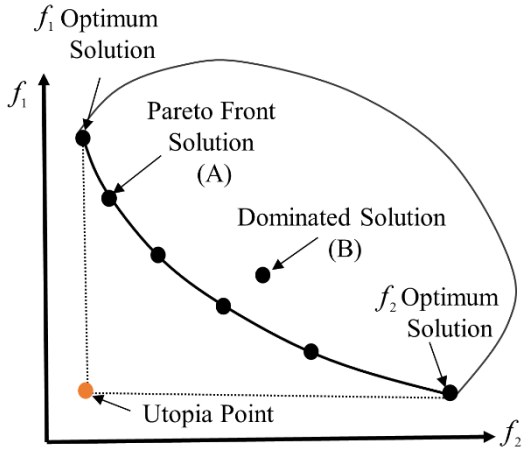

Figure 4-3 Domination relation between Pareto Front and dominated solution

The shape of the Pareto front can be concave, convex, mixed (partially convex and concave), or discontinuous depending on the nature of compromise between objectives (Parsopoulos and Vrahatis 2002). The shape of the Pareto front visually displays the level of compromise needed from one objective to improve the other. This kind of compromise reduces as the solutions approaching the extreme points of the Pareto front. In our formulation, the desired outcome is the-smaller-the-better for all three objectives, e.g., less cost of damping devices results in a higher repair cost, which leads to a monotonically decreasing shape of the Pareto front.

4.4. Case Study: Steel Moment-Resisting Frame with Fluid Viscous Dampers

4.4.1. Numerical Model of the Steel Frame

The conceptual framework is applied to a four-story office building. The prototype building is a steel moment-resisting frame and was designed based on seismic provisions (IBC-2003, AISC-2002, and AISC-2005) and was previously evaluated by Lignos (2008). The building is assumed to be located in the Los Angeles area with soil type D and risk category II.

A three-dimensional numerical model of the steel frame was developed using OpenSees (Open System for earthquake engineering simulation). All beams and girders are modeled as linear elastic. The nonlinearity of the column is modeled by the 'non-linear beam-column' element. All the components of the steel frame are assumed to be made of A992 grade 50 steel. A total of 24 FVDs are symmetrically placed on the exterior sides of the steel frame. The layout of the FVDs considers the seismic capacity of each story as well as the rationality of the architectural design, as shown in Figure 4-4.

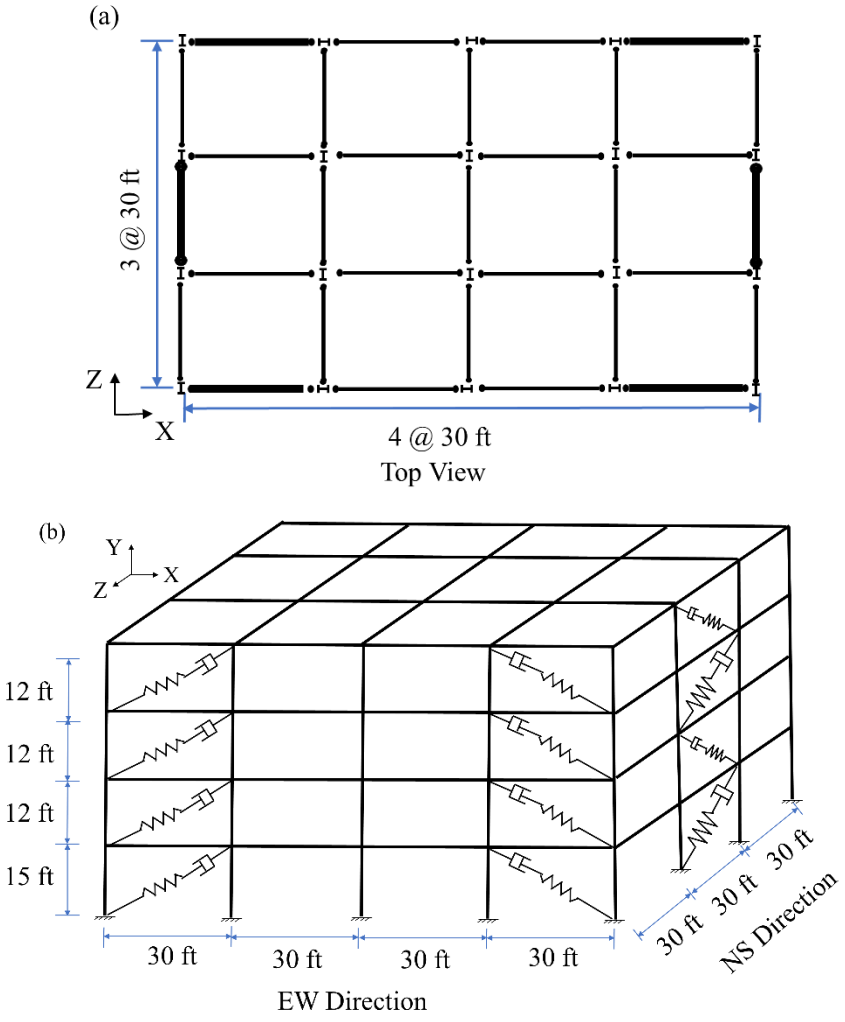

Figure 4-4 Plan view of the prototype office building

4.4.2. Description of Multi-Objective Optimization Design Procedure

The proposed multi-objective optimization design framework is applied to this office building. The stiffness of the brace and damper portion, K_d, the velocity exponent, α, and the damping coefficient C_d are selected as the design variables. Constraining K_d can ensure the damper systems able to sustain but not the unique source of lateral load stiffness and strength in the structure. Moreover, FVDs locate on the same floor, and the same horizontal direction of the structure are assigned the same values of design variables.

The far-field record set of FEMA-P695 PEER NGA database consists of 22 biaxial ground motion records. First, the first component of far-field ground motions is applied along the EW-direction of the numerical model and the second component is applied along NS-direction. Then, the records are rotated by 90 degrees and applied to the numerical model again. Hence, a total of 44-biaxial ground motions are considered in this case study. The optimization objectives serve as the outputs of the optimization loop, which is configured to minimize the repair cost of the structure, the total cost of all FVDs, and the COV of IDRs. The Pareto front as the ultimate result provides a series of optimum designs for decision markers to choose from.

Moreover, the repair cost of this office building is expressed as a percentage of the total replacement cost. It includes the repair costs of structural components, non-structural drift, and acceleration sensitive components. The non-structural components include exterior glass curtain wall, gypsum board partitions with steel studs, suspended ceiling, wall finishing, roof covering, and fire sprinkler system. The removable equipment and furnishings are not considered in this estimation. Table 4-2 provides the critical fragility information on the structural and non-structural components, in which M_{EDP} and β are the median and standard deviation of the EDP for the corresponding damage state. This critical fragility information is referenced from the PACT (Performance Assessment Calculation Tool) fragility database.

Table 4-2 Critical fragility information on structural and non-structural components

System	EDP	Damage State	M_{EDP}	β
Curtain wall	IDR	Glass cracking	0.0338	0.4
		Glass falls from frame	0.0383	0.4
Gypsum board partitions	IDR	Screw pop-out, slight crushing	0.005	0.4
		Moderate cracking or crushing	0.01	0.3
		Buckling of studs, significant cracking or crushing	0.021	0.2
Wall finishing	IDR	Wall paper warped and torn	0.0021	0.6
Suspended ceiling	PFA	5 % of ceiling grid, tile damage	1.47	0.3
		30% of ceiling grid, tile damage.	1.88	0.3
		50% of ceiling grid, tile damage.	2.03	0.3
Fire sprinkler drop	PFA	Spraying, dripping leakage at drop joints	0.95	0.4
Roof tile	PFA	Minor damage, tiles dislodged	1.1	0.4
		Major portion of tile dislodged	1.4	0.4
Steel moment frame	IDR	Local buckling	0.03	0.3
		Lateral-torsional distortion	0.04	0.3
		Fracture in buckled region	0.05	0.3

The default consequence functions reflect the 2011 repair costs of the structural and non-structural components for the Northern Californian region (FEMA P-58-2 2018). For this case study, it deems the cost as similar to the office building at the location of Southern California. The cost multiplier is set equal to one. The dispersion input is set to zero to reflect a precise value of unit cost. The total replacement cost of this building is estimated to be $8,640,000, which is $200 per square feet.

4.5. Optimization Results

4.5.1. Optimization Design Based on MCE Level

First, all ground motion records are scaled to the MCE level for the intensity-based performance assessment method. The specific variation ranges of each design variables are predefined as follows: (1) K_d can vary from 0 to 1500 kips/in with increasing interval of 250 kips/in. This limitation of the stiffness can ensure the brace of the supplemental damper

to be smaller than the size of the column. (2) α can vary from 0.3 to 1.0 with an increasing interval of 0.1. (3) C_d can vary from 0 to 70 kips-sec/in with an increasing interval of 10 kips-sec/in. The NSGA-II is implemented to solve this multi-objective optimization problem with 20 generations and 22 individuals in each generation.

The obtained optimum designs form the Pareto front, which provides the trade-off among the three optimization objectives, is shown in Figure 4-5 (d). The red points represent the optimum designs of the Pareto front, and the gray points denote all the dominated designs. The values of the optimum designs along the Pareto front and the corresponding values of design variables are listed in Table 4-3 and Table 4-4. The gathered Pareto front generally reveals that the COV_D and the $RC[C_{repair\_total}]$ are inverse proportional to the total dampers cost, while the COV_D is proportional to the $RC[C_{repair\_total}]$ of the structure. Herein, the dollar amounts for repair cost and the initial material cost are considered in today's dollars (not adjusted for inflation).

In general, for the given damper cost, both COV_D and $RC[C_{repair\_total}]$ can be significantly reduced after optimization. For instance, for a given damper cost of \$186,966, the COV_D can be improved from the worst design of 63.81% to the design of 54.99%, and $RC[C_{repair\_total}]$ can be improved from the worst design of 8.61% to the design of 3.23%. For identical COV_D or $RC[C_{repair\_total}]$, the damper cost can also significantly reduced after optimization, i.e., with COV_D as 60.43%, the damper cost can be reduced from \$186,966 to \$27,829; with $RC[C_{repair\_total}]$ as 5.50%, the damper cost can be reduced from \$186,966 to \$35,759.

Choosing a suitable, cost-effective design is critical for structural designers and construction investors. Three optimum designs are selected based on the damper cost. A more detailed comparison of the seismic performance of the selected designs will be presented in the later section.

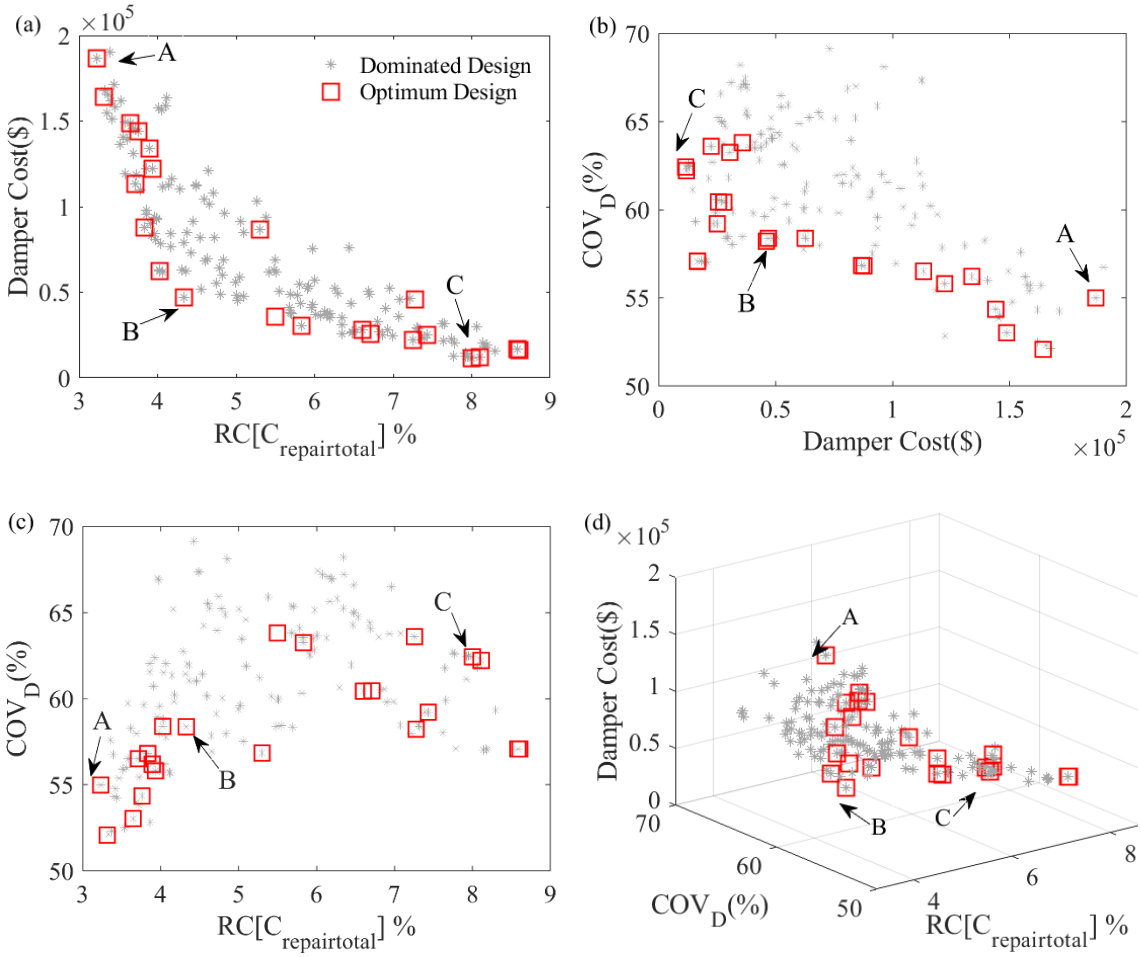

Figure 4-5 Pareto front and dominated designs of MCE level: (a) $RC[C_{repair\_total}]$ versus damper cost; (b) damper cost versus COV_D; (c) $RC[C_{repair\_total}]$ versus COV_D; (d) 3D view

Table 4-3 Properties of each FVD along the Pareto Front of MCE level-EW direction

	1st floor			2nd floor			3rd floor			4th floor			Objectives		
Number	C_d	K_d	α	C_d	K_d	α	C_d	K_d	α	C_d	K_d	α	RC (%)	DC ($)	COV_D (%)
1	50	1250	0.3	10	250	0.3	10	250	0.6	30	750	0.5	5.50	35759	63.81
2	10	250	1	50	1250	1	60	1500	0.6	60	1500	1	3.31	164342	52.09
3	50	1250	0.3	30	750	0.3	30	750	0.3	30	750	0.5	8.61	16503	57.08
4	10	250	0.3	60	1500	0.3	20	500	0.5	40	1000	0.5	8.00	11450	62.43
5	60	1500	0.9	30	750	0.9	50	1250	1	60	1500	1	3.23	186966	54.99
6	50	1250	1	50	1250	0.5	60	1500	0.7	40	1000	0.5	5.30	86734	56.84
7	10	250	1	60	1500	1	60	1500	0.6	50	1250	1	3.65	148781	53.03
8	50	1250	0.3	50	1250	0.3	60	1500	0.6	10	250	0.3	4.03	62578	58.39
9	50	1250	0.3	50	1250	0.3	60	1500	0.6	10	250	0.3	4.33	46956	58.38
10	40	1000	0.3	10	250	0.3	10	250	0.6	40	1000	0.5	7.44	25071	59.22
11	10	250	0.3	50	1250	0.3	20	500	0.5	60	1500	0.5	8.11	11941	62.23
12	50	1250	0.3	10	250	0.3	20	500	0.6	30	750	0.5	6.60	27829	60.43
13	50	1250	0.3	10	250	0.3	20	500	0.6	30	750	0.3	6.71	25518	60.46
14	10	250	1	60	1500	1	40	1000	0.9	60	1500	0.3	3.76	144129	54.36
15	10	250	1	10	250	1	50	1250	0.6	30	750	1	3.72	113336	56.51
16	10	250	1	60	1500	1	20	500	0.9	60	1500	0.3	3.94	122196	55.81
17	20	500	0.3	30	750	1	40	1000	0.3	30	750	0.5	7.28	45956	58.22
18	50	1250	0.4	30	750	0.3	40	1000	0.3	30	750	0.5	5.83	30472	63.24
19	10	250	1	60	1500	0.6	20	500	0.9	60	1500	0.3	3.84	87829	56.82
20	50	1250	0.3	30	750	0.7	20	500	0.6	30	750	0.5	7.26	22403	63.60
21	10	250	1	60	1500	1	60	1500	0.6	60	1500	0.4	3.90	133891	56.21
22	50	1250	0.3	30	750	0.3	40	1000	0.3	30	750	0.5	8.58	16596	57.08

Note: RC represents the normalized repair cost, $RC[C_{repair\_total}]$. DC represents the total cost of damper devices. The units of C_d and K_d are kips-sec/in and kips/in, respectively

Table 4-4 Properties of each FVD along the Pareto Front of MCE level-NS direction

	1st floor			2nd floor			3rd floor			4th floor			Objectives		
Number	C_d	K_d	α	C_d	K_d	α	C_d	K_d	α	C_d	K_d	α	RC (%)	DC ($)	COV_D (%)
1	10	250	0.9	20	500	0.8	20	500	1	60	1500	0.3	5.50	35759	63.81
2	40	1000	1	60	1500	0.7	20	500	1	50	1250	1	3.31	164342	52.09
3	10	250	0.9	20	500	0.3	60	1500	0.3	60	1500	0.4	8.61	16503	57.08
4	10	250	0.3	10	250	0.3	60	1500	0.3	50	1250	0.4	8.00	11450	62.43
5	40	1000	1	10	250	0.7	20	500	1	60	1500	1	3.23	186966	54.99
6	40	1000	0.8	20	500	0.5	20	500	0.7	20	500	0.3	5.30	86734	56.84
7	40	1000	1	30	750	0.6	20	500	1	40	1000	0.5	3.65	148781	53.03
8	50	1250	1	20	500	0.5	30	750	0.9	20	500	0.4	4.03	62578	58.39
9	20	500	1	20	500	0.5	30	750	0.9	20	500	0.4	4.33	46956	58.38
10	10	250	0.9	20	500	0.8	60	1500	0.5	60	1500	0.4	7.44	25071	59.22
11	10	250	0.3	60	1500	0.3	60	1500	0.3	10	250	0.4	8.11	11941	62.23
12	10	250	0.9	20	500	0.8	60	1500	0.6	60	1500	0.3	6.60	27829	60.43
13	10	250	0.9	20	500	0.8	60	1500	0.6	60	1500	0.3	6.71	25518	60.46
14	50	1250	1	30	750	0.6	20	500	1	10	250	0.5	3.76	144129	54.36
15	50	1250	1	30	750	0.6	20	500	1	40	1000	0.5	3.72	113336	56.51
16	50	1250	0.9	30	750	0.6	20	500	1	10	250	0.5	3.94	122196	55.81
17	10	250	0.9	20	500	0.3	60	1500	0.3	60	1500	0.4	7.28	45956	58.22
18	10	250	0.9	20	500	0.3	60	1500	0.8	60	1500	0.4	5.83	30472	63.24
19	60	1500	0.9	30	750	0.6	20	500	1	10	250	0.5	3.84	87829	56.82
20	10	250	0.3	20	500	0.3	60	1500	0.5	60	1500	0.4	7.26	22403	63.60
21	40	1000	1	60	1500	0.5	20	500	1	40	1000	1	3.90	133891	56.21
22	10	250	0.9	20	500	0.3	60	1500	0.3	60	1500	0.4	8.58	16596	57.08

Note: RC represents the normalized repair cost, RC[C_{repair_total}]. DC represents the total cost of damper devices. The units of Cd and Kd are kips-sec/in and kips/in, respectively.

4.5.2. Optimization Design Based on DBE Level

For a more cost-efficient consideration of the occurrence of earthquakes in real-life, the same optimization procedure is applied to the steel frame with all ground motions scaled to the DBE level. The scale factor of the DBE level is 2/3 of the MCE level. The variation ranges of K_d, C_d, and α remain the same as defined in section 4.4. NSGA-II is implemented to solve this multi-objective optimization problem with 20 generations and 22 individuals in each generation.

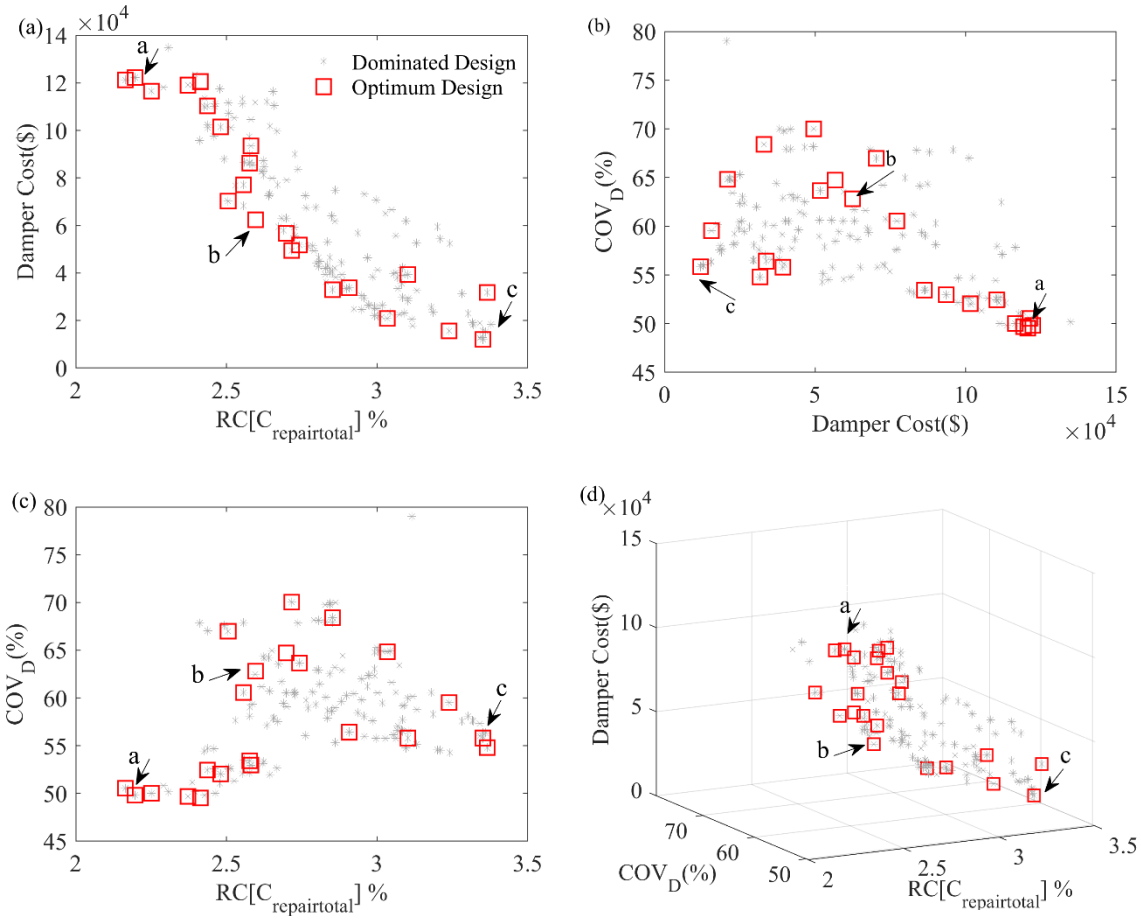

Figure 4-6 Pareto front and dominated designs of DBE level: (a) $RC[C_{repair\_total}]$ versus damper cost; (b) damper cost versus COV_D; (c) $RC[C_{repair\_total}]$ versus COV_D ; (d) 3D view

All the dominated designs are indicated in gray color and drawn in Figure 4-6 (d). The optimum designs along the Pareto front are highlighted in red. The values of design variables and optimum designs in the Pareto front are listed in Table 4-5 and Table 4-6, respectively.

With the damper cost of \$122,299, the COV_D can be improved from the worst design of 55.83% to the design of 49.81%, and $RC[C_{repair\_total}]$ can be improved from the worst design of 3.37% to the design of 2.20%.

In general, the required damper cost of the DBE level is smaller than the one under the MCE level. The maximum damper cost is reduced from \$186,966 to \$122,299, $RC[C_{repair\_total}]$ is reduced from 3.23% to 2.20%, and COV_D is reduced from 54.99% to 49.81%, when comparing the DBE results with those obtained under the MCE level.

In order to select the optimal performance and cost-efficiency design, three designs: design a, design b, and design c are selected along the Pareto front. In the following section, the seismic performance of these selected designs will be evaluated.

Table 4-5 Properties of each FVD along the Pareto Front of DBE level-EW direction

	1st floor			2nd floor			3rd floor			4th floor			Objectives		
Number	C_d	K_d	α	C_d	K	α	C_d	K_d	A	C	K_d	α	RC (%)	DC ($)	COV_D (%)
1	20	500	1	50	1250	1	20	500	1	10	250	0.5	2.41	120688	49.54
2	10	250	0.3	30	750	1	10	250	0.5	30	750	0.5	3.37	31735	54.79
3	50	1250	0.9	50	1250	0.5	60	1500	0.9	40	1000	0.5	2.20	122299	49.81
4	30	750	0.8	20	500	0.7	30	750	0.3	10	250	0.7	2.72	49551	70.01
5	10	250	0.3	10	250	0.5	10	250	0.5	30	750	0.5	3.35	11962	55.83
6	40	1000	0.9	50	1250	0.5	60	1500	0.9	40	1000	0.5	2.17	121231	50.53
7	60	1500	0.4	30	750	0.3	10	250	0.3	30	750	0.5	3.24	15574	59.53
8	10	250	1	50	1250	0.7	50	1250	0.7	30	750	0.5	3.10	39307	55.80
9	60	1500	0.4	30	750	0.3	10	250	0.3	30	750	0.5	3.03	20810	64.83
10	30	750	0.8	20	500	0.3	60	1500	0.7	30	750	0.7	2.56	77145	60.55
11	50	1250	1	50	1250	0.5	20	500	0.9	40	1000	0.5	2.25	116463	50.00
12	30	750	0.8	30	750	0.7	30	750	0.3	10	250	0.7	2.70	56652	64.72
13	30	750	0.8	10	250	0.3	60	1500	0.6	30	750	0.7	2.60	62462	62.81
14	50	1250	0.3	50	1250	0.3	40	1000	0.3	50	1250	1	2.51	70233	66.97
15	50	1250	1	50	1250	0.3	20	500	0.8	50	1250	0.5	2.48	101537	52.04
16	50	1250	1	50	1250	0.5	30	750	0.7	60	1500	0.5	2.58	86276	53.44
17	50	1250	0.3	40	1000	0.3	20	500	0.5	40	1000	0.5	2.85	32931	68.42
18	50	1250	0.3	30	750	0.3	20	500	0.5	40	1000	0.5	2.91	33778	56.43
19	60	1500	1	50	1250	0.5	30	750	0.7	40	1000	0.5	2.58	93530	52.97
20	50	1250	1	50	1250	0.8	20	500	1	10	250	0.5	2.37	119180	49.69
21	30	750	0.8	40	1000	0.3	60	1500	0.6	30	750	0.7	2.74	51699	63.65
22	60	1500	1	50	1250	0.5	30	750	0.7	60	1500	1	2.44	110307	52.45

Note: RC represents the normalized repair cost, $RC[C_{repair\_total}]$. DC represents the total cost of damper devices. The units of C_d and K_d are kips-sec/in and kips/in, respectively.

Table 4-6 Properties of each FVD along the Pareto Front of DBE level-NS direction

	1st floor			2nd floor			3rd floor			4th floor			Objectives		
Number	C	K_d	α	C_d	K_d	α	C_d	K	A	C_d	K_d	α	RC (%)	DC ($)	COV_D (%)
1	60	1500	1	20	500	0.3	60	1500	0.9	60	1500	1	2.41	120688	49.54
2	10	250	0.7	10	250	0.3	30	750	0.3	20	500	0.4	3.37	31735	54.79
3	60	1500	1	20	500	1	50	1250	1	50	1250	1	2.20	122299	49.81
4	60	1500	0.9	30	750	0.8	60	1500	0.3	20	500	0.8	2.72	49551	70.01
5	10	250	0.8	10	250	0.3	30	750	0.3	20	500	0.4	3.35	11962	55.83
6	60	1500	1	20	500	1	60	1500	1	50	1250	1	2.17	121231	50.53
7	60	1500	0.7	20	500	0.3	10	250	0.3	30	750	0.4	3.24	15574	59.53
8	10	250	0.9	60	1500	0.3	30	750	0.3	20	500	0.4	3.10	39307	55.80
9	60	1500	0.8	20	500	0.3	10	250	0.3	30	750	0.4	3.03	20810	64.83
10	60	1500	0.7	50	1250	1	50	1250	0.9	60	1500	1	2.56	77145	60.55
11	60	1500	1	20	500	1	50	1250	1	50	1250	1	2.25	116463	50.00
12	60	1500	0.9	30	750	0.8	60	1500	0.6	20	500	1	2.70	56652	64.72
13	60	1500	0.6	50	1250	1	50	1250	0.9	20	500	0.8	2.60	62462	62.81
14	60	1500	1	10	250	0.7	50	1250	0.4	60	1500	1	2.51	70233	66.97
15	60	1500	1	60	1500	0.3	60	1500	0.9	60	1500	1	2.48	101537	52.04
16	60	1500	1	20	500	0.7	20	500	1	20	500	0.6	2.58	86276	53.44
17	40	1000	1	50	1250	0.3	60	1500	0.5	60	1500	0.4	2.85	32931	68.42
18	40	1000	0.9	50	1250	0.3	60	1500	0.8	10	250	0.4	2.91	33778	56.43
19	60	1500	1	20	500	0.3	20	500	1	20	500	1	2.58	93530	52.97
20	60	1500	1	20	500	0.3	60	1500	0.9	60	1500	1	2.37	119180	49.69
21	60	1500	0.6	10	250	1	50	1250	0.9	20	500	0.8	2.74	51699	63.65
22	60	1500	1	20	500	0.3	20	500	1	10	250	1	2.44	110307	52.45

Note: RC represents the normalized repair cost, $RC[C_{repair\_total}]$. DC represents the total cost of damper devices. The units of C_d and K_d are kips-sec/in and kips/in, respectively.

4.5.3. Comparison of MCE and DBE Levels

In order to compare the optimization results of MCE and DBE levels, six designs along the Pareto front are selected based on the cost of dampers. The properties of the chosen designs are listed in Table 4-7 and Table 4-8. The cost of the dampers varies between \$11,450 and \$186,966. Generally, a damper with a higher cost results in better seismic performance of the structure.

For the MCE level, design A is the most expensive design with the minimum repair cost and COV_D. Design B is the design closest to the utopia point (the origin point). Design C is the design with the least damper cost and highest repair cost. The cost of the dampers increases from \$11,450 to \$46,956, but the $RC[C_{repair\_total}]$ and COV_D have significantly reduced from 8.00% to 4.33%, and 62.43% to 58.38%, respectively. The damper cost of design A is nearly four times than design B, but the $RC[C_{repair\_total}]$ is only increased by 3.67%. Similarly, three optimized designs of DBE level: design a, design b and design c are also, corresponding to the most expensive design, the design closest to the utopia point, and the design with the least damper cost, respectively.

Table 4-7 Properties of FVDs of the selected designs along the EW direction

	MCE									DBE								
	Design A			Design B			Design C			Design a			Design b			Design c		
	C_d	K_d	α	C_d	K_d	α	C_d	K_d	α	C_d	K_d	α	C_d	K_d	α	C_d	K_d	α
1st Floor	60	1500	0.9	50	1250	0.3	10	250	0.3	50	1250	0.9	30	750	0.8	10	250	0.3
2nd Floor	30	750	0.9	50	1250	0.3	60	1500	0.3	50	1250	0.5	10	250	0.3	10	250	0.5
3rd Floor	50	1250	1.0	60	1500	0.6	20	500	0.5	60	1500	0.9	60	1500	0.6	10	250	0.5
4th Floor	60	1500	1.0	10	250	0.3	40	1000	0.5	40	1000	0.5	30	750	0.7	30	750	0.5
$RC[C_{repair\_total}]$ (%)	3.23			4.33			8.00			2.20			2.60			3.35		
COV_D (%)	54.99			58.38			62.43			49.81			62.81			55.83		
Damper Cost ($)	186,966			46,956			11,450			122,299			62,462			11,962		

Table 4-8 Properties of FVDs of the selected designs along the NS direction

	MCE									DBE								
	Design A			Design B			Design C			Design a			Design b			Design c		
	C_d	K_d	α	C_d	K_d	α	C_d	K_d	α	C_d	K_d	α	C_d	K_d	α	C_d	K_d	α
1st Floor	40	1000	1.0	20	500	1.0	10	250	0.3	60	1500	1.0	60	1500	0.6	10	250	0.8
2nd Floor	10	250	0.7	20	500	0.5	10	250	0.3	20	500	1.0	50	1250	1.0	10	250	0.3
3rd Floor	20	500	1.0	30	750	0.9	60	1500	0.3	50	1250	1.0	50	1250	0.9	30	750	0.3
4th Floor	60	1500	1.0	20	500	0.4	50	1250	0.4	50	1250	1.0	20	500	0.8	20	500	0.4
$RC[C_{repair\_total}]$ (%)	3.23			4.33			8.00			2.20			2.60			3.35		
COV_D (%)	54.99			58.38			62.43			49.81			62.81			55.83		
Damper Cost ($)	186,966			46,956			11,450			122,299			62,462			11,962		

The seismic performance of the selected designs is evaluated under the effects of both MCE and DBE levels. The medium values of peak IDR and PFA along EW and NS directions are recorded and shown in Figure 4-7 and Figure 4-8.

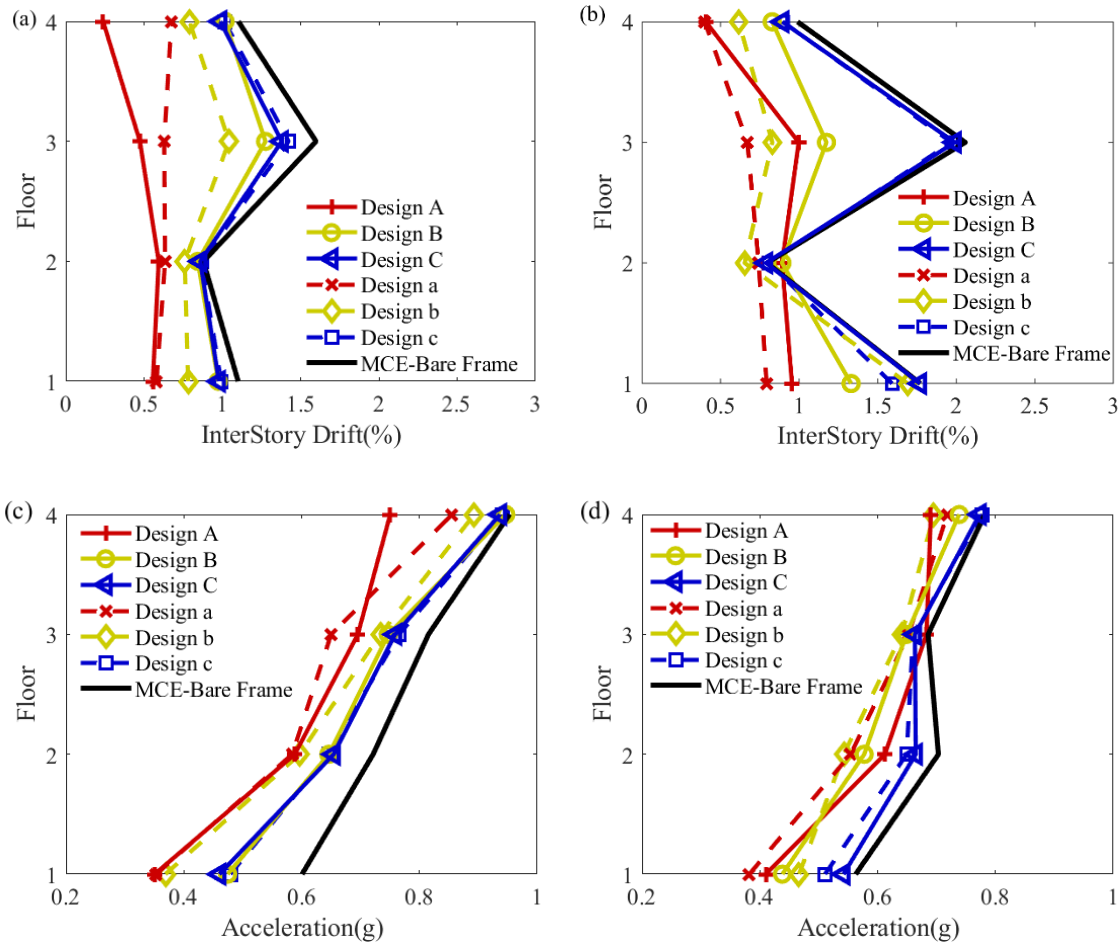

Figure 4-7 Seismic performance of selected designs under the effect of MCE level: (a) IDR of EW direction; (b) IDR of NS direction; (c) PFA of EW direction; (d) PFA of NS direction

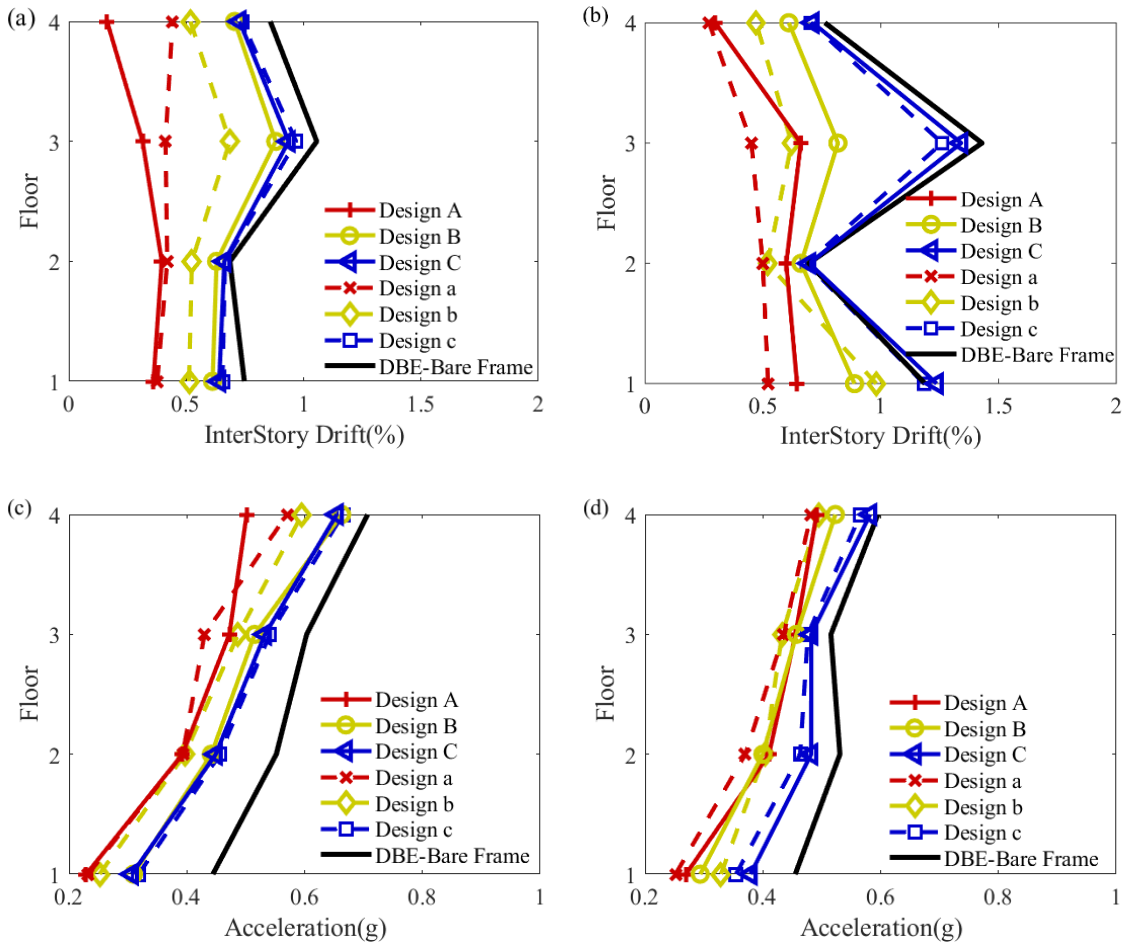

Figure 4-8 Seismic performance of selected designs under the effect of DBE level: (a) IDR of EW direction; (b) IDR of NS direction; (c) PFA of EW direction; (d) PFA of NS direction

The solid black lines represent the seismic responses of the bare frame (structure without installing any damper devices). It can be observed that the first and third stories of the NS-direction are the relative weaker stories, which have relatively higher IDR values. The solid and dashed red lines represent the seismic responses of design A and design a. For both MCE and DBE levels, the peak IDRs have significantly reduced in both EW and NS directions, as shown in Figure 4-7 (a), (b) and Figure 4-8 (a), (b). For design A, the medium value of IDR has reduced from 2.06% to 0.99% for the third floor and reduced

from 1.77% to 0.95% for the first floor under the MCE level. Meanwhile, the IDRs have decreased from 1.43% to 0.31% for the third floor, and 1.19% to 0.36% for the first floor under the DBE level. For design a, the IDRs of first and third floor have decreased from 1.77% to 0.79%, and 2.06% to 0.67% under the MCE level; also reduced from 1.19% to 0.52%, and 1.43% to 0.45% under the DBE level.

Furthermore, all the six designs yield reduced PFAs when compared to the bare frame, as shown in Figure 4-7 (c), (d), and Figure 4-8 (c), (d). It is observed that, even with a lower damper cost, design *a* results in a smaller PFA (better seismic performance) than design A. The PFA values of design a are 0.35g, 0.58g, 0.65g, and 0.86g, as shown in Figure 4-7 (c); 0.38g, 0.55g, 0.65g, and 0.72g, as shown in Figure 4-7 (d); 0.23g, 0.39g, 0.43g, and 0.57g, as shown in Figure 4-8 (c); and 0.25g, 0.37g, 0.44g, and 0.48g, as shown in Figure 4-8 (d).

The solid and dashed yellow lines represent the seismic responses of design B and design b. The IDR values reduced from 2.06% (bare frame) to 1.17% and 0.83 % on the third floor for design B and design b, respectively. However, the IDR values of the first floor only reduced from 1.77% to 1.76% and 1.59%, respectively, as shown in Figure 4-7 (b). The blue lines represent the seismic responses of design C and design c. The medium values of IDR have slightly reduced in the cases of design C and design c.

After comparing the median values of IDR and PFA of the selected designs, design a can be chosen as the optimum design since it has moderate damper costs, less structure repair cost and robustness measure (see Table 4-7 and Table 4-8). All the recorded values

of IDR for the design a, and the bare frame are shown in Figure 4-9 and Figure 4-10. It can be observed that the seismic performance of the steel frame has been dramatically improved under both the MCE and DBE levels.

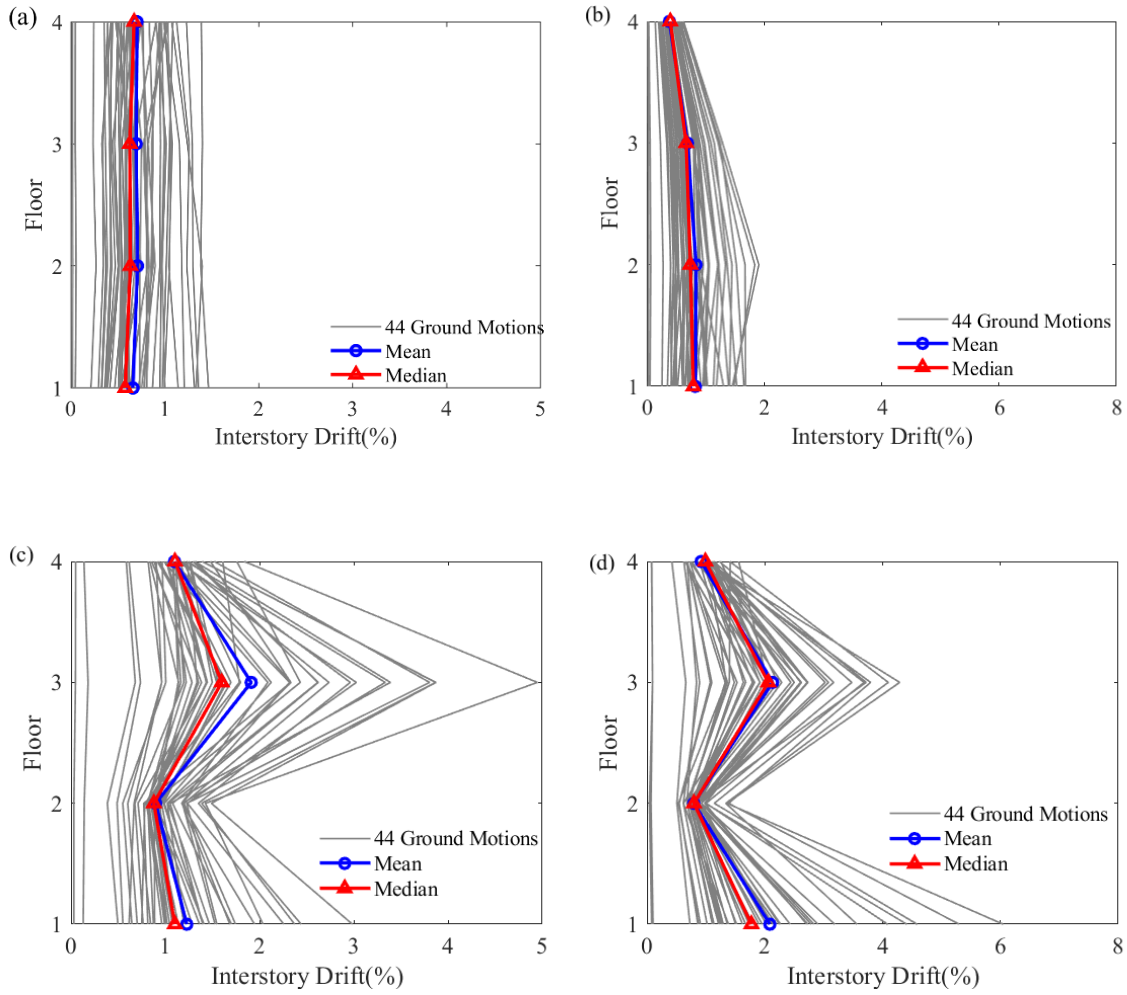

Figure 4-9 IDR of each floor under the effects of MCE level: (a) design a (EW direction); (b) design a (NS direction); (c) bare frame (EW direction); (d) bare frame (NS direction)

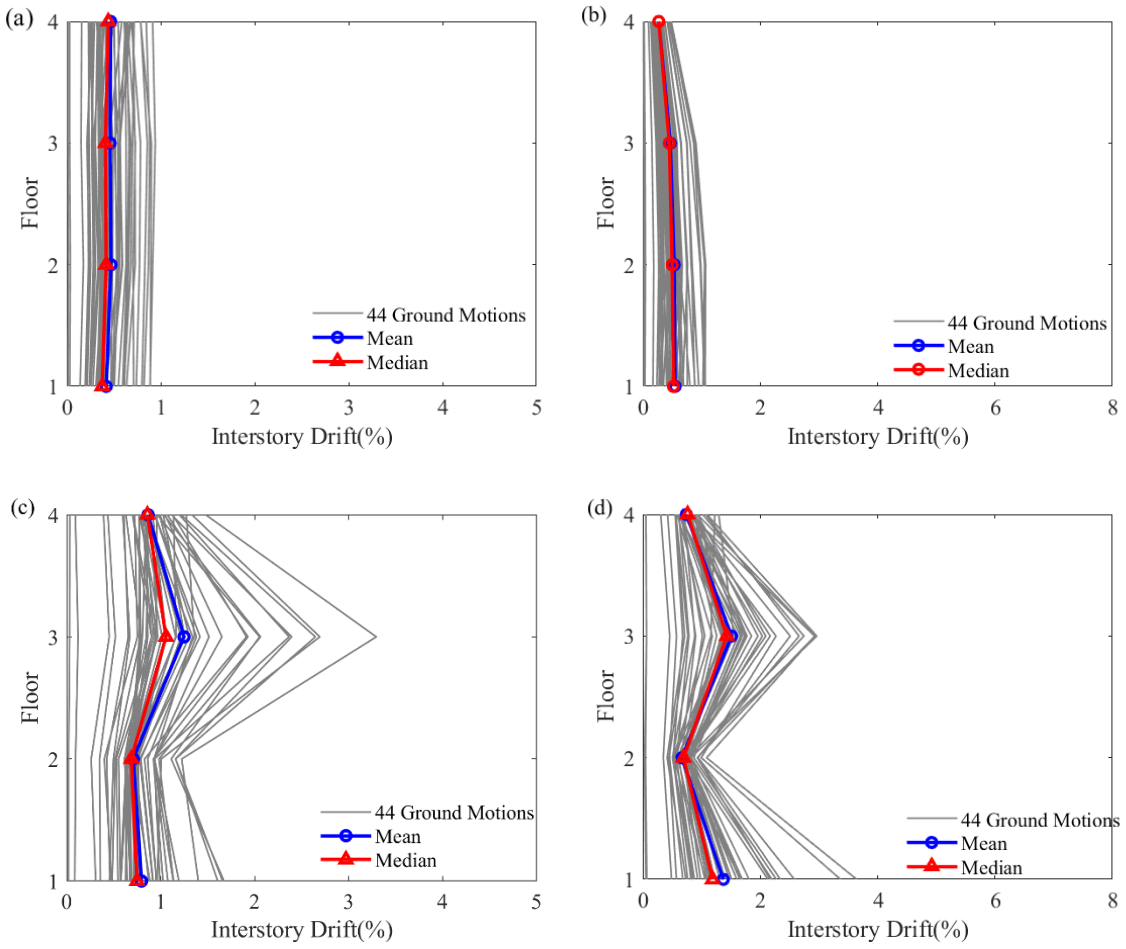

Figure 4-10 IDR of each floor under the effects of DBE level: (a) design a (EW direction); (b) design a (NS direction); (c) bare frame (EW direction); (d) bare frame (NS direction)

4.6. Summary

In this chapter, the performance-based multi-objective optimization structural design was formulated as an optimization problem of three conflicting objectives: the repair cost of the structure, the initial material cost (of the damper device), and robustness measure. Both the linear and nonlinear viscous dampers were considered in the structural design and the optimum design properties of the dampers were sought. The coefficient of variation of the IDRs was treated as the robustness measure.

The proposed optimization framework was applied to a three-dimensional steel frame modeled using the OpenSees software. The uncertainty of the earthquake loads was considered by applying a total of 44 biaxial ground motions. The NSGA-II-based multi-objective optimization approach was implemented in the proposed optimization framework. All the obtained optimum designs were found to be effective in reducing the IDR and PFA of the steel frame.

The optimization results revealed that the robustness measure does not have an utterly linear correlation with damper cost and the repair cost. The damper cost generally dominates the trade-off between the three objectives: the more cost of dampers could result in less repair cost and robustness measure. This kind of compromise decreases as the solutions approaching the extreme points of the Pareto front. Consequently, a continuous increase of the damper cost cannot infinitely improve the seismic performance of the structure.

Choosing the optimal design variables of the dampers is critical for decision-makers. Six optimum designs were selected based on the MCE and DBE levels. Those selected designs can help determine optimal performance and cost-effective design.

CHAPTER V
SIMULATION-BASED OPTIMIZATION OF STRUCTURAL PERFORMANCE INCORPORATING SOIL-STRUCTURE INTERACTION

5.1. Introduction

The overall performance of a structure with energy dissipation system is influenced by (1) its inherent properties, e.g., the dimensions of structural components, and the stiffness of connections; (2) the properties of the energy dissipation system, e.g. the load capacity of the energy dissipation system; (3) the interaction between the structure, the foundation, and the surrounding soil. The interaction between structure, foundation, and soil is referred to as soil-structure interaction (SSI) (Ghosh and Madabhushi 2004; Mason et al. 2013; Oh et al. 2009; Žižmond and Dolšek 2016). In the current seismic design of the structure with the energy dissipation system, the foundation of the structure is usually assumed to be rigid, i.e., a fixed base. Ignoring the effects of SSI may result in inaccurate estimations of the seismic responses of the structure.

Two groups of method can be used to incorporate SSI into the analysis process: (1) direct approach, which explicitly models soil, foundation, structure, and their interaction in a fully coupled way. The direct approach has been applied to the steel moment-resisting frame (Sáez et al. 2013). (2) sub-structural approach, which divides the structure into a superstructure and a substructure, then superimpose their effects. For the sub-structural approach, a series of springs are used to represent the soil-foundation interface (Li et al. 2014; Mason 2011). The sub-structural approach has been implemented in the bridges (Jeremić et al. 2004), reinforced concrete shear walls (Tang and Zhang 2011).

For the sub-structural approach, the ATC-40 (1996) and FEMA 356 (2000) specifications recommend using the elastic or elastic-plastic backbone Winkler-based model to simulate the soil-structure interface. Dutta et al. (2004) used linear and elasto-plastic springs to model the interface of soil-foundation. The authors concluded that the SSI model would result in an increasing force and ductility demand of the buildings. Raychowdhury (2008) proposed the beam-on-nonlinear-Winkler-foundation (BNWF) approach to model the soil-foundation interface and simulate the effect of the nonlinearity of foundation. The BNWF approach was implemented to the steel moment-resisting frame and shear wall building to assess the impacts of SSI on the seismic responses of the structures. The studies also concluded that the SSI would result in a decreasing in force, ductility, and inter-story drift demand (Raychowdhury 2008, 2011). In this chapter, the elastic Winkler-based SSI model is used to simulate the flexibility of the foundation.

In the context of performance-based structural design, an optimization framework is presented to consider multiple conflicting objectives: the seismic-induced losses of structure, the material cost of the energy dissipation system, and the influence of record-to-record variability of the ground motions. In this optimization framework, FEMA P58 is used to quantify the seismic-induced damages of structural and non-structural components (FEMA P-58-1 2018). As an effective energy dissipation system, the fluid viscous damper is used to improve the seismic capacity of the structure, so that it can reduce the earthquake-induced economic losses. The damper cost is served as the optimization objective since the seismic resistance force provided by the damper is proportional to its unit cost. Moreover, the influence of record-to-record variability of the ground motions is considered in the

optimization framework. A robustness measure is proposed to quantify the uncertainty of ground motions. A smaller robustness measure corresponds to a more robust structural design. This proposed optimization framework is applied to the simulation-based seismic design of the structure with flexible and fixed foundations.

This chapter is organized as follows: Section 5.2 illustrates the proposed optimization framework of the performance-based structural design. Section 5.3 demonstrates the details of a four-story steel moment-resisting frame and its numerical model. Section 5.4 presents the optimization results of both fixed and flexible foundations. Section 5.5 provides a summary of the study in this chapter.

5.2. Performance-Based Optimization Framework for Structural Design

In this chapter, an optimization framework of performance-based structural design is used to evaluate the impact of SSI on initial construction material cost, seismic performance, and the robustness measure of the structural design. For the initial construction material cost, only the material cost of the energy dissipation system is considered.

5.2.1. The Behavior of Fluid Viscous Damper under SSI Effects

The fluid viscous damper (FVD) is considered as an effective energy dissipation system to enhance the seismic performance of the structure and mitigate the earthquake-induced structure damage. FVD is a kind of velocity-based damper that dissipates the seismic energy by increasing the damping ratio of the structure.

For a structure with FVD, the total effective damping ratio of the structure consists of both structural inherent damping ratio and damper's damping ratio. The inherent damping ratio is usually assumed to be 5%. As specified in FEMA 356 (2000) and ASCE 41-17 (2017), the damper's damping ratio should be less than 30% of critical damping in the fundamental mode of the rehabilitated building. The calculation of damper's damping ratio is determined by the inherent properties of the structure and the damping coefficient of FVD.

The derivation of the damping coefficient for the linear FVD is presented as follows: for a given multi-degree of freedom (MDOF) system, the identical damping coefficient of linear FVDs are assumed to be distributed along with the building height. The MDOF system is assumed to be a flexible building and subjected to a sinusoidal displacement time history in both horizontal and vertical directions, expressed as:

$$u(t) = u_0 \sin \omega t, \quad 0 < t < \frac{2\pi}{\omega}$$
$$v(t) = v_0 \sin \omega t, \quad 0 < t < \frac{2\pi}{\omega} \tag{5.1}$$

where $u(t)$, u_o, and ω represent the horizontal displacement of the damper, the amplitude of the horizontal displacement, and the loading frequency. $v(t)$ and v_o represent the vertical displacement of the damper and its amplitude.

The seismic response of one floor in the MODF system is illustrated in Figure 5-1. The damper is diagonally placed with an inclination angle of θ. The horizontal and vertical

displacement of the damper at a moment of movement are represented by u and v, respectively.

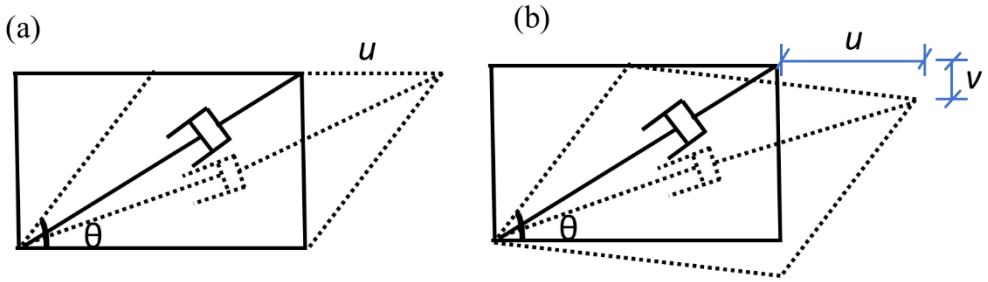

Figure 5-1 Fluid viscous damper behavior: (a) shear building assumption; (b) flexible building assumption

The axial elongation of the supplemental damper, u_d can be derived by:

$$u_d = u\cos\theta - v\sin\theta \tag{5.2}$$

The relative axial velocity of the damper can be calculated as:

$$\dot{u}_d = \frac{2\pi}{T}\cos\frac{2\pi t}{T}(u_0\cos\theta - v_0\sin\theta) \tag{5.3}$$

where $\dot{u}_d$ is the relative velocity between two ends of the damper, T is the fundamental period of the structure. The resistance force of the damper can be expressed as:

$$F_d = C_d\,\mathrm{sgn}\left(\dot{u}_d\right)\left|\dot{u}_d\right|^{\alpha} = K_d u(t) \tag{5.4}$$

where K_d is the stiffness of brace and damper portion, C_d is the supplemental damping coefficient, sgn is the signum function, and α is the velocity exponent of the damper.

The energy dissipated by one damper in one cycle of vibration can be derived as:

$$E_d = \int F_d d_{u_d} = \int C_d \dot{u}_d d_{u_d} = \int_0^{2\pi/\omega} C_d \dot{u}_d{}^2 d_t$$
$$= \pi C_d (u_0 \cos\theta - v_0 \sin\theta)^2 \omega \tag{5.5}$$

The relationship between the energy dissipated by all dampers in one cycle of vibration and the elastic strain energy of the MDOF system is given in FEMA 356 (2000), as:

$$\xi_d = \frac{\sum_{i=1}^{N_F} E_{d,i}}{4\pi \sum_{i=1}^{N_F} E_s} \tag{5.6}$$

where ξ_d is the damper's damping ratio in the fundamental vibration mode, $E_{d,i}$ represents the dissipated energy by the i-th damper in one cycle of vibration, N_F is the number of stories of the system, E_s is the elastic strain energy of the system, expressed as:

$$\sum_{i=1}^{N_F} E_s = \frac{2\pi^2}{T^2} \sum_{i=1}^{N_F} m_i \phi_i^2 \tag{5.7}$$

where m_i represents the mass of the i-th floor, and ϕ_i represents the horizontal displacement of the i-th floor. The energy dissipated by all dampers can be expressed as:

$$\sum_{i=1}^{N_F} E_{d,i} = \sum_{i=1}^{N_F} \pi C_d (u_i \cos\theta - v_i \sin\theta)^2 \omega$$
$$= \frac{2\pi^2}{T} \sum_{i=1}^{N_F} C_d (u_i \cos\theta - v_i \sin\theta)^2 \tag{5.8}$$
$$= \frac{2\pi^2}{T} \sum_{i=1}^{N_F} C_d (\phi_i \cos\theta_i - \phi_{v,i} \sin\theta_i)^2$$

where $\phi_{v,i}$ is the relative vertical displacement of the damper at the i-th story.

The damper's damping ratio, ξ_d can be calculated by substituting equation (5.7) and (5.8) into equation (5.6), which yields:

$$\xi_d = \frac{\frac{2\pi^2}{T}\sum_{i=1}^{N_F} C_d(\phi_i \cos\theta_i - \phi_{v,i}\sin\theta_i)^2}{4\pi\frac{2\pi^2}{T^2}\sum_{i=1}^{N_F} m_i\phi_i^2} = \frac{T\sum_{i=1}^{N_F} C_d(\phi_i \cos\theta_i - \phi_{v,i}\sin\theta_i)^2}{4\pi\sum_{i=1}^{N_F} m_i\phi_i^2} \tag{5.9}$$

C_d of the supplemental linear FVD at each floor can be expressed as:

$$C_d = \frac{4\pi\xi_d\sum_{i=1}^{N_F} m_i\phi_i^2}{T\sum_{i=1}^{N_F}(\phi_i \cos\theta_i - \phi_{v,i}\sin\theta_i)^2} \tag{5.10}$$

C_d is one major factor that determines the peak resistance force of the FVD (see Equation (5.4)). The unit cost of the damper is proportional to its peak resistance force, as listed in Table 5-1 (Liu 2010). The interpolation method is used when the peak resistance force is in the range of the provided values. Herein, the cost of FVD is treated as one of the optimization objectives.

Table 5-1 Unit damper device cost for different peak force (based on data from Liu 2010)

Peak Force (kips)	Cost (Dollars, $)
55	3,200
110	3,600
220	6,400
330	8,700
440	11,000

5.2.2. Seismic Repair Costs Estimation-FEMA P58

The FEMA P-58 method can be used to evaluate the seismic performance of a structure in terms of the repair cost (FEMA P-58-2 2018). The repair cost is composed of the costs of both structural and non-structural components. Each vulnerable structural and non-structural component has its corresponding fragility curve and the consequence function to estimate its repair cost. The components that are vulnerable to the same engineer demand parameter (EDP) can be categorized into the same performance group (PG). The EDP values are typically assumed to follow the lognormal distribution.

For a component could be experienced in four damage states, the total repair cost of this component can be calculated as:

$$RC[C_{repair}] = \sum_{i=1}^{4} P[D = DS_i \,|\, EDP] \cdot RC[C_{repair} \,|\, DS_i] \tag{5.11}$$

where $RC[C_{repair}|DS_i]$ the repair cost of the component under damage state DS_i. $RC[C_{repair}]$ represents the total repair cost of the component. The total repair cost of the structure is calculated by summing the repair costs of both structural and non-structural components, expressed as:

$$RC[C_{repair\_total}] = RC[C_{repair\_SS}] + RC[C_{repair\_NS}] \tag{5.12}$$

The critical fragility information of the structural components, non-structural drift, and acceleration sensitive components used in this study are provided in Table 5-2. M_{EDP} and β represent the median and standard deviation of the EDP values for each damage state.

This critical fragility information is referenced from the PACT (Performance Assessment Calculation Tool) fragility database. The cost multiplier is set to one. The dispersion input is set to zero, which reflects a precise value of unit cost. If the total repair cost of the building exceeds 40% of the replacement cost, the building is typically demolished (FEMA P-58-1 2018).

Table 5-2 Critical fragility information on structural and non-structural components

System	EDP	Damage State	M_{EDP}	β
Curtain wall	IDR	Glass cracking	0.0338	0.4
		Glass falls from frame	0.0383	0.4
Gypsum board partitions	IDR	Screw pop-out, slight crushing	0.005	0.4
		Moderate cracking or crushing	0.01	0.3
		Buckling of studs, significant cracking or crushing	0.021	0.2
Wall finishing	IDR	Wall paper warped and torn	0.0021	0.6
Suspended ceiling	PFA	5 % of ceiling grid, tile damage	1.47	0.3
		30% of ceiling grid, tile damage.	1.88	0.3
		50% of ceiling grid, tile damage.	2.03	0.3
Fire sprinkler drop	PFA	Spraying, dripping leakage at drop joints	0.95	0.4
Roof tile	PFA	Minor damage, tiles dislodged	1.1	0.4
		Major portion of tile dislodged	1.4	0.4
Steel moment frame	IDR	Local buckling	0.03	0.3
		Lateral-torsional distortion	0.04	0.3
		Fracture in buckled region	0.05	0.3

5.2.3. Robustness Measure Regarding Ground Motion Variability

In performance-based structural design, ASCE 7-10 (2010) explicitly defines that a minimum of three ground motion records should be applied to the structure model. Herein, the far-field record set of FEMA-P695 PEER NGA database is adopted in this study to consider the uncertainties of the ground motion records (FEMA P695 2009). This database consists of 22 pairs of biaxial ground motion records. By rotating each pair of

record 90 degrees, a total of 44 pairs of ground motions are generated and will be applied to the structure model in this study.

The concept of robust structural design is involved in this study to make the responses of the structure insensitive to the uncertainties of the ground motions. Thereby a reliable and efficient structural design can be provided to the designer. Generally, the mean and standard deviation values of the EDPs are treated as the robustness measures (Doltsinis and Kang 2004). In this study, the maximum COV value of IDRs is treated as the robustness measure and is incorporated in the optimization framework to seek the minimum value, expressed as:

$$COV_D = \max\left(\frac{\sigma_{NF}\left(IDR_i\right)}{u_{NF}\left(IDR_i\right)}\right),\ i = 1,2,\ldots,44 \tag{5.13}$$

where NF is the number of stories of the structure, μ and σ represent the mean and standard deviation of IDRs of each story, i represents the number of ground motions, COV_D is the maximum COV value. A smaller COV_D means that the structure is more robust against ground motion uncertainty.

Herein, the performance-based optimization framework for structural design can be formulated as: find optimal sets of design parameters (i.e., α, K_d, and C_d of FVD) such that the initial construction cost (i.e., the cost of FVD), the repair cost of the structure ($RC[C_{repair\_total}]$), and the robustness measure (COV_D) are minimized. These conflicting optimization objectives result in a multi-objective optimization problem. Herein, the Non-dominated Sorting Genetic Algorithm II (NSGA-II) as a fast-non-dominated sorting

procedure, a parameterless niching operator, and an elitist persevering approach is implemented to solve the multi-objective optimization problem. The basic principles of NSGA-II are selection, recombination, and mutation to populate a new generation until the solutions reach their optimum state (Deb et al. 2002). NSGA-II is used to determine the Pareto front since it can maintain a good distribution of the solutions and preserve a diversity of solutions (Erbas et al. 2006). The Pareto front consists of a set of non-dominated optimal solutions, which visually displays the level of compromise that needed from one objective to improve the other.

5.3. Case Study: Steel Moment-Resisting Frame Building with Viscous Dampers

5.3.1. Building Design

In order to evaluate the effects of SSI on the seismic response of the structure, a four-story steel frame (office building) adopted from Ray Chaudhuri and Villaverde (2008) is considered in this study. This steel frame is designed according to UBC-1994 (Uniform Building Code 1994), zone IV response spectra, which is a representative of a large quantity of existing steel frame buildings sitting on stiff soil in the California area.

The building has three bays in each direction, each bay of 24 ft (see Figure 5-2). This office building is assumed to be supported by isolated square footings. The soil beneath the footings is assumed to be dense silty soil and the site classification is D from NEHRP (2000). The size of the footings are 1.56 m×1.56 m×0.6 m for external footings, and 2.00 m×2.00 m×0.6 m for internal footings. The design loads are 2.8 MN and 5.6 MN

for the external and internal footings, respectively, which are based on the calculation procedures of a typical office building presented in a previous study (Raychowdhury 2011).

Both fixed and flexible foundations are considered in this case study. The fundamental periods of the frame with fixed and flexible foundations are 1.30 sec and 1.36 sec, respectively.

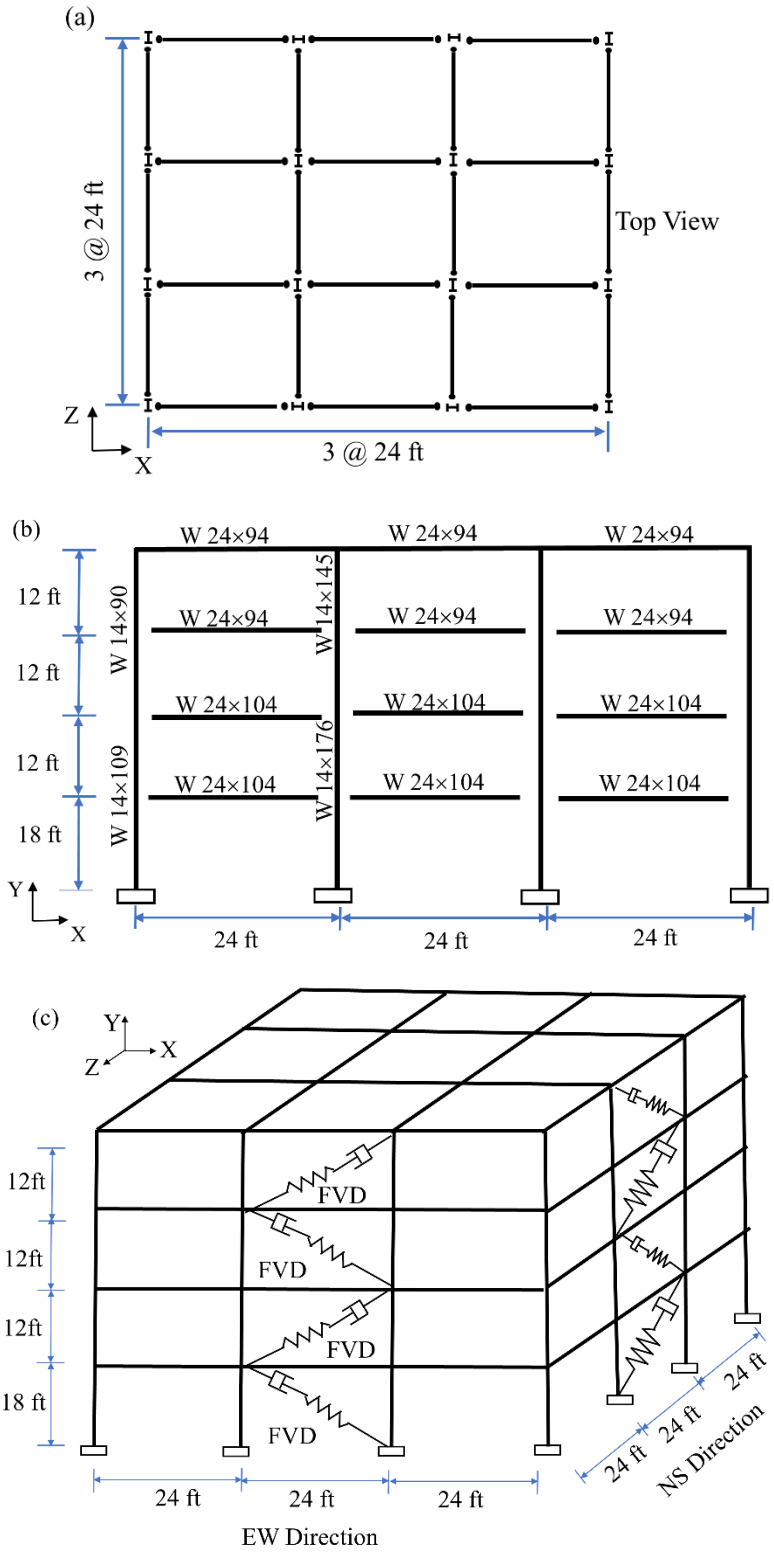

Figure 5-2 Plan view of the steel frame of the office building

5.3.2. Details of the foundation and SSI models

A 3D (three-dimensional) numerical model of the steel frame was developed using OpenSees (Open System for earthquake engineering simulation). The 3D numerical model can consider the influence of the soil beneath the foundations in multiple directions. The interaction between the soil and foundation interface is modeled using the elastic Winkler-based SSI model. The foundation is assumed to be placed on a series of elastic Winkler springs, and the lateral movement is represented by an elastic spring, as shown in Figure 5-3.

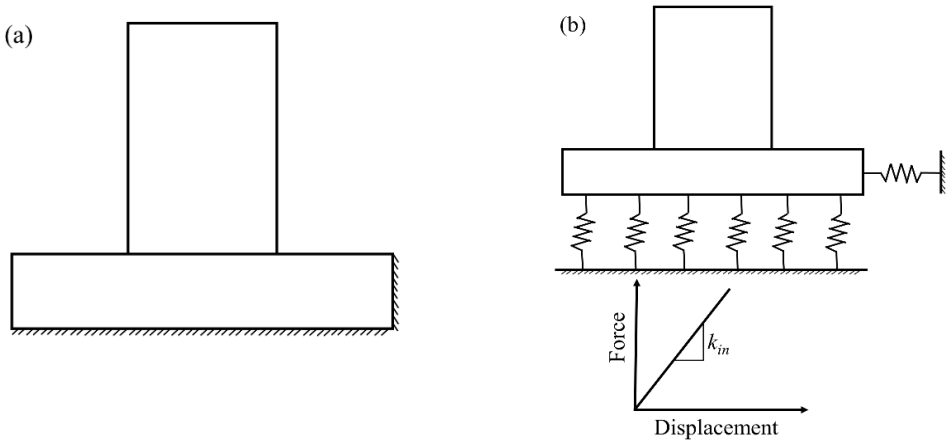

Figure 5-3: (a) fixed foundation; (b) flexible foundation: elastic Winkler-based SSI model

The stiffnesses of the springs are calculated according to the method from Gazetas (1991), as shown below:

The stiffness of the vertical spring, k_v:

$$k_v = \frac{GL}{1-v}[0.73+1.54(\frac{B}{L})^{0.75}] \tag{5.14}$$

The stiffness of the horizontal spring, k_x:

$$k_x = \frac{GL}{2-v}[2 + 2.5(\frac{B}{L})^{0.85}] \tag{5.15}$$

where G represents the shear modulus of the soil. v is the Poisson's ratio of soil. L and B are the length and width of the foundation.

The general bearing capacity of the foundation is calculated based on the equation from Terzaghi (1943), expressed as:

$$q_{ult} = cN_cF_{cs}F_{cd}F_{ci} + \gamma D_f N_q F_{qs} F_{qd} F_{qi} + 0.5\gamma BN_\gamma F_{\gamma s} F_{\gamma d} F_{\gamma i} \tag{5.16}$$

where q_{ult} is the ultimate bearing capacity per unit area of the footing. c is the cohesion. γ is the unit weight of soil. D_f is the depth of embedment. N_c, N_q, and N_γ are bearing capacity factors. F_{cs}, F_{qs}, and $F_{\gamma s}$ are shape factors. F_{cd}, F_{qd}, and $F_{\gamma d}$ are the depth factors. F_{ci}, F_{qi}, and $F_{\gamma i}$ are inclination factors.

The primary soil parameters that control the stiffness and strength of the foundation system are considered as follows: cohesion equal to 5kPa, friction angle equal to 38 deg, unit weight equal to 18 kN/m^3, shear modulus equal to 60MPa and the Poisson's ratio equal to 0.35. The values of those parameters are selected based on the available information of laboratory and field test data of dense silty sand in the Los Angeles area (Jones et al. 2002; NEHRP 2000). The stiffness intensity ratio of the spring is considered as 5. The end length ratio of the spring is assumed as 10%. The ratio of vertical spring spacing to the length of the foundation is assumed as 2%. The tension capacity is assumed to be 5% of the total

bearing capacity of the foundation. The nonlinear dynamic time history analysis is performed to assess the seismic behavior of the three-dimensional numerical model.

5.3.3. Validation of the Numerical Model

In order to verify the prediction ability of the 3D numerical model in terms of its seismic performance, the numerical model verification is required for the beam and column properties, the soil and spring parameters of the SSI model, and the properties of the foundation. Hence, an OpenSees model of the 4-story steel frame is developed to validate against the simulation results in the literature. According to the literature, the three-bay frame in the NS direction is considered, as shown in Figure 5-4 (a). Details of the sizes and dimensions of the selected frame are shown in Figure 5-4.

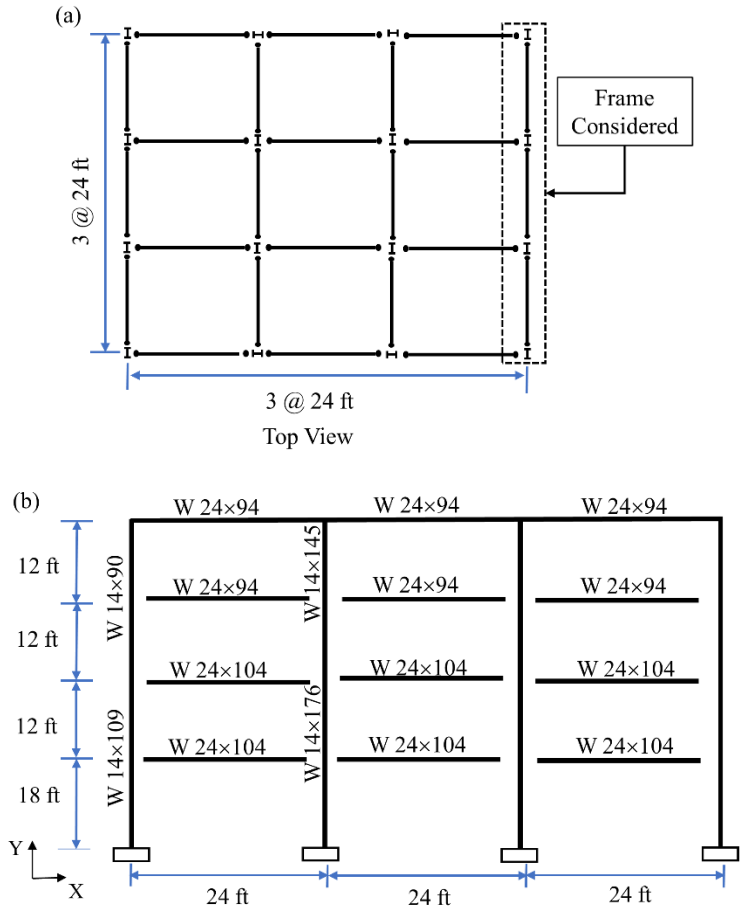

Figure 5-4 Section of the frame considered in numerical model validation

The beams of the numerical model are modeled as the nonlinear beams with hinges. The nonlinearities of columns are modeled using the nonlinear beam-column elements. The kinematic material hardening factor of 3% is considered for the nonlinear elements. The sizes of footings remain the same as described in section 5.3.1. The values of primary soil parameters and the properties of the springs remain the same as defined in section 5.3.2. In this case, the simulation results of the frame with fixed and flexible foundations are compared with those from Raychowdhury (2011).

Nonlinear time history analysis is performed to assess the seismic response of the frame under the scaled 1994 Northridge ground motion of MCE (maximum considered earthquake) level. The recorded time history of the 1994 Northridge ground motion is shown in Figure 5-5.

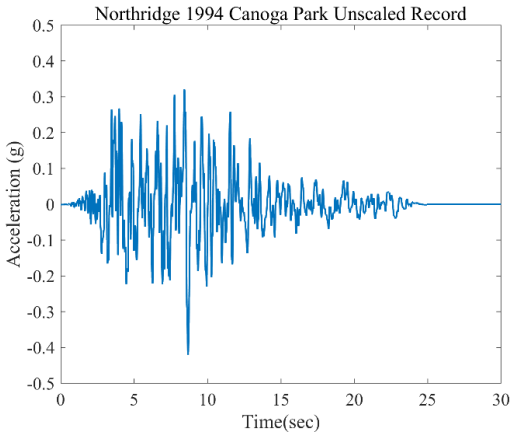

Figure 5-5 Time history of the 1994 Northridge ground motion

The story displacements are recorded and compared with the results in the literature. Figure 5-6 shows the recorded story displacement of the frame with fixed and flexible foundations. It can be observed that the story displacement dramatically increases as the foundation changed from fixed to flexible. The maximum difference of the recorded displacement occurs at the roof floor, which is 0.0128 m. Results using the model implemented in this study are in good agreement with those reported in the literature.

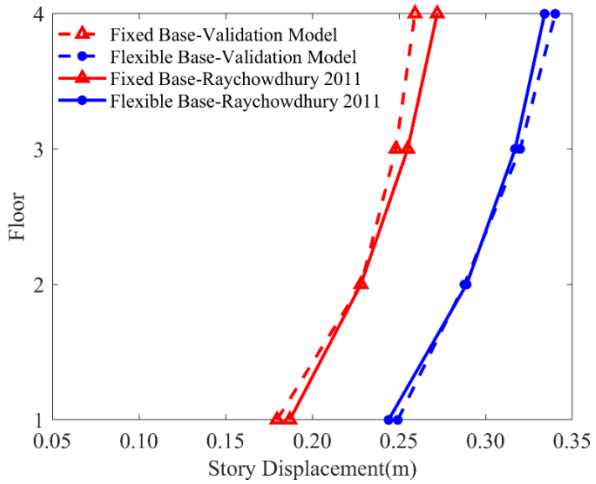

Figure 5-6 Peak story displacement of the validation frame

5.4. Optimization Results of Fixed and Flexible Foundation

5.4.1. Optimization Results: Fixed Foundation

As described in section 5.2, the proposed optimization framework is configured by minimizing the repair cost of the structure, the total cost of FVDs, and the robustness measure regarding the uncertainty of ground motion. The stiffness of brace and damper portion K_d, the velocity exponent α, and the damping coefficient C_d are selected as the design variables. The FVDs located on the same floor and the same direction of the building are assumed to have the same design parameters.

The variation ranges of each design variable are defined as follows: (1) K_d can vary from 0 to 1500 kips/in with an increasing interval of 120 kips/in. (2) α can vary from 0.3 to 1.0 with an increasing interval of 0.1. (3) C_d can vary from 0 to 70 kips-sec/in with an increasing interval of 10 kips-sec/in. All 44 biaxial ground motion records are scaled to the MCE level. The total replacement cost of the building is estimated to be $4,147,200, based

on a unit cost of $200 per square feet. The NSGA-II is implemented to solve this multi-objective optimization problem with 20 generations and 22 individuals in each generation.

In this case study, the performance-based optimization framework for structural design only considers the SSI of the steel frame on the site class D. Furthermore, the damages of the foundation and the FVD are not considered in the optimization framework. The seismic-induced damages only occur in the structural and non-structural components.

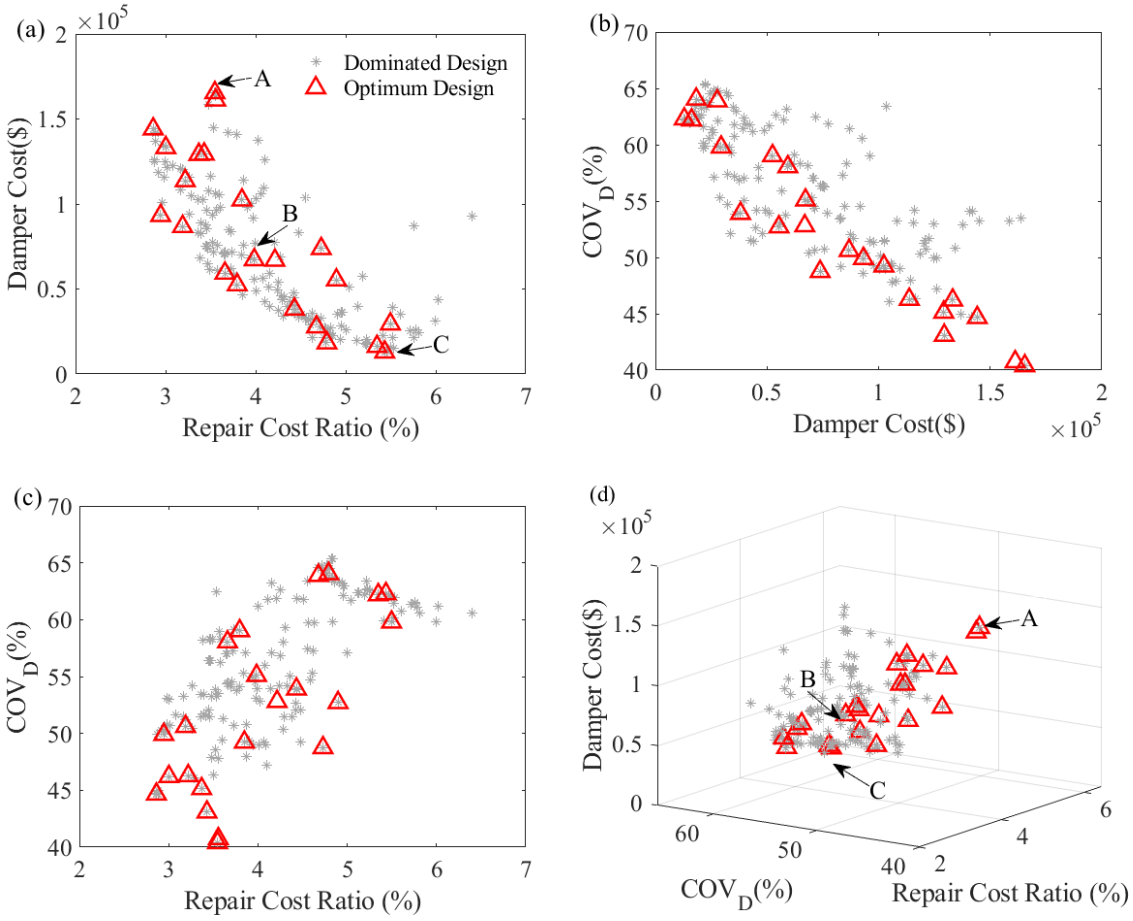

Figure 5-7 Pareto front and dominated designs of the frame with fixed foundation: (a) repair cost ratio versus damper cost; (b) damper cost versus COV_D; (c) repair cost ratio versus COV_D; (d) 3D view

Dominated designs and the corresponding Pareto front are shown in Figure 5-7. This Pareto front provides the trade-off among the three optimization objectives. Generally, a higher damper cost leads to a lower repair cost ratio. A smaller COV_D value indicates a more robust design of the structure. The values of the optimum designs along the Pareto front and the corresponding design parameters of each FVD are listed in Table 5-3 and Table 5-4. Herein, the repair cost ratio is normalized by the total replacement cost of the structure. Herein, the dollar amounts for repair cost and the initial material cost are considered in today's dollars (not adjusted for inflation).

The optimized damper cost varies from \$12,896 to \$165,474. In general, for a given damper cost, both COV_D and repair cost ratio can be significantly reduced, i.e., with the damper cost of \$66,893, the COV_D can be improved from the worst design of 64.05% to the design of 52.81%. The repair cost ratio can be improved from the worst design of 5.50% to the design of 4.21%. For a more robust design with smaller COV_D or a design with lower repair cost ratio, the damper cost can also be significantly changed, i.e., the damper cost can increase from \$66,893 to \$73,778 with COV_D as 48.75%; and the damper cost can increase from \$66,893 to \$93,191 with repair cost ratio as 2.95%.

Hence, choosing a suitable, cost-effective design is critical for structure designers and construction investors. In this case, three optimum designs: design A, design B, and design C, corresponding to the most expensive, the medium, and the least expensive damper design, are selected and their performance will be evaluated in details in a later section.

Table 5-3 Properties of each FVD along the Pareto Front of the frame with fixed foundation-EW direction

	1st floor			2nd floor			3rd floor			4th floor			Objectives		
Number	C_d	K_d	α	C_d	K_d	α	C_d	K_d	α	C_d	K_d	α	RC (%)	DC ($)	COV_D (%)
1	10	120	0.5	10	120	0.3	60	720	0.5	60	720	0.5	4.79	18250	64.05
2	40	480	0.5	10	120	0.4	20	240	0.5	30	360	0.3	5.43	12896	62.29
3	70	840	1.0	70	840	0.3	10	120	1.0	10	120	0.3	3.55	165474	40.39
4	70	840	0.8	70	840	0.9	10	120	1.0	10	120	0.3	2.86	144162	44.66
5	10	120	0.7	10	120	0.3	70	840	0.5	60	720	0.5	5.50	29438	59.79
6	10	120	0.3	40	480	0.3	10	120	1.0	10	120	0.3	4.90	55319	52.71
7	70	840	0.5	10	120	0.4	20	240	0.5	30	360	0.3	5.35	16189	62.20
8	60	720	0.8	10	120	0.9	10	120	1.0	50	600	0.3	3.99	67218	55.09
9	70	840	1.0	70	840	0.3	10	120	1.0	10	120	0.3	3.56	161158	40.74
10	70	840	0.8	10	120	0.9	10	120	0.7	60	720	0.4	3.19	86745	50.61
11	70	840	0.9	70	840	0.4	10	120	1.0	30	360	0.3	3.43	129382	43.09
12	20	240	0.5	10	120	0.7	20	240	0.6	60	720	0.3	4.43	38118	53.90
13	70	840	0.8	70	840	0.4	10	120	1.0	30	360	0.3	3.22	113707	46.28
14	70	840	0.8	50	600	0.9	10	120	1.0	30	360	0.3	3.37	129171	45.14
15	10	120	0.7	30	360	0.3	70	840	0.5	60	720	0.5	4.21	66893	52.81
16	20	240	0.8	50	600	0.6	50	600	0.5	70	840	0.7	3.66	59305	58.05
17	20	240	0.8	50	600	0.4	50	600	0.6	70	840	0.7	3.80	52452	59.03
18	70	840	0.8	70	840	0.3	50	600	0.7	10	120	0.3	2.95	93191	49.91
19	70	840	0.8	70	840	0.9	10	120	1.0	10	120	0.3	3.00	133169	46.21
20	70	840	0.7	70	840	0.3	10	120	1.0	30	360	0.3	3.85	102359	49.24
21	10	120	0.5	10	120	1.0	70	840	0.5	60	720	0.5	4.68	27694	63.89
22	10	120	0.3	70	840	0.4	10	120	1.0	10	120	0.3	4.73	73778	48.75

Note: RC represents the normalized repair cost. DC represents the total cost of damper devices. The units of C_d and K_d are kips-sec/in and kips/in, respectively.

Table 5-4 Properties of each FVD along the Pareto Front of the frame with fixed foundation-NS direction

	1st floor			2nd floor			3rd floor			4th floor			Objectives		
Number	C_d	K_d	α	C_d	K_d	α	C_d	K_d	α	C_d	K_d	α	RC (%)	DC ($)	COV_D (%)
1	70	840	0.5	70	840	0.5	70	840	0.6	40	480	0.4	4.79	18250	64.05
2	40	480	0.5	20	240	0.5	70	840	0.3	30	360	0.4	5.43	12896	62.29
3	70	840	1.0	70	840	1.0	50	600	1.0	70	840	1.0	3.55	165474	40.39
4	70	840	1.0	30	360	1.0	70	840	1.0	70	840	1.0	2.86	144162	44.66
5	10	120	0.5	70	840	0.5	70	840	1.0	40	480	0.4	5.50	29438	59.79
6	70	840	1.0	30	360	1.0	60	720	0.5	70	840	0.4	4.90	55319	52.71
7	40	480	0.5	20	240	0.5	70	840	0.3	30	360	0.7	5.35	16189	62.20
8	10	120	1.0	40	480	0.6	20	240	0.3	40	480	1.0	3.99	67218	55.09
9	70	840	1.0	70	840	1.0	50	600	0.9	70	840	1.0	3.56	161158	40.74
10	50	600	1.0	30	360	0.7	10	120	0.6	70	840	1.0	3.19	86745	50.61
11	70	840	1.0	30	360	1.0	50	600	1.0	10	120	1.0	3.43	129382	43.09
12	70	840	0.9	20	240	0.3	70	840	0.5	20	240	0.6	4.43	38118	53.90
13	70	840	1.0	30	360	1.0	70	840	1.0	20	240	1.0	3.22	113707	46.28
14	70	840	1.0	30	360	1.0	70	840	1.0	70	840	0.4	3.37	129171	45.14
15	60	720	1.0	70	840	0.5	70	840	1.0	40	480	1.0	4.21	66893	52.81
16	60	720	0.8	30	360	0.3	10	120	1.0	40	480	1.0	3.66	59305	58.05
17	40	480	0.8	30	360	0.3	10	120	1.0	20	240	1.0	3.80	52452	59.03
18	70	840	0.9	30	360	0.3	60	720	1.0	70	840	1.0	2.95	93191	49.91
19	70	840	1.0	10	120	1.0	50	600	1.0	70	840	1.0	3.00	133169	46.21
20	70	840	1.0	70	840	1.0	50	600	1.0	10	120	1.0	3.85	102359	49.24
21	70	840	0.5	70	840	0.5	70	840	0.6	40	480	0.4	4.68	27694	63.89
22	70	840	1.0	30	360	1.0	60	720	1.0	20	240	0.4	4.73	73778	48.75

Note: RC represents the normalized repair cost. DC represents the total cost of damper devices. The units of C_d and K_d are kips-sec/in and kips/in, respectively.

5.4.2. Optimization Results: Flexible Foundation

In order to incorporate the influence of SSI on the seismic responses of structure, the same performance-based optimization framework is applied to the steel frame with a flexible foundation. The ranges of K_d, C_d, and α of FVD remain the same as defined in section 5.4.1. NSGA-II is implemented to solve this multi-objective optimization problem with 20 generations and 22 individuals in each generation.

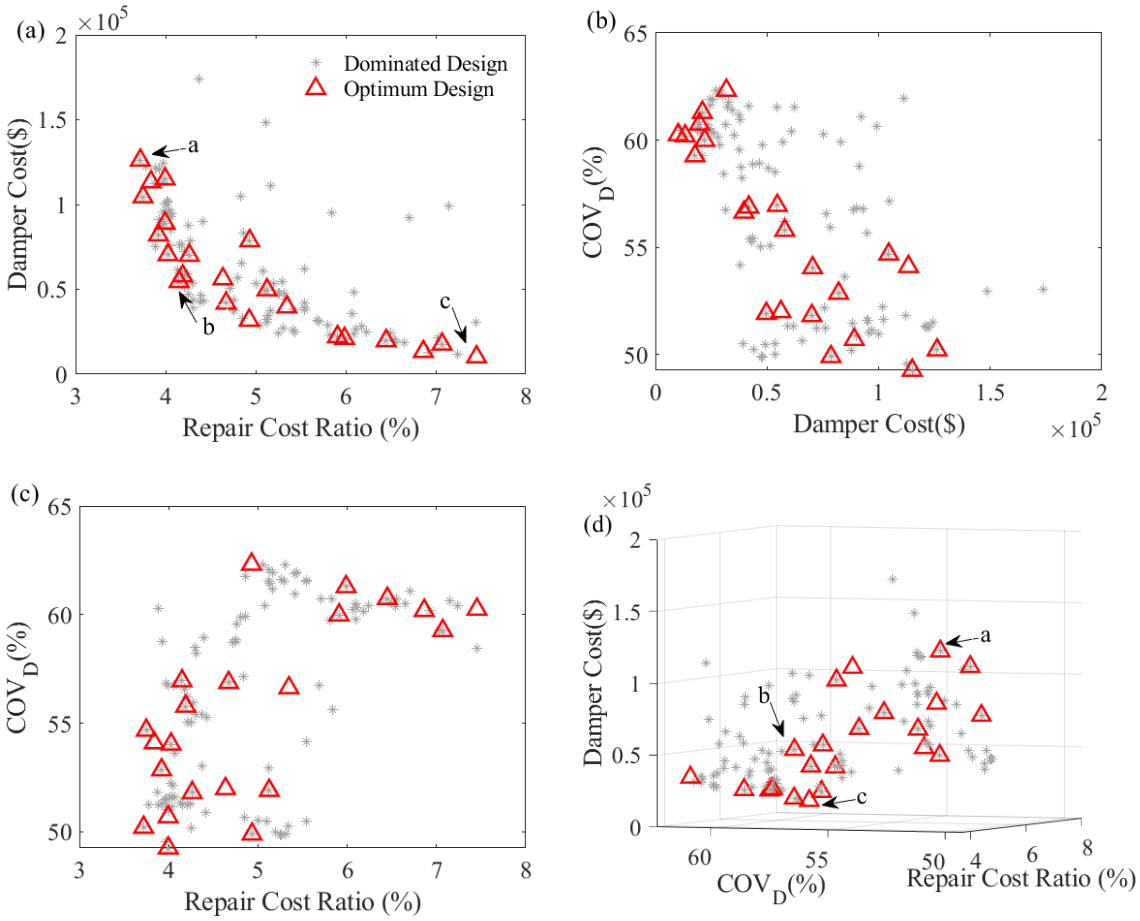

Figure 5-8 Pareto front and dominated designs of the frame with flexible foundation: (a) repair cost ratio versus damper cost; (b) damper cost versus COV_D; (c) repair cost ratio versus COV_D; (d) 3D view

Dominated designs and the corresponding Pareto front are shown in Figure 5-8 (d). The values of the optimum design variables of each FVD and the corresponding values of objectives are listed in Table 5-5 and Table 5-6. With the highest damper cost of $126,168, the COV_D can be improved from the worst design of 62.32% to the design of 50.21%, and the repair cost ratio can be improved from the worst design of 7.45% to the design of 3.72%.

It is observed that the repair cost ratio and the COV_D of the frame with a fixed foundation are slightly lower than the one with a flexible foundation when the damper cost is similar. For example, for the case of the fixed foundation with a damper cost of $59,305, the repair cost ratio is 3.66%. For the case of the flexible foundation with a damper cost of $57,938, the repair cost ratio is 4.19%. The value of COV_D is reduced from 58.05% (fixed foundation) to 55.79% (flexible foundation).

In order to select the best performing model with optimal design variables of FVDs, three optimum designs: design a, design b, and design c, corresponding to the most expensive, the medium, and the least expensive damper design, are selected and and their seismic performance will be evaluated in details in the followed section.

Table 5-5 Properties of each FVD along the Pareto Front of the frame with flexible foundation-EW direction

	1st floor			2nd floor			3rd floor			4th floor			Objectives		
Number	C_d	K_d	α	C_d	K_d	α	C_d	K_d	α	C_d	K_d	α	RC (%)	DC ($)	COV_D (%)
1	10	120	0.4	10	120	0.6	20	240	0.3	60	720	0.3	7.45	10189	60.25
2	50	600	0.6	50	600	0.3	20	240	0.3	70	840	0.6	4.93	31778	62.32
3	40	480	0.6	60	720	1.0	50	600	0.5	60	720	1.0	4.00	115040	49.26
4	60	720	0.6	60	720	1.0	50	600	1.0	60	720	0.8	3.72	126168	50.21
5	10	120	0.4	10	120	0.6	20	240	0.3	60	720	0.3	7.07	17714	59.27
6	10	120	0.6	20	240	0.6	20	240	0.6	10	120	0.5	6.45	19731	60.75
7	40	480	0.6	60	720	1.0	50	600	0.5	60	720	1.0	3.75	104531	54.68
8	60	720	0.7	10	120	0.3	20	240	1.0	30	360	0.5	4.19	57938	55.79
9	60	720	0.7	10	120	1.0	20	240	0.6	30	360	0.5	3.92	82050	52.86
10	60	720	0.7	30	360	0.3	20	240	0.7	30	360	0.6	4.15	54597	56.95
11	10	120	0.6	20	240	0.6	20	240	0.6	10	120	0.6	5.99	21012	61.29
12	50	600	0.3	10	120	0.6	60	720	0.7	10	120	0.5	5.35	39655	56.64
13	40	480	0.6	60	720	0.8	50	600	0.5	30	360	0.5	4.26	70067	51.81
14	60	720	0.7	10	120	0.6	20	240	1.0	30	360	0.6	4.03	70399	54.04
15	40	480	0.3	60	720	0.7	20	240	1.0	60	720	1.0	3.99	89080	50.70
16	30	360	0.3	30	360	0.4	20	240	0.3	70	840	0.9	4.93	78632	49.90
17	70	840	0.4	10	120	0.6	50	600	0.3	60	720	0.4	6.86	13318	60.19
18	40	480	0.6	60	720	1.0	50	600	1.0	30	360	0.5	3.84	113351	54.10
19	20	240	0.7	10	120	0.3	30	360	0.6	30	360	0.3	4.64	56193	51.99
20	60	720	0.7	40	480	0.3	20	240	0.3	30	360	0.5	4.67	41831	56.87
21	10	120	0.6	10	120	0.6	70	840	0.3	40	480	0.5	5.13	49688	51.91
22	10	120	0.6	10	120	0.6	20	240	0.3	60	720	0.5	5.91	22097	59.98

Note: RC represents the normalized repair cost. DC represents the total cost of damper devices. The units of C_d and K_d are kips-sec/in and kips/in, respectively.

Table 5-6 Properties of each FVD along the Pareto Front of the frame with flexible foundation-NS direction

	1st floor			2nd floor			3rd floor			4th floor			Objectives		
Number	C_d	K_d	α	C_d	K_d	α	C_d	K_d	α	C_d	K_d	α	RC (%)	DC ($)	COV_D (%)
1	40	480	0.3	10	120	0.6	70	840	0.5	10	120	0.3	7.45	10189	60.25
2	70	840	0.5	20	240	0.9	70	840	0.6	20	240	0.3	4.93	31778	62.32
3	60	720	0.9	30	360	0.7	70	840	1.0	20	240	0.8	4.00	115040	49.26
4	60	720	0.9	30	360	0.7	70	840	0.8	20	240	1.0	3.72	126168	50.21
5	40	480	0.3	10	120	0.6	50	600	0.6	70	840	1.0	7.07	17714	59.27
6	50	600	0.3	30	360	0.6	10	120	0.7	40	480	0.6	6.45	19731	60.75
7	60	720	0.8	30	360	0.7	70	840	1.0	20	240	0.8	3.75	104531	54.68
8	20	240	0.9	20	240	0.3	70	840	0.6	70	840	0.6	4.19	57938	55.79
9	40	480	1.0	50	600	0.3	70	840	0.8	70	840	1.0	3.92	82050	52.86
10	40	480	0.8	20	240	0.3	70	840	0.3	70	840	1.0	4.15	54597	56.95
11	50	600	0.4	30	360	0.6	10	120	0.7	40	480	0.6	5.99	21012	61.29
12	50	600	0.8	10	120	0.3	70	840	0.5	30	360	0.8	5.35	39655	56.64
13	60	720	0.9	30	360	0.7	70	840	0.3	20	240	1.0	4.26	70067	51.81
14	20	240	0.9	10	120	0.3	60	720	1.0	70	840	0.6	4.03	70399	54.04
15	60	720	0.9	70	840	0.7	70	840	0.7	50	600	0.8	3.99	89080	50.70
16	60	720	0.9	30	360	1.0	70	840	0.9	20	240	0.9	4.93	78632	49.90
17	40	480	0.3	10	120	0.3	70	840	0.5	70	840	0.5	6.86	13318	60.19
18	70	840	0.8	30	360	0.7	70	840	1.0	20	240	0.8	3.84	113351	54.10
19	40	480	1.0	50	600	0.4	70	840	0.8	30	360	0.5	4.64	56193	51.99
20	10	120	0.9	70	840	0.4	10	120	0.3	70	840	0.8	4.67	41831	56.87
21	40	480	1.0	20	240	0.6	50	600	0.6	40	480	1.0	5.13	49688	51.91
22	40	480	0.3	20	240	0.6	50	600	0.6	40	480	1.0	5.91	22097	59.98

Note: RC represents the normalized repair cost. DC represents the total cost of damper devices. The units of C_d and K_d are kips-sec/in and kips/in, respectively.

5.4.3. Comparison of Fixed and Flexible Foundation

In this section, the optimization results of fixed and flexible foundation cases are compared. The design variables of each FVD are listed in Table 5-7 and Table 5-8. The nonlinear time history analysis is used to assess the seismic responses of the steel frame under the total of 44 biaxial ground motions. The median values of the inter-story drifts are plotted in Figure 5-9 and Figure 5-10. The solid black line represents the seismic response of the bare frame. It can be observed that all the selected designs are effectively improved the seismic performance of the steel frame. The solid and dashed red lines represent the seismic responses of design A and design a. The solid and dashed yellow lines represent the seismic responses of design B and design b. The blue lines represent the seismic responses of design C and design c.

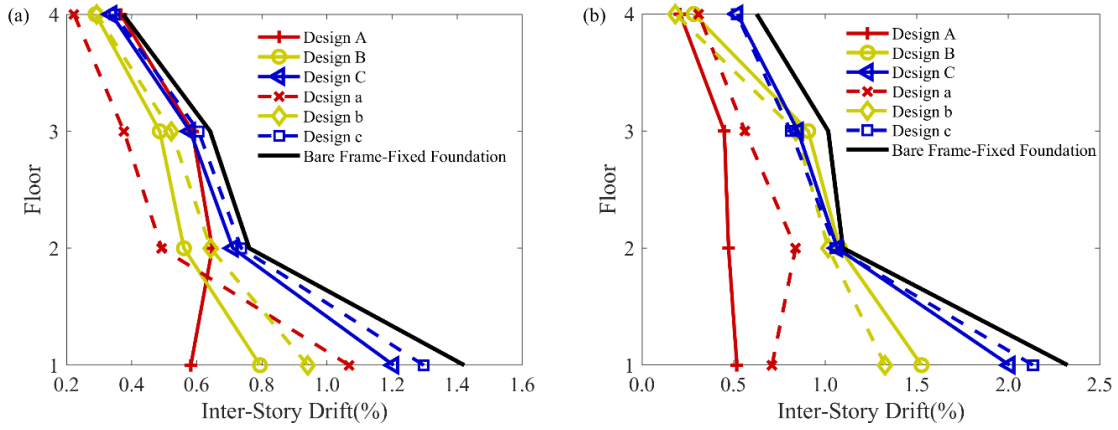

Figure 5-9 Seismic response of selected designs under the effect of fixed foundation: (a) IDR of EW direction; (b) IDR of NS direction

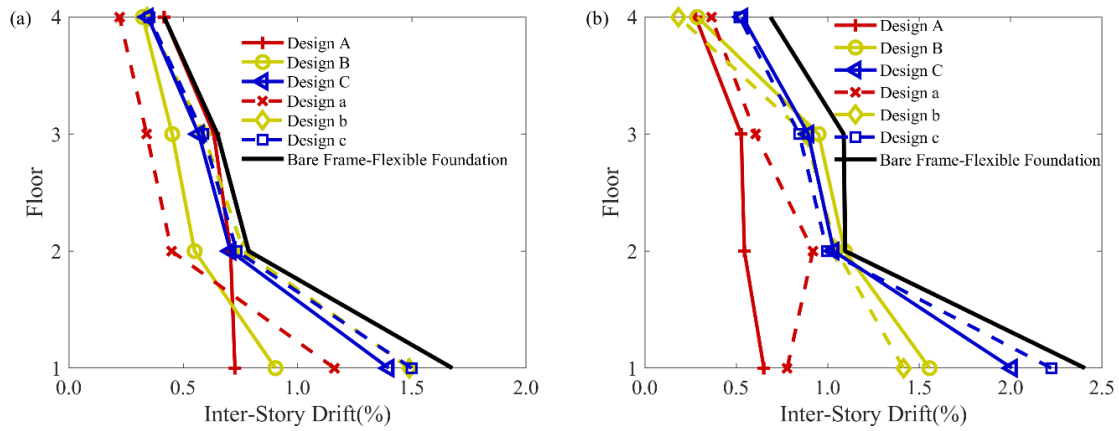

Figure 5-10 Seismic response of selected designs under the effect of flexible foundation: (a) IDR of EW direction; (b) IDR of NS direction

For the frame of design A, which has the fixed foundation, the medium values of peak IDR have reduced to 0.58%, 0.64%, 0.58% and 0.37% of each floor in the EW direction, and 0.52%, 0.47%, 0.45% and 0.21% of each floor in the NS direction. For the same frame of design A, which has the flexible foundation, the medium values of peak IDR have reduced to 0.73%, 0.70%, 0.63%, and 0.42% of each floor in the EW direction, and 0.65%, 0.54%, 0.53%, and 0.28% of each floor in the NS direction. It can be concluded that the steel frame on the site class D has large IDR values by considering the flexibility of the foundation.

For design a, the IDRs have reduced to 1.07%, 0.49%, 0.38%, and 0.22% of each floor in EW direction, and 0.71%, 0.84%, 0.56%, and 0.31% in the NS direction of the frame with the fixed foundation. It can be observed that design A can result in a better seismic performance of the frame in the NS direction, but relatively weaker performance in the first floor of the EW direction. The same conclusion can be drawn for the frame with a flexible foundation.

Table 5-7 Properties of FVDs of the selected designs along the EW direction

	Fixed Foundation									Flexible Foundation								
	Design A			Design B			Design C			Design a			Design b			Design c		
	C_d	K_d	α	C_d	K_d	α	C_d	K_d	α	C_d	K_d	α	C_d	K_d	α	C_d	K_d	α
1st Floor	70	840	1.0	60	720	0.8	40	480	0.5	60	720	0.6	60	720	0.7	10	120	0.4
2nd Floor	70	840	0.3	10	120	0.9	10	120	0.4	60	720	1.0	30	360	0.3	10	120	0.6
3rd Floor	10	120	1.0	10	120	1.0	20	240	0.5	50	600	1.0	20	240	0.7	20	240	0.3
4th Floor	10	120	0.3	50	600	0.3	30	360	0.3	60	720	0.8	30	360	0.6	60	720	0.3
RC (%)	3.55			3.99			5.43			3.72			4.15			7.45		
Damper Cost ($)	165,474			67,218			12,896			126,168			54,597			10,189		
COV_D (%)	40.39			55.09			62.29			50.21			56.95			60.25		

Table 5-8 Properties of FVDs of the selected designs along the NS direction

	Fixed Foundation									Flexible Foundation								
	Design A			Design B			Design C			Design a			Design b			Design c		
	C_d	K_d	α	C_d	K_d	α	C_d	K_d	α	C_d	K_d	α	C_d	K_d	α	C_d	K_d	α
1st Floor	70	840	1.0	10	120	1.0	40	840	0.5	60	720	0.9	40	480	0.8	40	480	0.3
2nd Floor	70	840	1.0	40	480	0.6	20	240	0.5	30	360	0.7	20	240	0.3	10	120	0.6
3rd Floor	50	600	1.0	20	240	0.3	70	840	0.3	70	840	0.8	70	840	0.3	70	840	0.5
4th Floor	70	840	1.0	40	480	1.0	30	360	0.4	20	240	1.0	70	840	1.0	10	120	0.3
RC (%)	3.55			3.99			5.43			3.72			4.15			7.45		
Damper Cost ($)	165,474			67,218			12,896			126,168			54,597			10,189		
COV_D (%)	40.39			55.09			62.29			50.21			56.95			60.25		

In order to select the best-performance design, the effectiveness of these selected designs is evaluated using two measures: (1) the improvement of the structural performance over the bare frame; (2) the uniformity of the inter-story drift along with the building height. The improvement of the structural performance is quantified by the index, μ_{IDR}, expressed as:

$$\mu_{IDR} = \frac{\sum_{i=1}^{N_F} (IDRB_i - IDRD_i)}{N_F}, \quad \text{i=1,2}\ldots N_F \tag{5.17}$$

where *IDRB* and *IDRD* represent the inter-story drift of the bare frame and the frame with dampers, respectively. The overall seismic capacity of the structure is declined with a negative number. Furthermore, the seismic capacity of the structure is enhanced with a positive number.

The values of μ_{IDR} of each selected design are plotted in Figure 5-11. The seismic performance of all the selected designs is improved by applying the FVDs. It is observed that design A has significantly improved the seismic performance of the frames with both fixed and flexible foundations, especially in the NS direction. While design a also significantly improves the seismic performance of the frames with both fixed and flexible foundations, especially in the EW direction.

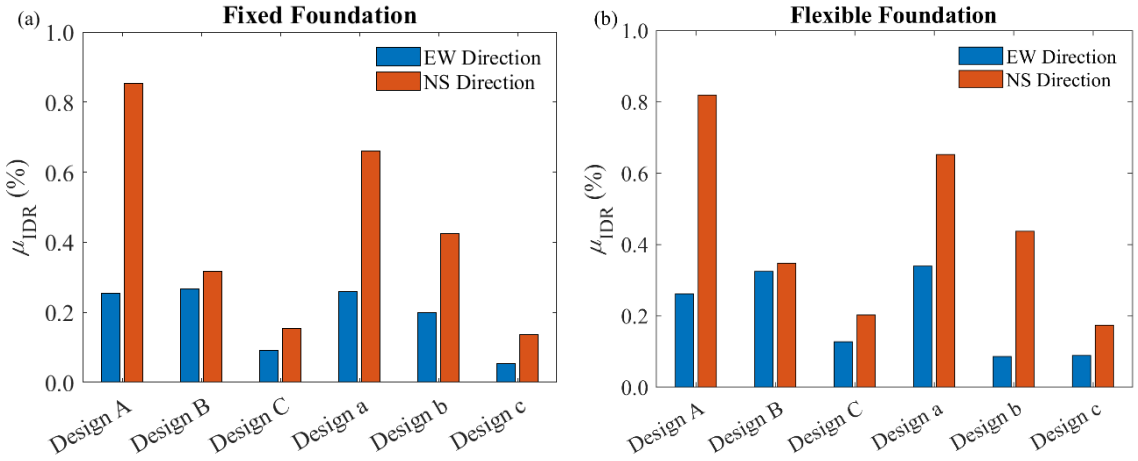

Figure 5-11 Mean value of the inter-story drift improvement over the bare frame: (a) frame with the fixed foundation; (b) frame with the flexible foundation

For the second measure of effectiveness, the uniformity of the inter-story drift along the building height is shown in Figure 5-12. The inter-story drift of each floor is recorded under the 44 biaxial ground motions. The median values of those recorded inter-story drifts of each floor are used to quantify the uniformity of the inter-story drifts, as:

$$COV = \frac{\sigma}{\mu} \tag{5.18}$$

where μ represents the mean value of the inter-story drifts, σ represents the standard deviation of the inter-story drifts, the coefficient of variance (COV) of the inter-story drift ratios is served as the index to quantify the uniformity.

A smaller COV means a more uniformly distributed inter-story drift. In this case, design A (optimized results of the frame with fixed foundation) yields the most uniformly distributed inter-story drift of the frames with both the fixed and flexible foundations.

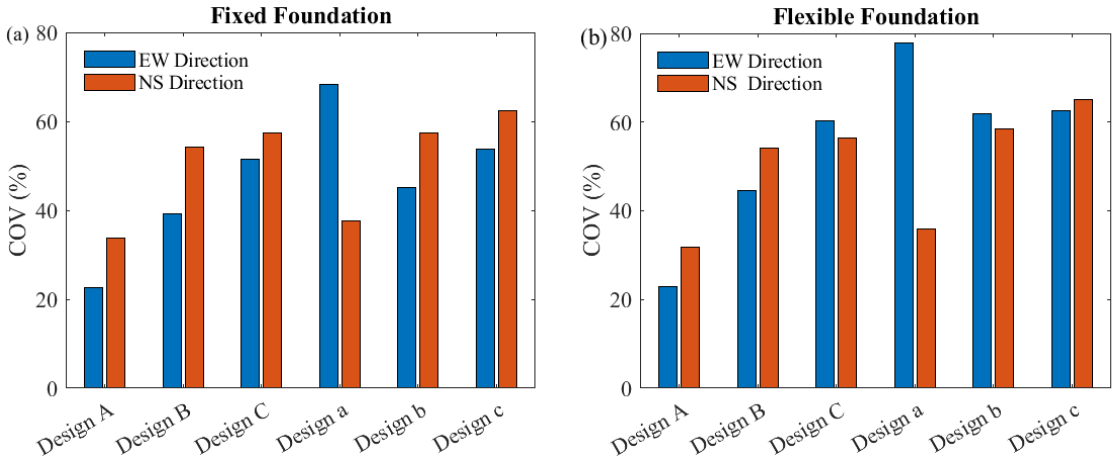

Figure 5-12 Coefficient of variance (*COV*) of the inter-story drift uniformity: (a) fixed foundation; (b) flexible foundation

In this case study, design A can provide the best seismic performance of the structure. It has the smallest repair cost of the structure and produces the most robust design. That is, the properties of each FVD listed in design A can be chosen as the optimum design. It can be visually observed that the seismic performance of the steel frame has been dramatically improved under the MCE level.

5.5. Summary

In this chapter, the effect of soil-structure interaction was incorporated in the proposed optimization framework of performance-based seismic design of the structure. The proposed optimization framework was formulated by three conflicting objective functions: the seismic repair cost of the structure, damper cost, and the robustness measure of ground motion uncertainty. The properties of the axial stiffness, damping coefficient, and the velocity exponent of fluid viscous dampers were selected as the design variables.

The performance-based optimization framework has been applied to a four-story steel moment-resisting frame building. Two scenarios were considered in the optimization framework: one with a fixed foundation, and the other one with a flexible foundation. The flexibility of the foundation was simulated by the elastic Winkler-based SSI model. The soil beneath the foundation was assumed to be dense silty soil and the site classification is D. The damages of the foundation and the FVD were not considered in the optimization framework. The seismic performance of the steel frame was evaluated by considering a total of 44 biaxial ground motions under the MCE level.

The multi-objective optimization results in a family of non-dominated solutions, effectively forming a Pareto front. The obtained designs along the Pareto front were found to improve the seismic performance of the steel frame. Several optimized designs were selected along the Pareto fronts regarding the two optimization scenarios. For the site class of D, the frame with a flexible foundation was found to have a larger inter-story drift in each floor when compared to the frame with a fixed foundation. Moreover, the frame with a flexible foundation has a higher seismic repair cost and is less sensitive to the uncertainty of the ground motion.

The guideline for selecting the best-performance design is based on the inter-story drift ratio, which can be considered as an engineering demand parameter of the structure design. Two performance indices, i.e., the improvement of the inter-story drift (compared to a bare frame without energy dissipation systems) and the uniformity of the inter-story drift, were proposed to evaluate the effectiveness of the selected designs. In this case,

design A (optimized results of the frame with fixed foundation) has significantly reduced the inter-story drift and yields the most uniformly distributed inter-story drift of the frames with both the fixed and flexible foundations.

CHAPTER VI
CONCLUSION AND RECOMMENDATIONS

6.1. Conclusions

Energy dissipation systems such as fluid viscous dampers can effectively improve the seismic performance of a structure and are widely implemented in engineering projects. This dissertation aims to improve and simulate the seismic performance of structures with energy dissipation systems, consider soil-structure interaction that can affect the seismic performance of structures, and also provide the guideline for choosing the best performing and cost-effective structural design.

In this dissertation, the seismic performance of structures with energy dissipation systems, specifically fluid viscous dampers (FVD), was investigated using three-dimensional (3D) numerical models. Four different damping coefficient distribution methods of the FVD have been extended and applied to the 3D numerical model of structures. Based on that, the seismic performance of all structures has been significantly improved. Among the four different damping coefficient distribution methods, the story shear strain energy distribution (SSSED) method was recommended to distribute the damper's damping coefficient within the 3D numerical model. Moreover, a performance-based optimization framework for the structural design was developed that considers multiple conflicting objectives. Based on this proposed optimization framework, the optimal design variables of the energy dissipation systems can be selected. Those optimal design variables can help to achieve the desired performance level of the structure with

moderate initial material cost, structural repair cost, and robustness measure. Furthermore, the impact of soil-structure interaction was incorporated into the proposed optimization framework. Both the fixed foundation and flexible foundation were considered in the analysis. Two performance indices, that the improvement of the inter-story drift (compared to a bare frame without energy dissipation systems) and the uniformity of the inter-story drift, were proposed to select the best-performance design.

Key findings of the three main chapters (chapters III to V) are summarized in the following:

Chapter III: Damping Coefficient Distribution of Energy Dissipation System Applied to the 3D Numerical Model of Building

(1) The uniform distribution (UD), inter-story drift proportional distribution (IDPD), SSSED, and efficient story shear strain energy distribution (ESSSED) methods were extended to distribute the damper's damping coefficient within the 3D numerical model. The seismic performance of all structures has been significantly improved.

(2) The uniformity of distributed inter-story drift and the improvement of inter-story drift were considered as the performance measures to evaluate the effectiveness of different damping coefficient distribution methods.

(3) The SSSED method was found to improve the inter-story drift of the structure while also providing the most uniformly distributed inter-story drift.

(4) The ESSSED method could not provide the stable seismic performance of the structure when extending it to the 3D numerical models.

Chapter VI: Performance-Based Optimization for Seismic Design of Steel Frame with Energy Dissipation System

(1) The developed performance-based optimization framework for the structural design was effective in improving the seismic performance of structures. The applicability and capability of the proposed framework were demonstrated by applying it to the 3D numerical model of the steel frame with the energy dissipation system.

(2) All obtained optimum designs were found to dramatically decrease the inter-story drift and peak floor acceleration of the steel frame.

(3) The Pareto fronts of both the MCE and DBE levels revealed that the damper cost generally dominates the trade-off between the three distinct objectives: the more cost of dampers could result in less repair cost and robustness measure. Moreover, the Pareto fronts revealed that the robustness measure does not have an utterly linear correlation with damper cost and the repair cost.

(4) The optimal design variables of the dampers were selected by comparing the seismic performance of the optimized designs at the MCE and DBE levels. The selected design can achieve the desired performance levels of the structure with moderate initial material cost, structural repair cost, and robustness measure.

Chapter V: Simulation-Based Optimization of Structural Performance Incorporating Soil-Structure Interaction

(1) The effect of soil-structure interaction was incorporated into the proposed optimization framework of performance-based seismic design of the structure (presented in Chapter IV). Two scenarios have been applied to the proposed optimization framework: one with a fixed foundation, and the other one with a flexible foundation.

(2) All the obtained optimal designs were found to be improved the seismic performance of the structure, which sits on the site class of D. The frame with a flexible foundation was found to have a larger inter-story drift in each floor when compared to the frame with a fixed foundation. Moreover, the frame with a flexible foundation has a higher seismic repair cost and is less sensitive to the uncertainty of the ground motion.

(3) The guideline for selecting the best-performance design was based on the inter-story drift ratio. The improvement and the uniformity of the inter-story drift were proposed as the performance indexes to evaluate the effectiveness of the selected designs. The optimized result of the frame with a fixed foundation was selected as the best-performance design. Because the selected design can significantly reduce the inter-story drift and yields the most uniformly distributed inter-story drift of the frames with both the fixed and flexible foundations.

6.2. Recommendations

To further expand the work presented in this dissertation, some research topics may be undertaken, which include the following:

(1) It is recommended to consider the higher modes and their coupled effects of the 3D model while applying the damping coefficient distribution methods described in Chapter III.

(2) The performance-based optimization framework for structural design only considers the SSI of the structures on the site class D. It is recommended to investigate the influence of different site classes on the proposed optimization framework. Moreover, the damages of the foundation and the FVD can be considered in the optimization framework.

(3) The proposed performance-based optimization framework for structural design can be implemented using many other building types. Thus, future study is recommended to further develop this approach by using design variables of structural components other than those considered in chapter IV and chapter V.

REFERENCE

Achour, Nebil, Masakatsu Miyajima, Masaru Kitaura, and Andrew Price. 2011. "Earthquake-Induced Structural and Nonstructural Damage in Hospitals." Earthquake Spectra 27(3):617–34.

Aittokoski, Timo and Kaisa Miettinen. 2008. "Cost Effective Simulation-Based Multiobjective Optimization in the Performance of an Internal Combustion Engine." Engineering Optimization 40(7):593–612.

Applied Technology Council (ATC). 1996. "Seismic Evaluation and Retrofit of Concrete Buildings, ATC-40, Volume 1 and 2."

Aristizabal-Ochoa, J. Datio. 1986. "Disposable Knee Bracing: Improvement in Seismic Design of Steel Frames." Journal of Structural Engineering 112(7):1544–52.

ASCE 07-10. 2010. Minimum Design Loads for Buildings and Other Structures.

ASCE 41-17. 2017. Seismic Evaluation and Retrofit of Existing Buildings.

Askari, Mohsen, Jianchun Li, and Bijan Samali. 2017. "Cost-Effective Multi-Objective Optimal Positioning of Magnetorheological Dampers and Active Actuators in Large Nonlinear Structures." Journal of Intelligent Material Systems and Structures 28(2):230–53.

Banazadeh, Mehdi and Ali Ghanbari. 2017. "Seismic Performance Assessment of Steel Moment-Resisting Frames Equipped with Linear and Nonlinear Fluid Viscous Dampers with the Same Damping Ratio." Journal of Constructional Steel Research 136:215–28.

Bao, Yihai and Sashi K. Kunnath. 2010. "Simplified Progressive Collapse Simulation of

RC Frame–Wall Structures." Engineering Structures 32(10):3153–62.

Basoz, Nesrin I., Anne S. Kiremidjian, Stephanie A. King, and Kincho H. Law. 1999. "Statistical Analysis of Bridge Damage Data from the 1994 Northridge, CA, Earthquake." Earthquake Spectra 15(1):25–54.

Bertero, Raul D. and Vitelmo V. Bertero. 2002. "Performance-Based Seismic Engineering: The Need for a Reliable Conceptual Comprehensive Approach." Earthquake Engineering and Structural Dynamics 31(3):627–52.

Bommer, J. J., R. J. Chandler, and C. E. Rodrıguez. 1999. "Earthquake-Induced Landslides : 1980 – 1997." Soil Dynamics and Earthquake Engineering 18:325–46.

Buckle, I. G. 2000. "Passive Control of Structures for Seismic Loads." Bulletin of the New Zealand Society for Earthquake Engineering 33(3):209–21.

Charmpis, D. C., P. Komodromos, and M. C. Phocas. 2012. "Optimized Earthquake Response of Multi-storey Buildings with Seismic Isolation at Various Elevations." Earthquake Engineering & Structural Dynamics 41(15):2289–2310.

Chaudhuri, S. R. and R. Villaverde. 2008. "Effect of Building Nonlinearity on Seismic Response of Nonstructural Components: A Parametric Study." Journal of Structural Engineering 134(4r):661–70.

Confesor, Jr R. B. and G. W. Whittaker. 2007. "Automatic Calibration of Hydrologic Models With Multi-Objective Evolutionary Algorithm and Pareto Optimization 1." JAWRA Journal of the American Water Resources Association, 43(4):981–89.

Constantinou, M. C., T. T. Soong, and G. F. Dargush. 1998. Passive Energy Dissipation Systems for Structural Design and Retrofit.

Constantinou, M. C. and I. G. Tadjbakhsh. 1983. “Optimum Design of a First Story Damping System.” Computers & Structures 17(2):305–10.

Deb, K., S. Agrawal, A. Pratap, and T. Meyarivan. 2000. “A Fast Elitist Non-Dominated Sorting Genetic Algorithm for Multi-Objective Optimization: NSGA-II.” Pp. 849–58 in International conference on parallel problem solving from nature.

Deb, K., A. Pratap, S. Agarwal, and T. Meyarivan. 2002. “A Fast and Elitist Multiobjective Genetic Algorithm: NSGA-II.” IEEE Transactions on Evolutionary Computation 6(2):182–97.

Deb, Kalyanmoy. 2001. Multi-Objective Optimization Using Evolutionary Algorithms. John Wiley & Sons.

Deng, Peng, Shiling Pei, John W. van de Lindt, Hongyan Liu, and Chao Zhang. 2017. “An Approach to Quantify the Influence of Ground Motion Uncertainty on Elastoplastic System Acceleration in Incremental Dynamic Analysis.” Advances in Structural Engineering 20(11):1744–56.

Dogruel, Seda, Oren Lavan, and Gary F. Dargush. 2008. “A Unified Framework for Evolutionary Optimization with Application to Structural Engineering.” International Conference on Engineering Optimization 1–12.

Doltsinis, Ioannis and Zhan Kang. 2004. “Robust Design of Structures Using Optimization Methods.” Computer Methods in Applied Mechanics and Engineering 193(23–26):2221–37.

Dutta, Sekhar Chandra, Koushik Bhattacharya, and Rana Roy. 2004. “Response of Low-Rise Buildings under Seismic Ground Excitation Incorporating Soil–Structure

Interaction.” Soil Dynamics and Earthquake Engineering 24(12):893–914.

Erbas, Cagkan, Selin Cerav-Erbas, and Andy D. Pimentel. 2006. “Multiobjective Optimization and Evolutionary Algorithms for the Application Mapping Problem in Multiprocessor System-on-Chip Design.” IEEE Transactions on Evolutionary Computation 10(3):358–74.

FEMA-273. 1997. “NEHRP Guidelines for the Seismic Rehabilitation of Buildings.” (FEMA 273).

FEMA-356. 2000. “Prestandard and Commentary for the Seismic Rehabilitation of Buildings.”

FEMA P-58-1. 2018. “Seismic Performance Assessment of Buildings Volume 1—Methodology.” Technical Report FEMA-P58.

FEMA P-58-2. 2018. “Seismic Performance Assessment of Buildings Volume 2—Implementation Guide.” Technical Report FEMA-P58.

FEMA P695. 2009. “Quantification of Building Seismic Performance Factors.” Fema P695.

Ferracuti, Barbara, Rui Pinho, Marco Savoia, and Roberto Francia. 2009. “Verification of Displacement-Based Adaptive Pushover through Multi-Ground Motion Incremental Dynamic Analyses.” Engineering Structures 31(8):1789–99.

Furtado, André, Hugo Rodrigues, and António Arêde. 2015. “Modelling of Masonry Infill Walls Participation in the Seismic Behaviour of RC Buildings Using OpenSees.” International Journal of Advanced Structural Engineering 7(2):117–27.

Gazetas, George. 1991. “Formulas and Charts for Impedances of Surface and Embedded Foundations.” 117(9):1363–81.

Ghobarah, Ahmed. 2001. “Performance-Based Design in Earthquake Engineering: State of Development.” Engineering Structures 23(8):878–84.

Gholizadeh, Saeed and Amir Baghchevan. 2017. “Multi-Objective Seismic Design Optimization of Steel Frames by a Chaotic Meta-Heuristic Algorithm.” Engineering with Computers 33(4):1045–60.

Ghosh, B. and S. P. G. Madabhushi. 2004. “Dynamic Soil Structure Interaction for Layered and Inhomogeneous Ground: A Compartitive Study.” Pp. 1–15 in In Proceedings of the the 13th World Conference on Earthquake Engineering, Vancouver, BC, Canada.

Gidaris, Ioannis and Alexandros A. Taflanidis. 2015. “Performance Assessment and Optimization of Fluid Viscous Dampers through Life-Cycle Cost Criteria and Comparison to Alternative Design Approaches.” Bulletin of Earthquake Engineering 13(4):1003–28.

Del Gobbo, G. M., Anthony. Blakeborough, and M. S. Williams. 2018. “Improving Total-Building Seismic Performance Using Linear Fluid Viscous Dampers.” Bulletin of Earthquake Engineering 16(9):4249–72.

Del Gobbo, G. M., Martin S. Williams, and Anthony Blakeborough. 2018. “Comparing Fluid Viscous Damper Placement Methods Considering Total-Building Seismic Performance.” Earthquake Engineering and Structural Dynamics 47(14):2864–86.

Gonzalez, D., C. Ash, W. Brown, J. Ahlport, and M. Abdi. 2013. “Seismic Retrofit of a 1960’s Steel-Frame Industrial Building in Washington State Using Viscous Dampers.” In Structures Congress 2013: Bridging Your Passion with Your Profession 1046–57.

Gorum, Tolga, Xuanmei Fan, Cees J. van Westen, Run Qiu Huang, Qiang Xu, Chuan Tang,

and Gonghui Wang. 2011. “Distribution Pattern of Earthquake-Induced Landslides Triggered by the 12 May 2008 Wenchuan Earthquake.” Geomorphology 133(3–4):152–67.

Güneyisi, E. M. 2012. “Seismic Reliability of Steel Moment Resisting Framed Buildings Retrofitted with Buckling Restrained Braces.” Earthquake Engineering & Structural Dynamics 41(5):853–74.

Guo, Tong, Jia Xu, Weijie Xu, and Zhiqiang Di. 2014. “Seismic Upgrade of Existing Buildings with Fluid Viscous Dampers: Design Methodologies and Case Study.” Journal of Performance of Constructed Facilities 29(6):04014175.

Hejazi, F., I. Toloue, M. S. Jaafar, and J. Noorzaei. 2013. “Optimization of Earthquake Energy Dissipation System by Genetic Algorithm.” Computer-Aided Civil and Infrastructure Engineering 28(10):796–810.

Hwang, J. S., S. L. Yi, and S. Y. Ho. 2004. “Equivalent Damping Ratios of Structures with Supplemental Viscous Dampers.” Engineering Structures 26:346–65.

Hwang, Jenn Shin, Yin Nan Huang, Shy Lian Yi, and Song Yen Ho. 2008. “Design Formulations for Supplemental Viscous Dampers to Building Structures.” Journal of Structural Engineering 134(1):22–31.

Hwang, Jenn Shin, Wang Chuen Lin, and Nian Juan Wu. 2013. “Comparison of Distribution Methods for Viscous Damping Coefficients to Buildings.” Structure and Infrastructure Engineering 9(1):28–41.

Ishihara, K. 1993. “Liquefaction and Flow Failure during Earthquakes.” Géotechnique 43(3):351–451.

Jeremić, Boris, Sashi Kunnath, and Feng Xiong. 2004. “Influence of Soil–Foundation–Structure Interaction on Seismic Response of the I-880 Viaduct.” Engineering Structures 26(3):391–402.

Jiang, Jian and Asif Usmani. 2013. “Modeling of Steel Frame Structures in Fire Using OpenSees.” Computers and Structures 118:90–99.

Jones, Allen L., Steven L. Kramer, and Pedro Arduino. 2002. “Estimation of Uncertainty in Geotechnical Properties for Performance-Based Earthquake Engineering.” Technical Report 2002/16, Pacific Earthquake EngineeringR Esearch Center, PEER.

Kang. 2005. “Robust Design Optimization of Structures under Uncertainties.” Ph.D. Thesis, Institute Fur Statik Und Dynamik Der Luft - Und Raumfahrkon - Struktionen Universitat Stuttgart 161.

Kaplan, H., S. Yilmaz, N. Cetinkaya, and E. Atimtay. 2011. “Seismic Strengthening of RC Structures with Exterior Shear Walls.” Sadhana 36(1):17.

Karavasilis, Theodore L. 2016. “Assessment of Capacity Design of Columns in Steel Moment Resisting Frames with Viscous Dampers.” Soil Dynamics and Earthquake Engineering 88:215–22.

Kasai, Kazuhiko, Hiroshi Ito, Yoji Ooki, Tsuyoshi Hikino, Koichi Kajiwara, Shojiro Motoyui, Hitoshi Ozaki, and Masato Ishii. 2010. “Full-Scale Shake Table Tests of 5-Story Steel Building with Various Dampers.” 7th International Conference on Urban Earthquake Engineering (7CUEE) & 5th International Conference on Earthquake Engineering (5ICEE) 11–22.

Kaveh, A., B. Farahmand Azar, A. Hadidi, F. Rezazadeh Sorochi, and S. Talatahari. 2010.

"Performance-Based Seismic Design of Steel Frames Using Ant Colony Optimization." Journal of Constructional Steel Research 66(4):566–74.

Kuczera, G. 1997. "Efficient Subspace Probabilistic Parameter Optimization for Catchment Models." Water Resources 33(1):177–85.

Kumar, P. Santhosh, M. Vasudeva Naidu, S. Madhan Mohan, and S. Sreenatha Reddy. 2016. Application of Fluid Viscous Dampers in Multi-Story Buildings.

Landi, Luca, Filippo Conti, and Pier Paolo Diotallevi. 2015. "Effectiveness of Different Distributions of Viscous Damping Coefficients for the Seismic Retrofit of Regular and Irregular RC Frames." Engineering Structures 100:79–93.

Lavan, O. and O. Amir. 2014. "Simultaneous Topology and Sizing Optimization of Viscous Dampers in Seismic Retrofitting of 3D Irregular Frame Structures." Earthquake Engineering & Structural Dynamics 43(9):1325–42.

Lavan, O., G. F. Dargush, and A. M. Reinhorn. 2008. "Multi-Objective Evolutionary Optimization of Passive Energy Dissipation Systems under Seismic Loading." Earthquake Engineering.

Lavan, Oren and Gary F. Dargush. 2009. "Multi-Objective Evolutionary Seismic Design with Passive Energy Dissipation Systems." Journal of Earthquake Engineering 13(6):758–90.

Lee, D. and D. P. Taylor. 2001. "Viscous Damper Development and Future Trends." Structural Design of Tall Buildings 10(5):311–20.

Li, Mengke, Xiao Lu, Xinzheng Lu, and Lieping Ye. 2014. "Influence of Soil–Structure Interaction on Seismic Collapse Resistance of Super-Tall Buildings." Journal of Rock

Mechanics and Geotechnical Engineering 6(5):477–85.

Lignos, D. G. 2008. “Sidesway Collapse of Deteriorating Structural Systems under Seismic Excitations.”

Lignos, D. G. and H. Krawinkler. 2010. “Deterioration Modeling of Steel Components in Support of Collapse Prediction of Steel Moment Frames under Earthquake Loading.” Journal of Structural Engineering 137(11):1291–1302.

Lignos, D. G., H. Krawinkler, and A. S. Whittaker. 2011. “Prediction and Validation of Sidesway Collapse of Two Scale Models of a 4-story Steel Moment Frame.” Earthquake Engineering & Structural Dynamics 40(7):807–25.

Lin, W. H. and A. K. Chopra. 2003. “Earthquake Response of Elastic Single-Degree-of-Freedom Systems with Nonlinear Viscoelastic Dampers.” Journal of Engineering Mechanics 129(6):597–606.

Liu, Junshan. 2010. “Risk-Based Seismic Design Optimization of Steel Building Systems with Passive Damping Devices.”

Liu, Wen and F. Yamazaki. 2018. “Extraction of Collapsed Buildings Due to the 2016 Kumamoto, Japan, Earthquake Using Two-Temporal Lidar Data.” in SPIE 10779, Lidar Remote Sensing for Environmental Monitoring XVI. Vol. 10779.

Liu, Yang and Fan Sun. 2010. “Sensitivity Analysis and Automatic Calibration of a Rainfall-Runoff Model Using Multi-Objectives.” Ecological Informatics 5(4):304–10.

Liu, Z. 2013. “Robust Design Optimization: Ensuring Robustness against Uncertainty in Structural Design.”

Lu, Xiao, Xinzheng Lu, Hong Guan, and Lieping Ye. 2013. “Collapse Simulation of

Reinforced Concrete High-Rise Building Induced by Extreme Earthquakes." Earthquake Engineering and Structural Dynamics 42(5):705–23.

Madsen, Henrik. 2003. "Parameter Estimation in Distributed Hydrological Catchment Modelling Using Automatic Calibration with Multiple Objectives." Advances in Water Resources 26(2):205–16.

Madsen, Henrik, Geoffrey Wilson, and Hans Christian Ammentorp. 2002. "Comparison of Different Automated Strategies for Calibration of Rainfall-Runoff Models." Journal of Hydrology 261(1–4):48–59.

Mason, H. B. 2011. "Seismic Performance Assessment in Dense Urban Environments." Doctoral Dissertation, UC Berkeley.

Matsagar, Vasant A. and R. S. Jangid. 2008. "Base Isolation for Seismic Retrofitting of Structures." Practice Periodical on Structural Design and Construction 13(4):175–85.

Meunier, Patrick, Niels Hovius, and John Allan Haines. 2008. "Topographic Site Effects and the Location of Earthquake Induced Landslides." Earth and Planetary Science Letters 275(3–4):221–32.

Mishra, K. K. and S. Harit. 2010. "A Fast Algorithm for Finding the Non Dominated Set in Multi-Objective Optimization." International Journal of Computer Applications 1(25):35–39.

Miyamoto, H. K., A. S. Gilani, A. Wada, and C. Ariyaratana. 2010. "Limit States and Failure Mechanisms of Viscous Dampers and the Implications for Large Earthquakes." Earthquake Engineering & Structural Dynamics 39(11):1279–97.

Miyamoto, Kit, Amir S. J. Gilani, and Robert S. Glasgow. 2007. "Seismic Retrofit of a

Hospital Building with Supplementary Damping Devices." In New Horizons and Better Practices 1–10.

Narkhede, D. I. and R. Sinha. 2012. "Shock Vibration Control of Structures Using Fluid Viscous Dampers." in 15th World Conference on Earthquake Engineering (15WCEE).

NEHRP. 2000. "Recommended Provisions for Seismic Regulations for New Buildings." Building Seismic Safety Council. Washington (DC).

Obermeier, Stephen F. 1996. "Use of Liquefaction-Induced Features for Paleoseismic Analysis—an Overview of How Seismic Liquefaction Features Can Be Distinguished from Other Features and How Their Regional Distribution and Properties of Source Sediment Can Be Used to Infer the Locatio." Engineering Geology 44(1–4):1–76.

Oesterle, Michael Gerhardt. 2003. "Use of Incremental Dynamic Analysis to Assess the Performance of Steel Moment-Resisting Frames with Fluid Viscous Dampers."

Ou, Jinping and Hui Li. 2009. "Design Approaches for Active, Semi-Active and Passive Control Systems Based on Analysis of Characteristics of Active Control Force." Earthquake Engineering and Engineering Vibration 8(4):493–506.

Parsopoulos, K. E. and M. N. Vrahatis. 2002. "Particle Swarm Optimization Method in Multiobjective Problems." Pp. 603–7 in Proceedings of the 2002 ACM symposium on Applied computing.

Pollini, N., O. Lavan, and O. Amir. 2017. "Minimum-cost Optimization of Nonlinear Fluid Viscous Dampers and Their Supporting Members for Seismic Retrofitting." Earthquake Engineering & Structural Dynamics 46(12):1941–61.

Pollini, Nicolò, Oren Lavan, and Oded Amir. 2016. "Towards Realistic Minimum-Cost

Optimization of Viscous Fluid Dampers for Seismic Retrofitting." Bulletin of Earthquake Engineering 14(3):971–98.

Raghunandan, M. and A. B. Liel. 2013. "Effect of Ground Motion Duration on Earthquake-Induced Structural Collapse." 41:119–33.

Ras, A. and N. Boumechra. 2016. "Seismic Energy Dissipation Study of Linear Fluid Viscous Dampers in Steel Structure Design." Alexandria Engineering Journal 55(3):2821–32.

Raychowdhury, Prishati. 2008. "Nonlinear Winkler-Based Shallow Foundation Model for Performance Assessment of Seismically Loaded Structures (Doctoral Dissertation, UC San Diego)."

Raychowdhury, Prishati. 2011. "Seismic Response of Low-Rise Steel Moment-Resisting Frame (SMRF) Buildings Incorporating Nonlinear Soil–Structure Interaction (SSI)." Engineering Structures 33(3):958–67.

Sáez, Esteban, Fernando Lopez-Caballero, and Arezou Modaressi-Farahmand-Razavi. 2013. "Inelastic Dynamic Soil–Structure Interaction Effects on Moment-Resisting Frame Buildings." Engineering Structures 51:166–77.

Seo, C. Y., T. L. Karavasilis, J. M. Ricles, and R. Sause. 2014. "Seismic Performance and Probabilistic Collapse Resistance Assessment of Steel Moment Resisting Frames with Fluid Viscous Dampers." Earthquake Engineering & Structural Dynamics 43(14):2135–54.

Shukla, A. K. and T. K. Datta. 1999. "Optimal Use of Viscoelastic Dampers in Building Frames for Seismic Force." Journal of Structural Engineering 125(4):401–9.

Silwal, Baikuntha, Robert J. Michael, and Osman E. Ozbulut. 2015. “A Superelastic Viscous Damper for Enhanced Seismic Performance of Steel Moment Frames.” Engineering Structures 105:152–64.

Silwal, Baikuntha, Osman E. Ozbulut, and Robert J. Michael. 2016. “Seismic Collapse Evaluation of Steel Moment Resisting Frames with Superelastic Viscous Damper.” Journal of Constructional Steel Research 126:26–36.

Singh, M. P. and L. M. Moreschi. 2002. “Optimal Placement of Dampers for Passive Response Control.” Earthquake Engineering & Structural Dynamics 31(4):955–76.

Sirois, Frédéric and Grilli Francesco. 2015. “Potential and Limits of Numerical Modelling for Supporting the Development of HTS Devices.” Superconductor Science and Technology 28(4).

Soong, T. T. and G. F. Dargush. 1997. “Passive Energy Dissipation Systems in Structural Engineering.”

Soong, T. T. and B. F. Spencer. 2002. “Supplemental Energy Dissipation: State-of-the-Art and State-of-the-Practice.” Engineering Structures 24(3):243–59.

Sorace, S. and G. Terenzi. 2008. “Seismic Protection of Frame Structures by Fluid Viscous Damped Braces.” Journal of Structural Engineering 134(1):45–55.

Sorace, S. and G. Terenzi. 2009. “Fluid Viscous Damped-Based Seismic Retrofit Strategies of Steel Structures: General Concepts and Design Applications.” 5(3):322–39.

Stewart, J. P., G. L. Fenves, and R. B. Seed. 1999. “Seismic Soil-Structure Interaction in Buildings. I: Analytical Methods.” Journal of Geotechnical and Geoenvironmental Engineering 125(1):26–37.

Symans, M. D. and M. C. Constantinou. 1998. “Passive Fluid Viscous Damping Systems for Seismic Energy Dissipation.” ISET Journal of Earthquake Technology 35:185–206.

Takewaki, I. 1997. “Optimal Damper Placement for Minimum Transfer Functions.” Earthquake Engineering & Structural Dynamics 26(11):1113–24.

Tang, Yuchuan and Jian Zhang. 2011. “Probabilistic Seismic Demand Analysis of a Slender RC Shear Wall Considering Soil–Structure Interaction Effects.” Engineering Structures 33(1):218–29.

Terzaghi, K. 1943. “Theoretical Soil Mechanics.” New York: Wiley.

Terzic, V., S. A. Mahin, and M. Comerio. 2014. “Comparative Life-Cycle Cost and Performance Analysis of Structural Systems for Buildings.” In Tenth US National Conference on Earthquake Engineering.

Tong, Xiaohua, Xiaofei Lin, Tiantian Feng, Huan Xie, Shijie Liu, Zhonghua Hong, and Peng Chen. 2013. “Use of Shadows for Detection of Earthquake-Induced Collapsed Buildings in High-Resolution Satellite Imagery.” ISPRS Journal of Photogrammetry and Remote Sensing 79:53–67.

Torunbalci, N. 2004. “Seismic Isolation and Energy Dissipating Systems in Earthquake Resistant Design.” Pp. 1–13 in Proceedings in 13th World Conference on Earthquake Engineering.

Uang, Chia-Ming and Vitelmo V. Bertero. 1990. “Evaluation of Seismic Energy in Structures.” Earthquake Engineering & Structural Dynamics 19(1):77–90.

Uniform Building Code. 1994. “Structural Engineering Design Provisions. Vol.2.” In

International Conference of Building Officials.

Veerappa, Varsha and Emmanuel Letier. 2011. “Understanding Clusters of Optimal Solutions in Multi-Objective Decision Problems.” Proceedings of the 2011 IEEE 19th International Requirements Engineering Conference, RE 2011 89–98.

Wang, Shanshan, Jiun Wei Lai, Matthew J. Schoettler, and Stephen A. Mahin. 2017. “Seismic Assessment of Existing Tall Buildings: A Case Study of a 35-Story Steel Building with Pre-Northridge Connection.” Engineering Structures 141:624–33.

Wong, K. K. 2011. “Seismic Energy Analysis of Structures with Nonlinear Fluid Viscous Dampers—Algorithm and Numerical Verification.” The Structural Design of Tall and Special Buildings 20(4):482–96.

Wu, Bo, Jin-ping Ou, and T. T. Soong. 1997. “Optimal Placement of Energy Dissipation Devices for Three-Dimensional Structures.” Engineering Structures 19(2):113–25.

Wu, X. 2014. “A Study of Nonlinear Time History Analysis vs. Current Codes Analysis Procedure of Comparing Linear Dynamic Demand with Nonlinear Static Capacity for Ordinary Standard Bridge.” In Challenges and Advances in Sustainable Transportation Systems 467–80.

Wu, Xiaoyun. 2014. “A Study of Nonlinear Time History Analysis vs. Current Codes Analysis Procedure of Comparing Linear Dynamic Demand with Nonlinear Static Capacity for Ordinary Standard Bridge.” In Challenges and Advances in Sustainable Transportation Systems 467–80.

Yang, T. Y., J. P. Moehle, Y. Bozorgnia, F. Zareian, and J. W. Wallace. 2012. “Performance Assessment of Tall Concrete Core-wall Building Designed Using Two

Alternative Approaches." Earthquake Engineering & Structural Dynamics 41(11):1515–31.

Zeng, Xiang, Xinzheng Lu, T. Y. Yang, and Zhen Xu. 2016. "Application of the FEMA-P58 Methodology for Regional Earthquake Loss Prediction." Natural Hazards 83(1):177–92.

Zhang, R. H. and T. T. Soong. 1992. "Seismic Design of Viscoelastic Dampers for Structural Applications." Journal of Structural Engineering 118(5):1375–92.

Zitzler, E. 1999. Evolutionary Algorithms for Multiobjective Optimization: Methods and Applications. Vol. 63.

Zou, X. K. and C. M. Chan. 2004. "Integrated Time History Analysis and Performance-Based Design Optimization of Base-Isolated Concrete Buildings." Proc. 13th World Conference on Earthquake Engineering (1314):1314.

Zou, X. K., C. M. Chan, G. Li, and Q. Wang. 2007. "Multiobjective Optimization for Performance-Based Design of Reinforced Concrete Frames." Journal of Structural Engineering 133(10):1462–74.